HIPPO SIGNALING KINASE LATS CONTROLS EPICARDIAL PROGENITOR CELL DIFFERENTIATION AND MAINTAINS ADULT HEART HOMEOSTASIS

A Dissertation

by

YANG XIAO

Submitted to the Office of Graduate and Professional Studies of
Texas A&M University
in partial fulfillment of the requirements for the degree of

DOCTOR OF PHILOSOPHY

Chair of Committee,	Fen Wang
Co-Chair of Committee,	James F. Martin
Committee Members,	Richard Behringer
	Ali J. Marian
Head of Program,	Warren Zimmer

December 2017

Major Subject: Medical Sciences

ABSTRACT

The epicardium, the heart's outermost layer, contains progenitors for essential non-cardiomyocyte lineages that support coronary vascular development. The Hippo pathway, a conserved kinase cascade, controls organ size in the developing heart and inhibits regeneration in the adult heart. In the first study, using high-throughput single cell RNA-seq (scRNA-seq), we investigated the function of Hippo pathway kinases, Lats1 and Lats2 (Lats1/2) in epicardial development. *Lats1/2* mutant cells fail to activate the fibroblast differentiation program, but instead remain suspended in an intermediate progenitor cell state with characteristics of epicardial cells and fibroblasts. Computational analysis and lineage tracing revealed an arrested developmental trajectory for *Lats1/2* mutant cells that resulted in an abnormal extracellular matrix composition and an altered extracellular growth factor milieu, leading to defective coronary vascular remodeling.

In the second study, we focused on the minor lineage endothelial cell which rarely comes from epicardium at normal state. Lats mutant epicardium preferentially generated endothelial cells. Genes associated with F-actin polymerization were upregulated in Lats mutant epicardium. Super-resolution microscopy and atomic force microscopy indicated that Lats mutant epicardium was stiffer with more intracellular F-actin bundles. Explant studies revealed that epicardial progenitors cultured on stiff matrices acquired an endothelial phenotype independently of Lats , while on softer, more physiologic matrices Lats inhibited

the endothelial phenotype. Thus, Lats inhibits Wt1 derived endothelial lineage expansion in cooperation with cytoskeletal state.

In the third study, we investigated the role of Lats1/2 in adult cardiac fibroblast. Inactivation of *Lats1/2* in fibroblasts resulted in hyper-proliferation of cardiac fibroblast. *Lats1/2*CKO hearts also showed reduced collagen production after injury, suggesting defective injury response. We compared the transcriptome of these two groups at homeostasis without surgery. Interestingly, interferon responding genes and genes associated with T cell activation were decreased, suggesting common cross-talk between fibroblasts and immune cells at resting condition. To be noted, these *Lats1/2* mutant fibroblasts exhibited pronounced Myc expression, which were accompanied with significant apoptosis in surrounding cells, suggesting cell competition between *Lats1/2* mutant cells and neighboring “wild type” cells. Taken together, our study revealed a pivotal role of Lats kinase in heart homeostasis maintenance and injury response.

ACKNOWLEDGEMENTS

I'd like to express my sincere appreciation to the following persons who made my research and Ph.D. study possible:

My mentor Dr. James F. Martin set an example of a good scientist for me since my first day of rotation in this lab. He provided me an extraordinary platform to conduct cardiac research, collaborative environment to learn new things from other labs and precious opportunities to attend national and international meetings. He trained me to be an independent and innovative scientist by giving me the freedom to try new things, to explore cutting-edge techniques. All of these are the extremely valuable experience for my future career as well as my life.

Interaction with Dr. Ali J. Marian as one of my committee members provided me with excellent opportunities to grow as a scientist. He offered valuable advice for my research, grants and career plan.

My committee members, Dr. Fen Wang, and Dr. Richard R. Behringer spent plenty of time for my committee meeting and asked insightful questions to urge me to think more. They wrote me great letters for my grant and job application.

Dr. Yun Huang agreed to attend my dissertation defense to substitute Dr. Richard R. Behringer due to latter's conflict schedule. Dr. Yun Huang and our group have close collaboration on the cardiac project and we learned a lot from each other. She also kindly provided her support for my sequencing experiments.

Dr. Joshua D. Wythe offered great help on epicardium project. He provided valuable ideas on vessel imaging and manuscript writing.

My great lab members, Jun Wang, Yan Bai, Yuka Morikawa, Matthew C. Hill, Elzbieta A. Klysik, Thuy Tien Tran, Paul G. Swinton, Min Zhang, Ge Tao, Vaibhav Deshmukh, Chris Hine III, Peter Kahr, Zachary A. Kadow, John P. Leach, Tanner O. Monroe, Thomas Martin, Lele Li, Todd R. Heallen, Bao H. Nguyen, Mahdis Rahmani, Ann Bromley, Idaliz Michelle Martinez-Traverso, Neha Singha, Shijie Liu, Yocheved Schindler, Solange Gonzalez Vazquez, Sandra Mena Gerges Riad, Jong Hwan Kim. The tremendous help from them to make my Ph.D. study possible. Especially Jun Wang and Yan Bai's guidance for my research and personal life. They helped me settle down in the US when I just arrived in Houston from China. Matthew C. Hill, Min Zhang and Thomas Martin invested a great amount of time for NGS analysis, taught me bioinformatics analysis. Those innovative findings cannot be done without their analysis. Matthew C. Hill always discusses with me and offers intriguing and innovative thoughts to my projects. Yuka Morikawa taught me immunostaining which is a valuable tool for my studies. Elzbieta A. Klysik, Thuy Tien Tran, Paul G. Swinton, Ge Tao, Vaibhav Deshmukh, Lele Li, Todd R. Heallen, Bao H. Nguyen, Ann Bromley and Neha Singha they always offer help without any hesitation.

Dr. Marian’s lab members Suet Nee Chen, Raffaella Lombardi, Priyatansh Gurha, Jennifer Karmouch and Evelyn Capadocia. They always kindly provided their research resources and suggested valuable ideas.

My friends Shanshan Gao, Suet Nee Chen, Raffaella Lombardi, Junchen Liu, Li Lai, Yanqing Huang, Yi Liang, Shaohai Fang. They bring so much fun and support to my Ph.D. life. Their company makes me realize I am not alone to fight for what I dream about.

I also want to thank my family, my parents, and grandparents unconditional love and support, which always give me the courage to move forward.

CONTRIBUTORS AND FUNDING SOURCES

Contributors

This work was supervised by dissertation committee consisting of Dr. James F. Martin of Baylor College of Medicine, Dr. Ali.J Marian of University of Texas, Houston, Dr. Fen Wang of Texas A&M Health Science Center, and Dr. Richard R. Behringer of University of Texas, Houston.

The Drop-seq data in Chapter II was analyzed by Matthew C. Hill, Min Zhang, and Thomas Martin of Baylor College of Medicine. Some immunostaining in Chapter II was done by Yuka Morikawa of Texas Heart Institute. The RNA-seq data in Chapter III was analyzed by Min Zhang of Baylor College of Medicine. TRAP-seq in Chapter IV was completed with the help from Vaibhav Deshmukh of Baylor College of Medicine.

All other work for the dissertation was completed by the student independently.

Funding Sources

This work was supported in part by an Intellectual and Developmental Disability Research Center grant (1U54 HD083092) from the Eunice Kennedy Shriver National Institute of Child Health & Human Development; the Mouse Phenotyping Core at Baylor College of Medicine with funding from the National Institutes of Health (U54 HG006348); grants from the National Institutes of Health (DE 023177, HL 127717, HL 130804, and HL 118761 to J.F.M.), the Vivian L. Smith Foundation (to J.F.M.) and transatlantic Network of Excellence Award

LeDucq Foundation Transatlantic Networks of Excellence in Cardiovascular Research 14CVD01: “Defining the genomic topology of atrial fibrillation”

TABLE OF CONTENTS

Page

Page

LIST OF FIGURES

Figure Page

Figure Page

CHAPTER I

INTRODUCTION

Heart disease is the leading cause of death in developed world. Since adult mammalian heart has very limited regeneration ability, heart muscle once damaged is often accompanied with fibrotic scar which results cardiac function decline. Current studies have been searching efficient therapeutics to reverse or alleviate this disease progress from the aspects as follows. Firstly, although adult mammalian heart is considered as a post-mitotic organ, several group have shown that cardiomyocyte indeed undergo slow turnover rate. This observation offered us a great hint of manipulating cardiomyocyte growth to promote heart repair. Secondly, stem cell therapy for other organ has raised a tremendous hope of replenishing functioning cells after injury. The question that whether stem cell exists in adult heart is still debatable. Nonetheless, several cell types, such as epicardial cells, with higher plasticity indeed exert reparative function after heart injury. Thirdly, as the main source of fibrosis after heart insult, cardiac fibroblast has been shown to participate initial adaptive phase to prevent heart rupture as well as the later maladaptive phase of heart remodeling. Studies have demonstrated that either reprogramming fibroblast into cardiomyocyte, or manipulating fibroblast *per se*, can be an exciting path to promote heart repair. Here in our study, we are going to focus on the latter two aspects.

Hippo signaling is an ancient signaling pathway controlling organ size through modulating cell proliferation and differentiation. Its components include ste-20 family kinases Mst1 and Mst2 (Mst1/2), which complex with the scaffold adaptor protein Salvador (Salv) to phosphorylate the nuclear dbf2-related (NDR) family kinases Lats1 and Lats2 (Lats1/2). Yap and Taz, the Hippo pathway effectors, are transcriptional co-factors that are substrates for Lats1/2 kinases. Upon phosphorylation by Lats1/2 kinases, Yap and Taz are excluded from the nucleus and their transcriptional activity is inhibited. Work from our lab revealed that removing Hippo pathway components in the embryonic or adult myocardium releases the downstream effector Yap from Hippo-dependent suppression, promoting cardiomyocyte proliferation and tissue regeneration (1-3).

CHAPTER II

SINGLE CELL TRANSCRIPTOMICS REVEAL AN ESSENTIAL ROLE FOR HIPPO SIGNALING IN CELL STATE TRANSITIONS DURING CARDIAC FIBROBLAST DEVELOPMENT

Introduction

Embryonic epicardium originates from pro-epicardium. At mouse embryonic day (E)9.5, proepicardial cells attach to myocardium and spread as a continuous epithelial sheet over the myocardium. A subset of epicardial cells delaminate from the epicardium, undergo epithelial mesenchymal transition, and generate EPDC (4). Although epicardial cells are quiescent in the adult, they are activated upon injury and contribute to the repair process in part by modulating the inflammatory response. The activated epicardium post-injury expresses many developmental genes indicating that developmental programs are reactivated after injury in the adult heart (5,6). This reactivation of developmental programs has considerable clinical significance since the adult epicardium is also the source of pro-inflammatory signals that regulate the amount of fibrosis after myocardial infarction.

During heart development, subset of epicardial cells delaminate from the epicardium, undergo epithelial to mesenchymal transition (EMT) and generate epicardial-derived cells (EPDCs). EPDCs first populate the subepicardial space between epicardium and myocardium, forming the subepicardial mesenchyme, and then invade the myocardium where they differentiate into the essential

supporting cells of the heart (4). In mammals, EPDCs derived from the Wt1-expressing lineage primarily give rise to vascular smooth muscle cells and fibroblasts, two supporting cell types that are important for coronary vascular and myocardial development.

The Hippo signaling pathway is a conserved organ size control pathway that inhibits cell proliferation and promotes apoptosis (7). Work from our lab revealed that removing Hippo pathway components in the embryonic or adult myocardium releases the downstream effector Yap from Hippo-dependent suppression, promoting cardiomyocyte proliferation and tissue regeneration (1-3).

Here, we used single cell transcriptomics to investigate *Lats1/2* function in epicardial progenitor cell diversification. A high-throughput single cell (sc) RNA-sequence (seq) platform, Drop-seq, was adopted for the first time to characterize E13.5 and E14.5 cardiac cellular composition and heterogeneity at high resolution in *Lats1/2* deficient and control hearts (8). Importantly, our data revealed that Lats1/2 activity is required for EPDC progression from a transient subepicardial mesenchymal phenotype to a fully differentiated cardiac fibroblast identity.

Materials and Methods

Mice

Wt1^{CreERT2} (9), *Lats1/2*$^{flox/flox}$ (3), *Yap/Taz* $^{flox/flox}$(10),*Rosa26*^{mTmG} (11) alleles have been described previously. Mice were on a mixed genetic background of C57BL/6 and 129SV. Tamoxifen was dissolved in peanut oil with 5% ethanol at

10mg/ml. For *Wt1*^{CreERT2}, 0.1mg/g body weight tamoxifen was administrated to plugged female by intraperitoneal injection at embryonic (E) day 11.5.

Cell preparation and Drop-seq workflow

Atria were removed prior to single cell suspension preparation, droplet generation, cDNA amplification, and library preparation. Following sequencing of Drop-seq libraries, a minimum gene per cell threshold of 500 was set for inclusion into the data set resulting in a final digital gene expression matrix with a median of 1,005 genes per cell and 1,500 Unique Molecular Identifiers (UMI) per cell (Fig. S2A). Batch effects were corrected for and principle components analysis was carried out. Cells were dissociated as previously described (12). Hearts were chopped into several pieces and digested by 1mg/ml collagenase I for 20 min at 37°C. Every 10min, the sample was gently pipetted sample up and down to mechanically dissociate the cells. 10% FBS in DMEM was applied to quench the protease, and samples were passed through a 100μm strainer. Following tissue dissociation cells were diluted to a concentration of 150,000 cells/mL in PBS with 0.1% BSA. Next, Drop-seq was performed according to Macosko et. al (8). Briefly, cells were co-encapsulated into nano-liter sized droplets containing barcoded microparticles (ChemGenes, catalog number Macosko201110) and lysis buffer using a Drop-seq specific microfluidics device (custom made by FlowJEM, Toronto, Canada). After droplet breakage, reverse transcription, and exonuclease treatment, total cDNA was amplified, pooled, and purified with Ampure XP beads and then quality control, quantification and size determination was performed

using a Fragment analyzer (Advanced Analytical Technologies, Inc.) for quality control, quantification, and size determination. Tagmentation and library preparation was performed with the Illumina Nextera XT kit. Final libraries were triple purified with a successive Ampure XP based protocol, whereby two successive 0.6X (beads to sample ratio) purifications were performed, followed by a final 1X purification step. All libraries were sequenced on an Illumina Nextseq500 instrument.

Drop-seq data analysis

Sequencing data was processed as described in *Shekhar* et. al. (2016) (8,13). Briefly, raw fastq files were converted to BAMs with Picard tools (MergeSamFiles) and then used as input for STAR alignment (14), cell barcode correction, and digital gene expression (DGE) matrix generation via the Drop-seq tools software package (available at http://mccarrolllab.com/dropseq/). Next, DGEs from each experiment were merged. We then imported the comprehensive DGE into Seurat (version 1.4.0.5) where normalization was performed according to package default settings (15). Batch effects were corrected for with the application of Combat, from the R SVA package (version 3.18.0), and by further regressing out the number of molecules per cell and the percentage of mapped mitochondrial reads with the RegressOut function (Seurat package) (16). Next, principle components analysis was performed and significant PCs were used as input for graph-based clustering. Finally, 2-dimesnsional visualization of the multi-dimensional data set was done with tSNE(17). Differential expression of the

various clusters was also performed with Seurat, using the likelihood-ratio test for single cell gene expression (18). For pseudotime analysis, the normalized data from the indicated clusters calculated in Seurat was then passed directly into Monocle2 (19). The Monocle2 branched expression analysis modeling (BEAM) statistical test was utilized to isolate the branch-specific gene expression patterns (256 genes with qval <0.1). Motif enrichment analysis was carried out with the Cytoscape plug-in iRegulon using the mouse genome's default parameters (20). All gene ontology (GO) analysis was performed with the Metascape tool (http://metascape.org) (21).

Histology, immunofluorescence, and RNA in situ hybridization

Epicardium-restricted-*Lats1/2* mutant embryos (*Lats1/2* CKO) were generated by crossing $Wt1^{CreERT2}$ with $Lats1/2^{flox/flox}$ or $Lats1/2^{flox/flox}$; $Rosa26^{mTmG}$. Control embryos were generated by crossing $Wt1^{CreERT2}$ with $Rosa26^{mTmG}$ or Cre negative littermate control. For H&E staining and immunofluorescence staining, hearts were fixed in 4% PFA overnight at 4°C and dehydrated in a serial ethanol, xylene and embedded in paraffin. Sections of 7μm thick sections were stained with H&E for histological analyses (22). For some immunofluorescence staining, cryosections were used. Antibodies used for immunofluorescence staining were as follows: GFP(1:200, Abcam ab290, ab6673), phospho-YAP (1:200, Cell signaling technology,4911), Yap(1:200, Novus NB110-583538), PECAM-1(1:100-1:200, BD Pharmingen 550274), Vimentin (1:200, Abcam, ab92547), Wt1(1:200, Abcam, ab89901), Podoplanin (1:200, Developmental Studies Hybridoma Bank,

8.1.1) , α -actinin (1:200, Abcam, ab68687), Collagen I (1:200, Abcam, ab21286), Dpp4 (1:100, Biolegend, H194-112). To visualize some antigens, Alexa-647 was employed. When applications required green and red co-staining, sections were pre-treated with 0.3% H_2O_2 in PBS for 20min at room temperature to quench the endogenous GFP and Tomato signals, which come from the *Rosa26*^{mTmG} reporter line. In some cases, Tyramide Signal Amplification Systems (1:100, Perkin Elmer) were used to amplify signal. PECAM-1 whole mount staining was performed as previously described (Monica Zamora, 2007, (23)). PECAM-1(1:100) staining was followed either by anti-rat-HRP (1:200, Life Technologies, 62-9520) and a DAB kit (Vector lab) for color development or anti-rat-Alexa-647 (1:200, Thermo Fisher Scientific) for immunofluorescence staining. The vessel pattern was quantified by Angiotool. The tissues for RNA in situ hybridization were prepared as described above except adding Diethylpyrocarbonate (DEPC) was added to avoid RNAse contamination. RNA in situ hybridization was performed by the RNA In Situ Hybridization Core at Baylor College of Medicine. The *Twist1*(24) and *Snai2*(25) probes were previously described. Gross heart images were captured by Zeiss SteREO Discovery.V12 microscope. Histology and RNA In Situ images were captured by Nikon Eclipse 80i microscope. Immunofluorescence images were captured on a Leica TCS SP5 confocal microscope, a Zeiss LSM 780 confocal microscope or Nikon A1-Rs inverted laser scanning microscope. Sample size labels on the corresponding bar graph indicate the number of hearts being

analyzed, otherwise n=3 in all groups. Three fields of views were analyzed in each heart.

EdU incorporation assay

To study cell proliferation, pregnant females were injected with 0.08mg/g body weight EdU 2hr before harvesting embryos. Hearts were processed as described above. EdU incorporation was assayed using the Click-it EdU imaging kit (Life Technologies).

FACS analysis

Cells were dissociated as previously described in the method section of "Cell preparation and Drop-seq workflow". Antibodies used for flowcytometry were: PDGFRα (BD Bioscience 562774), isotype conjugated with BV421 (BD Bioscience 562602). Cells were analyzed using BD Biosciences CORP Aria I and BD Biosciences LSRII and images were processed with FlowJo software.

Motif analysis and ChIP-q-PCR

Gene regulatory region information was extracted from GEO database: E14.5 H3K27ac (GSM1264374), P0 H3K27ac (GSM1264378) and Heart DHS (GSM1014166). TEAD motif was analyzed by Homer. Chromatin immunoprecipitation was performed with an anti-Yap antibody (Novus NB110-58358) in the MEC1 epicardial cell line (26). Three biological replicates were included in each group. The primers used for detecting TEAD binding region at *Dhrs3* and *Dpp4* are:

Dpp4 site1-Forward 5'- GGAGGAAGATTATGCACAACAAC -3';

Dpp4 site1-Reserve 5'- TGTGGAGACATGAAAGACTAAGG -3';

Dpp4 site2-Forward 5'- GGAGCTCATGAATGCCTGATT -3';

Dpp4 site2-Reserve 5'- CTGCAGAAGAACTGTGCTCTTA -3';

Dhrs3-Forward 5'- CCTACCCACACAAGACATCAA -3';

Results

Epicardial deletion of *Lats1/2* results in defective coronary vessel development and embryonic lethality

We deleted *Lats1/2* in epicardium at E11.5 using the $Wt1^{CreERT2}$ allele. *Lats1/2* conditional knock out (CKO) embryos were embryonic lethal and failed to survive past E15.5 (Fig. 2.1A). At E14.5, gross morphology and histology revealed that *Lats1/2* CKO hearts appeared normal, but at E15.5 mutant hearts were smaller, with less compacted myocardium (Fig. 2.1 B-D). In addition to these cardiac defects, mutant embryos displayed severe surface hemorrhages, as well as, herniated livers and intestines (Fig. 2.1E-G).

E14.5 to E15.5 is a critical developmental window for coronary vessel morphogenesis, as the initial vascular plexus remodels to meet the increased oxygen demands of the expanding ventricular wall. We examined overall vessel patterning by whole-mount PECAM-1 immunostaining at E14.5. In *Lats1/2* CKO embryos compared to controls, the coronary vasculature was disorganized with reduced vessel coverage and decreased density (Fig. 2.2 B). PECAM-1 immunofluorescence (IF) staining with confocal microscopy revealed that the dorsal vasculature exhibited decreased branching (Fig. 2.2 C). Automated

quantification also indicated reduced vessel coverage with fewer junctions and increased lacunarity (Fig.2.2 D).

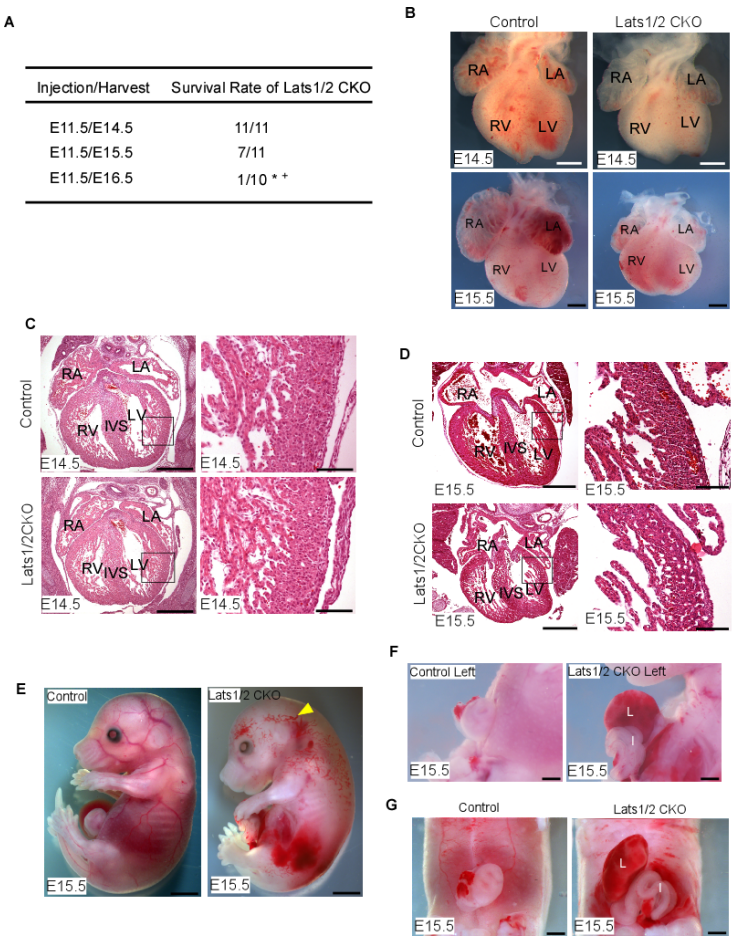

Fig. 2.1 Knocking out *Lats1/2* leads to embryonic lethality at E15.5. (A) Activity of Cre was induced at E11.5 by tamoxifen injection. *Lats1/2* CKO survival rate was determined at different harvest time series. **P* <0.001 between E16.5 and E14.5, Fisher's exact test. $^{+}$*P* <0.05 between E16.5 and E15.5, Fisher's exact test. (B-D) Gross heart morphology and H&E stained sections from at E14.5 and E15.5. (E-G) Non-cardiac defects in *Lats1/2* CKO at E15.5, including hemorrhage (yellow arrowheads) and herniated liver (L) and intestine (I). Scale bar: B 400μm; C left panel 400 μm; right panel 80 μm; D left panel 500 μm; right panel 100 μm; E 2000μm; F-G 1000μm.

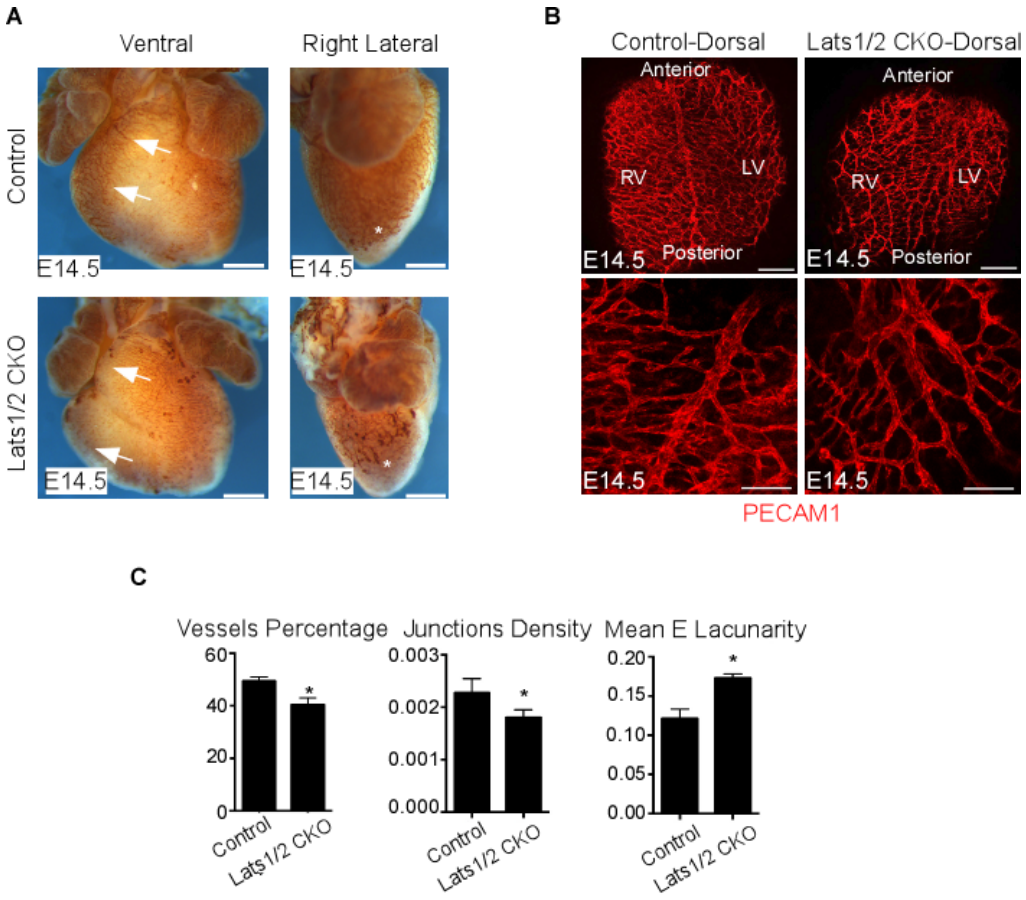

Fig. 2.2 Knocking out *Lats1/2* leads to coronary vessel defects. (A) Coronary vessels were visualized by PECAM-1 whole-mount staining at E14.5. *Lats1/2* CKO hearts exhibited decreased vessel coverage (arrows) and disorganized vessel patterning (asterisks) on ventral and lateral side of the heart. (B) PECAM-1 immunofluorescent whole-mount staining. *Lats1/2 CKO* exhibited malformed coronary vessel patterning. (C) Quantitative analysis of vasculature in B (n=3 in each group). Data shown are means ± SD. $p<0.1$ was by Mann-Whitney U test. A 500μm; B upper panels 200μm, bottom panels 100μm. RV: right ventricle; LV: left ventricle;

To exclude the possibility that *Wt1*^{CreERT2} heterozygosity contributed to the vascular phenotype, we injected tamoxifen to *Wt1*^{CreERT2} /+ embryos and Cre negative littermates to compare the coronary vessel phenotype. As another control, we injected vehicle (peanut oil) to *Wt1*^{CreERT2}; *Lats1/2* $^{f/f}$ and their Cre negative littermates to compare coronary vessel phenotype. In both of these controls, coronary vessel development was normal (Fig. 2.3 A,B).

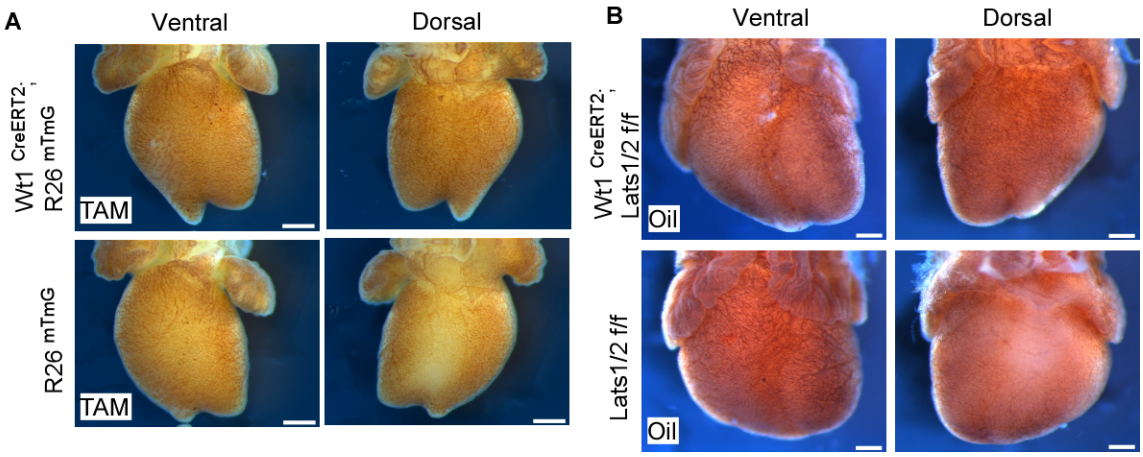

Figure 2.3. Control experiments to validate coronary vessel development defects in *Lats1/2* CKO.(A)*Wt1* $^{CreERT2/+}$; *Rosa26* ^{mTmG} injected with Tamoxifen (TAM) exhibited well-formed coronary vasculature compared with *Rosa26* ^{mTmG} littermate at E14.5. (B) *Wt1* $^{CreERT2/+}$; *Lats1/2* $^{f/f}$ hearts exhibited organized coronary vessel injected with vehicle control peanut oil compared with *Lats1/2* $^{f/f}$ littermate at E15.0. Scale bar: 400μm.

Next, we examined Yap sub-cellular localization and Yap phosphorylation (p-Yap) and as a readout of Lats kinase activity in *Lats1/2* CKO and control embryos. Yap localization in *Lats1/2* CKO hearts, detected by total Yap IF and co-labeling with podoplanin, revealed increased nuclear Yap in both epicardium and subepicardium of *Lats1/2* CKO hearts (Fig. 2.4 A-B). p-Yap IF revealed decreased p-Yap in *Lats1/2* CKO epicardium and subepicardium as compared to control hearts (Fig. 2.4 C). We noted that podoplanin, while restricted to the epicardium in control embryos, was also expressed in subepicardium in *Lats1/2* CKO embryos suggesting that EMT occurred prior to repression of epicardial gene program (Fig.2.4C). To determine if Yap function was required for the *Lats1/2* CKO mutant vascular phenotype, we performed a genetic suppression experiment by genetically reducing endogenous *Yap* and *Taz* levels in *Lats1/2* CKO embryos. We generated $Wt1^{CreERT2}$; $Lats1/2^{f/f;}$ $Yap/Taz^{f/+}$ embryos and induced Cre activity at E11.5. All compound mutant embryos were viable at E15.5, although the herniated liver and intestinal phenotypes persisted (data not shown). The morphology of $Wt1^{CreERT2}$; $Lats1/2^{f/f}$; $Yap/Taz^{f/+}$ hearts appeared to be similar to the Cre negative littermate controls, with no evidence of major coronary vasculature defects (Fig. 2.4 D-E).

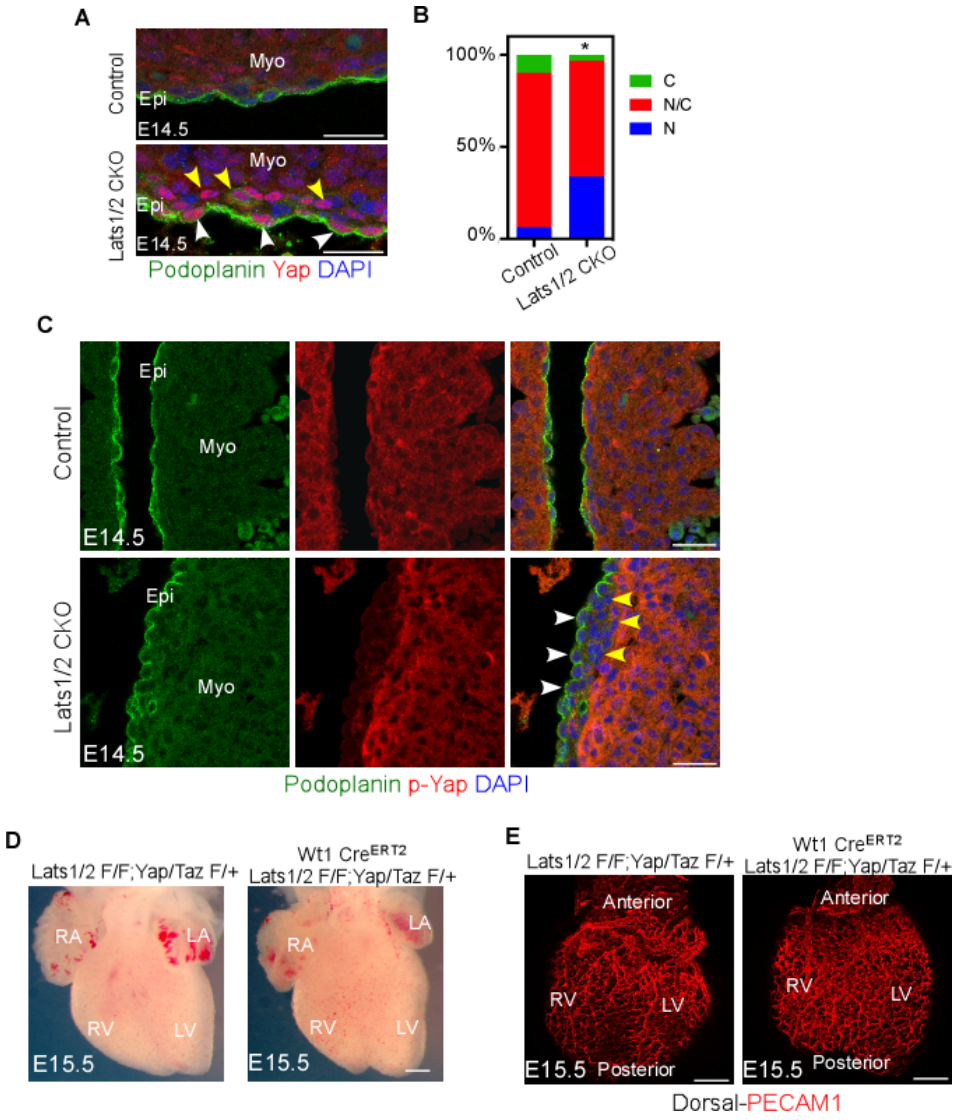

Figure 2.4. Reducing Yap/Taz activity rescues the phenotype resulted from *Lats1/2* deficiency.(A) Podoplanin labels the epicardium and *Lats1/2 CKO* hearts show increased nuclear Yap localization in the epicardium (white arrows) and subepicardium(yellow arrows). (B) Quantification of Yap cellular localization. Data shown are means ± SD. p<0.1 Nuclear Yap percentage (%) was by Mann-Whitney U test. (C) Phosphorylation status of YAP (p-YAP) is a direct readout for Lats1/2 activity. *Lats1/2* CKO showed decreased p-Yap in epicardium (white arrows) and subepicardial region (yellow arrows). (D-E) *Lats1/2 CKO* hearts with reduced Yap/Taz activity appeared to be normal at E15.5 compared to their littermate controls. A 25μm; C 25μm, D 400μm,E 200μm. Scale bar: LA: left atrium; RA: right atrium; LV: left ventricle; IVS: interventricular septum. RV: right ventricle; LV: left ventricle; N: Nuclear Yap; N/C Nuclear/Cytoplasmic Yap; C: Cytoplasmic Yap; Epi: epicardium; Myo: myocardium.

Recent work indicated that deletion of *Yap* and its paralog *Taz* in the epicardium led to defective EMT and reduction of epicardial-derived lineages (27). We performed *in situ* hybridization to examine EMT marker expression. Expression of a canonical EMT regulator, the gene encoding the zinc finger transcription factor *Snai2* was elevated in the mutant hearts, while another EMT marker,*Twist1,* was unchanged (Fig.2.5). These results suggest that Lats1/2 kinases are required for normal coronary vessel development by restricting epicardial and subepicardial Yap activity.

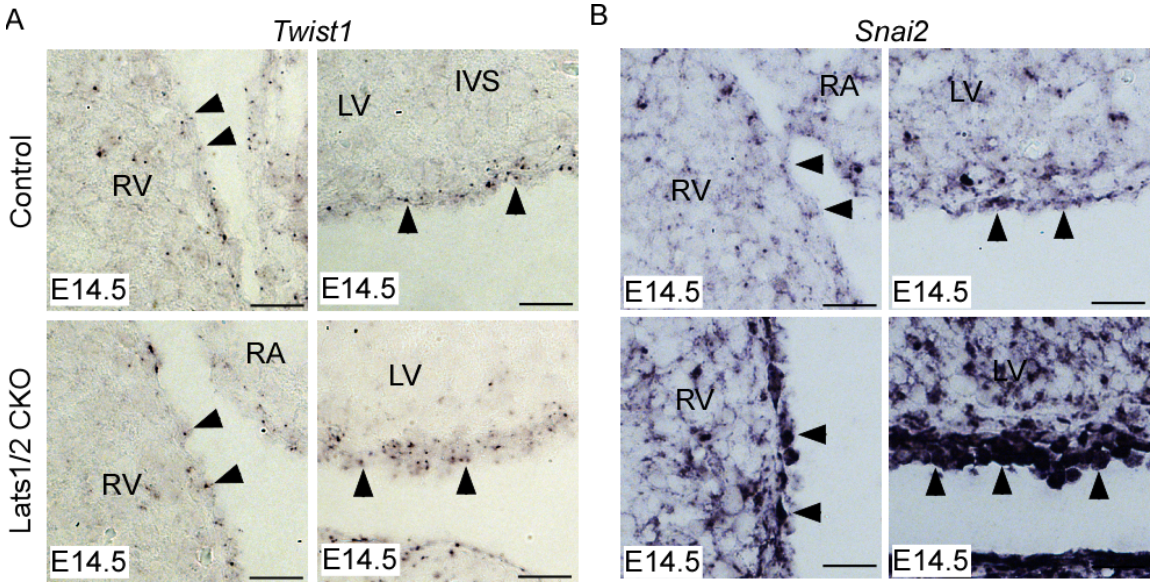

Figure 2.5 EMT factors expression in epicardium and EPDC. EMT factors *Twist1* and *Snai2* detected by *in situ* probe at E14.5. Scale bar: 25 μm.

Unbiased single-cell transcriptome profiling of embryonic cardiac tissue at E13.5 and E14.5

To simultaneously capture the cellular states of all cardiac cell types in control and *Lats1/2* mutants, we performed Drop-seq to profile cardiac tissue from control and *Lats1/2* CKO embryos at E13.5 and E14.5, the stages preceding *Lats1/2* CKO embryonic lethality. Graph based clustering was performed on significant principle components and the results visualized through the non-linear dimensional reduction algorithm, t-Disributed Stochastic Neighbor Embedding (tSNE) (8,17,28-30). Embedding 18,166 single cells across two time points and two genotypes into the final projection that revealed 28 distinct clusters (Fig. 2.6 A,B). Differential expression analysis on spatially proximal clusters was carried out to identify transcriptionally well-defined clusters. Clusters without appreciable transcriptional distinctions were merged and classified based on the expression of known markers (Fig. 2.6 C).

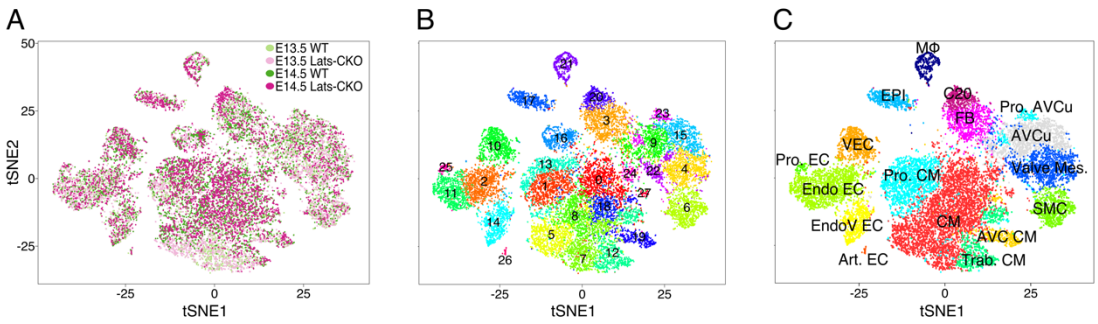

Figure 2.6. High-throughput single cell RNA-seq of wild type and *Lats1/2* CKO embryonic cardiac tissue. (A) two-dimensional tSNE representation of 18,757 single-cell transcriptomes colored by experimental group. (B) tSNE visualization of graph-based clustering carried out on the comprehensive embryonic mutant and non-mutant dataset. (C) Classification and merging of clusters shown in Figure 2B. Red blood cells and platelets, cluster 16, are removed.

The main cardiac cell types, including cardiomyocytes, endothelial cells, smooth muscle cells, mesenchymal cells, macrophages, and epicardial cells had cluster sizes in the range of 63 to 4,716 cells (Fig. 2.7 B). We first evaluated non-epicardial-derived lineage, specifically cardiomyocytes and endothelial cells. A comprehensive analysis of E13.5-E14.5 heart tissue, excluding the atria, revealed a cellular composition that is distinct from adult murine cardiac tissue (Fig. 2.7 B). Adult cardiac tissue is made up of approximately 31% cardiomyocytes and 43% endothelial cells (Pinto et al., 2016). Our results indicated that the E13.5-E14.5 murine heart contains 43% cardiomyocytes and only 19% endothelial cells.

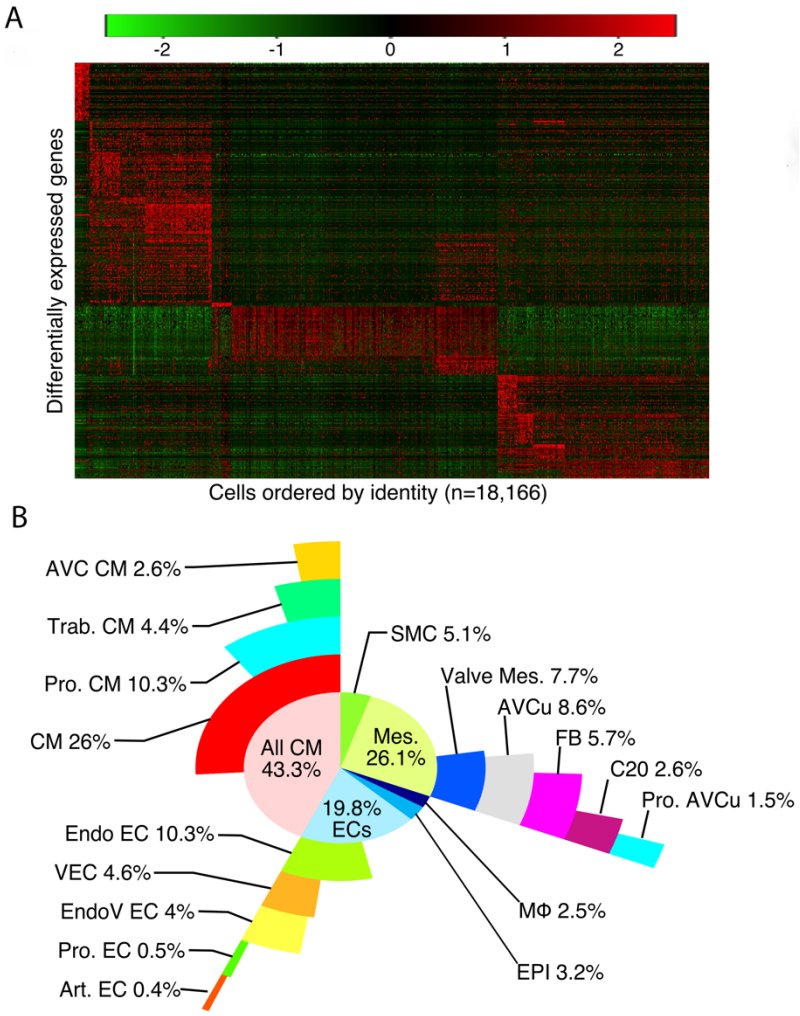

Figure 2.7. Cell type composition of wild type and *Lats1/2* CKO embryonic cardiac tissue at E13.5 and E14.5. (A) Heatmap of differentially expressed genes (rows) across the final 18,166 cells (columns). (B) Sunburst plot of E13.5-E14.5 cardiac cell composition as determined by Drop-seq.

Importantly, these cardiac cell types displayed considerable heterogeneity and were further sub-categorized (Fig. 2.8). Within the cardiomyocyte lineage, the two rarest cardiomyocyte populations were atrioventricular canal (AVC) and trabecular cardiomyocytes. AVC cardiomyocytes were identified based on a molecular signature that included the Wnt-pathway gene Rspo3 and the Bmp-pathway gene Bmp2 (Fig. 2.8, Fig. 2.9) (Cambier et al., 2014). Trabecular cardiomyocytes were identified by a signature that included Nppa and Gja5 (Fig. 2.8, Fig. 2.9)(Jensen et al., 2012). In addition to Bmp2, we detected several other AVC cardiomyocyte markers, including Pitx2, Shox2, Wisp1, Tbx2, Tbx3, Tbx5, and Bmp7 (Campione et al., 2001; Habets et al., 2002) (Fig. 2.9). Further clustering revealed several known and novel cardiomyocyte markers, as well as, transcriptional signatures of proliferating cardiomyocytes (Fig. 2.9) (Li et al., 2016).

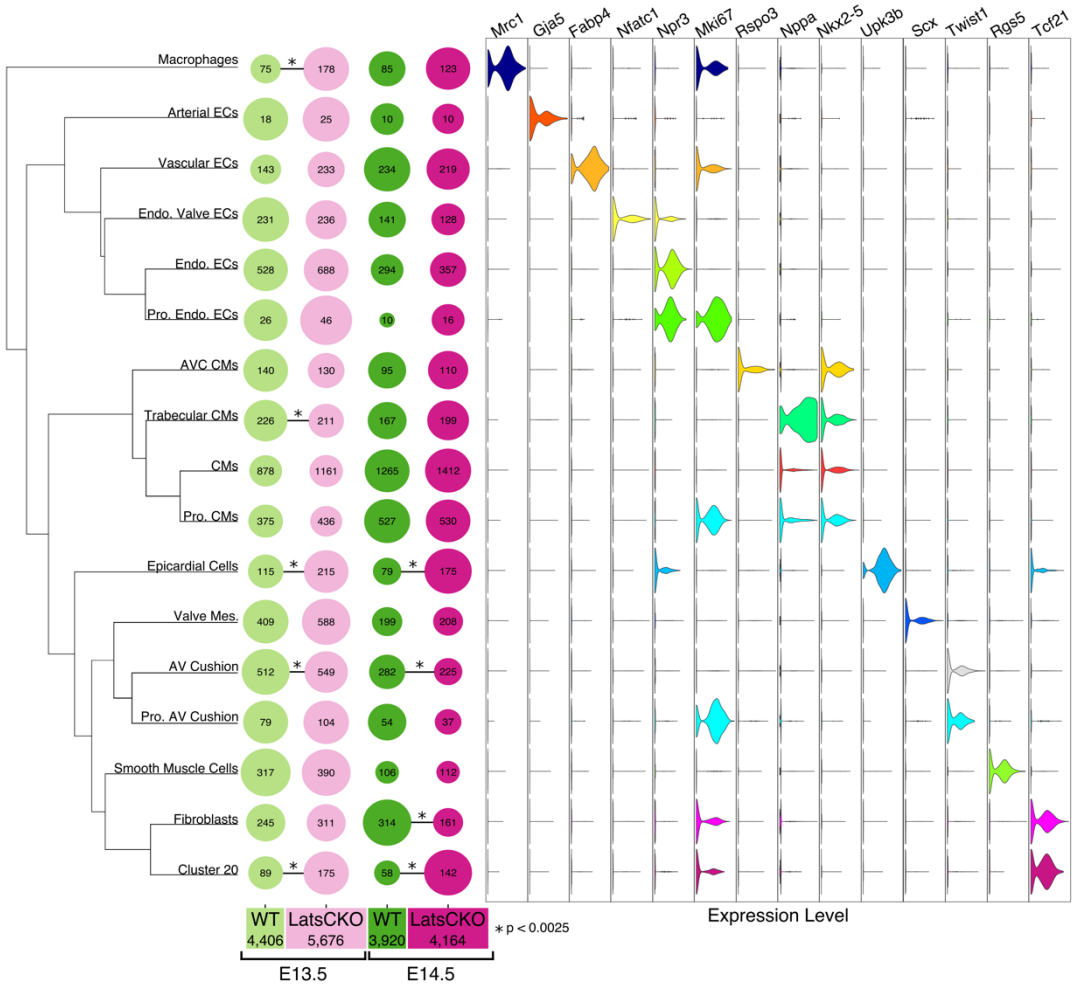

Figure 2.8 *Lats1/2* CKO and wild type (WT) single-cell composition for individual cluster categories. Phylogenetic tree showing the relationship of each identified cell type based on 3,217 appreciably expressed genes with high dispersion (> 2 standard deviations above average dispersion) (left). Dot plot showing the relative proportion of cells belonging to each genotype across E13.5 and E14.5 time points colored according to Figure 2A. The size of the dots represents the percentage of cells within each identity class. Numbers on the dots are the actual cell numbers in the corresponding cluster and the numbers below each genotype are the total cell numbers we analyzed in each experimental group (middle, Chi-squared analysis, * p-value < 0.0025). Violin plot of gene expression for representative markers of each categorical class colored according to Figure 2.6C(right).

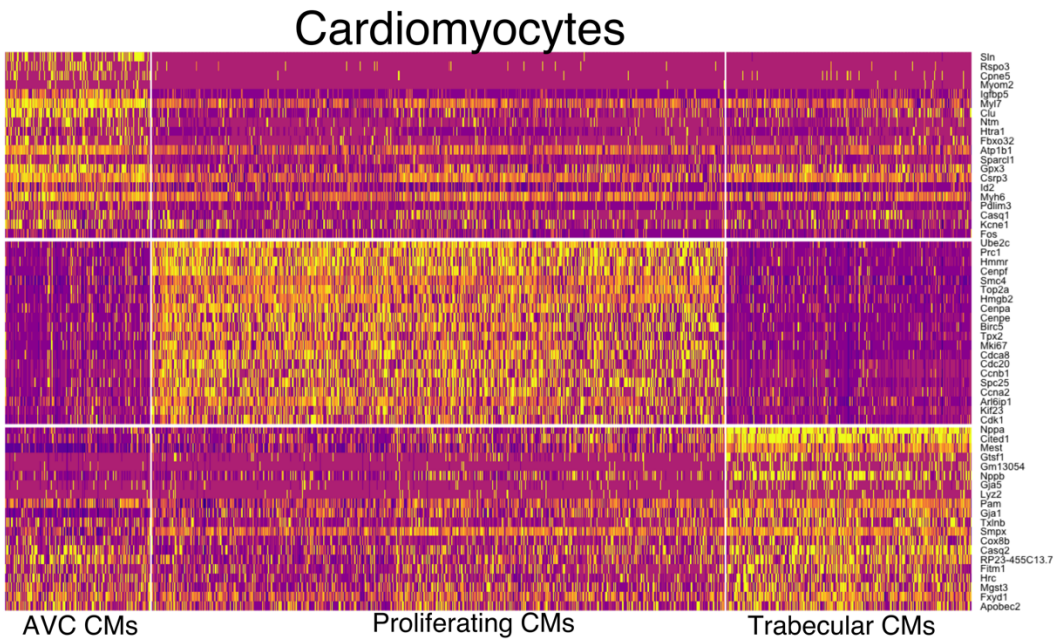

Figure 2.9 Cardiomyocyte subclusters at E14.5. Heatmap of top differentially expressed genes among rare cardiomyocyte cell populations. Highly expressed genes are shown as yellow/orange.

Endothelial cells, well represented in our data set, comprised a total of 5 clusters. Arterial endothelial cells were distinguished by several markers, including Gja5, Fbln2, Fbln5, and Sox17 (Fig. 2.7B, Fig.2.8 and Fig. 2.10) (Liu et al., 2015). Vascular endothelial cells were clearly distinguishable by Fabp4 and Apln expression (Fig. 2.10) (He et al., 2014; Liu et al., 2015). Endocardial cells were characterized by high level of Npr3 (Zhang et al., 2016) in addition to other, previously unknown markers including Ednrb, Adgrg6, Plvap, and Smoc1 (Fig. 2.10). This comprehensive and novel characterization of endothelial cell

heterogeneity in the developing heart may reflect the distinct cellular origins of endothelial cells and their unique functions although this possibility will require further investigation.

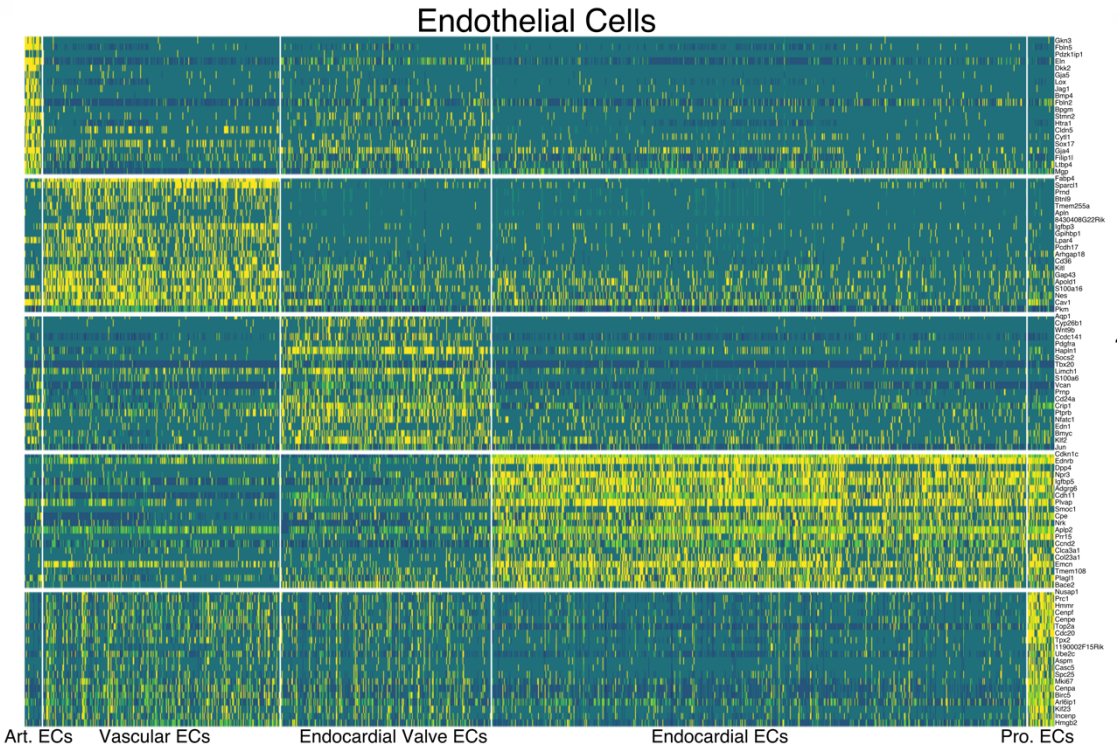

Figure 2.10 Endothelial cell subclusters at E14.5. Heatmap displaying the top differentially expressed genes across all endothelial-like cells. Highly expressed genes are yellow.

Our data revealed several cell types with critical roles in valve development. We performed graph base clustering and tSNE visualization of the valve data subset (Fig. 2.1G and Fig. 2.2D) including Scx-positive valve mesenchymal cells, Twist1-positive atrioventricular valve and cushion cells, Bmp2-positive AVC cardiomyocytes, and Nfatc1-positive valve endocardial cells (Fig. 2.1F) (Chakraborty et al., 2008; Gong et al., 2014; Katz et al., 2012; Ma et al., 2005; Wu et al., 2011). We found AV cushion mesenchymal cells expressed Wnt-pathway genes Lef1 and Tbx20 while valve mesenchyme expressed Sfrp2 and Dkk3 (Fig. 2.1 H, Fig. 2.2 D) (Cai et al., 2013).

Interestingly, we discovered three distinct clusters of Nfatc1 positive cells (EndoV1-EndoV3) revealing a previously unappreciated heterogeneity within the valvular endocardium, including the EndoV3 cluster that displayed high expression of endocardial-to-mesenchymal transition (EMT) associated genes Enpp2, Prox1, and Fzd10 (Fig. 2.1 G,H) (Gong et al., 2014; Lu et al., 2012; Shaul et al., 2014). The heterogeneity of valve endocardial cells may be the result of dynamic cellular phenotypic changes during EMT. We also noted heterogeneous expression across these endocardial valve clusters of different aquaporin (AQPs) family genes (e.g. Aqp8 and Aqp1). AQP genes, encoding water channel proteins controlling cellular osmotic balance, have not previously been implicated in valve endocardial development (Fig. 2.2 C, D). Due to their potential roles in osmotic stress, for example after ischemia-reperfusion (Au et al., 2004), AQPs may be interesting targets for future studies.

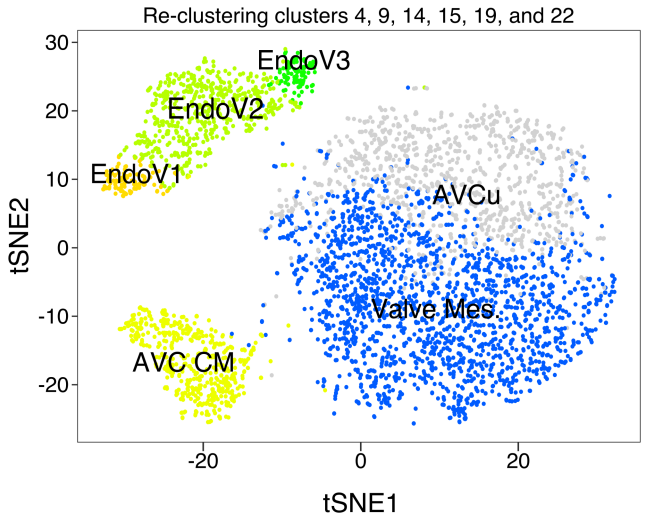

Figure 2.11. Clustering and tSNE visualization of 4,183 cells implicated in valvulogenesis.

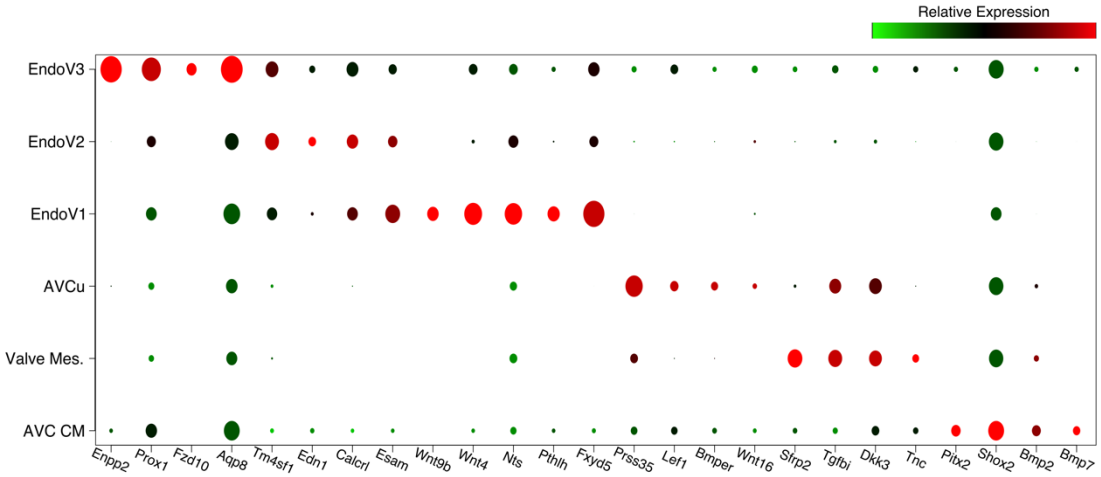

Figure 2.12. Single-cell markers of cardiac valve development. The relative expression levels of each gene (column) are shown as dots for each of the 6 cardiac valve clusters identified in Figure 2.8.

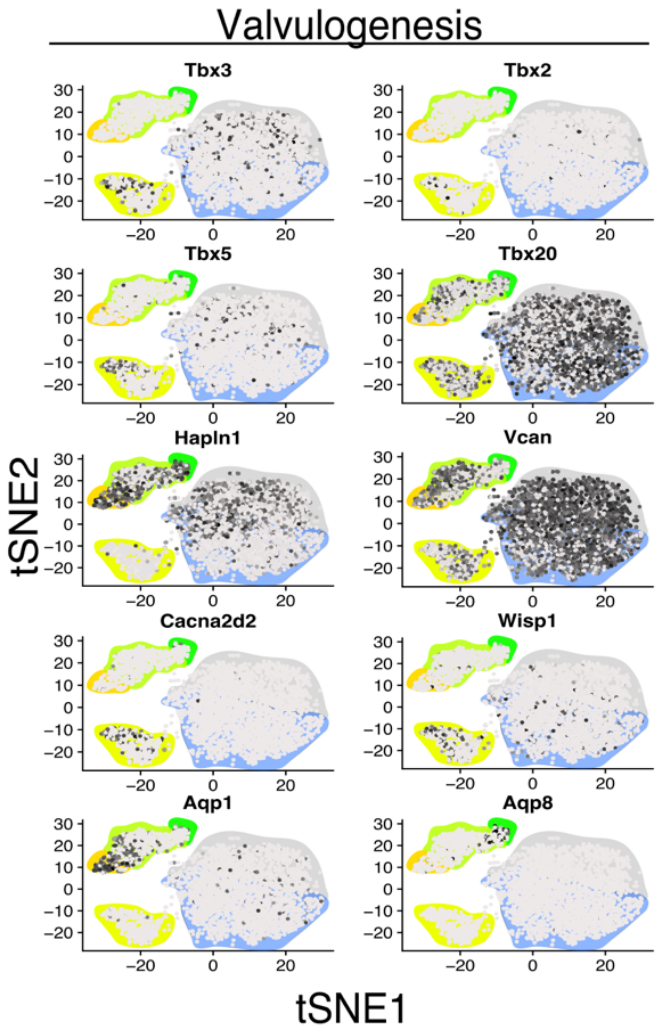

Figure 2.13 Feature expression plots of the classic, as well as some novel genes expressed during valvulogenesis. Gene expression is indicated by dark black, and the background color indicates the cluster/cellular identity shown in Figure 2.11.

Identification of an epicardial-derived cell population composed primarily of *Lats1/2* deficient cells

To investigate the molecular changes resulting from loss of epicardial Lats1/2 kinase function, we compared the relative proportions of each cell type between control and *Lats1/2* mutant hearts (Fig. 2.8). Although we saw differences in a few non-epicardial-derived cell types, such as macrophages and trabeculated myocardium, for this study we focused our attention on the epicardial lineage. Two clusters showed statistically significant enrichment of *Lats1/2* mutant cells compared to control (chi-squared test, $p < 0.0025$). One of these was the epicardial cluster, which suggests increased proliferation and self-renewal or defective differentiation of the *Lats1/2* mutant epicardium. The second predominantly mutant cluster, designated as Cluster 20 (C20), possessed a gene signature intermediate between that of fibroblasts and epicardium. C20 cells expressed *Tcf21*, a gene encoding a basic helix loop helix transcription factor whose expression demarcates epicardial cells committed to the cardiac fibroblast lineage and resting cardiac fibroblasts (Fig. 2.8) (31). We also observed a reduction in the number of cardiac fibroblasts in E14.5 mutant hearts, suggesting a defect in epicardial to fibroblast transition (Fig. 2.8). There was no difference in the smooth muscle lineage, the other major EPDC-derived cell type, between control and *Lats1/2* mutant hearts (Fig. 2.8).

To further determine the transcriptional distinctions between C20, epicardial cells, and cardiac fibroblasts, we performed iterative clustering. We

included vascular endothelial cells (VECs) in our analysis given the defective coronary vessel phenotype. Cell barcodes were selected from each cell type and deposited into a new digital expression matrix prior to principle component analysis (PCA), graph based clustering, and tSNE visualization. We evaluated these cell types and performed differential expression analysis (likelihood-ratio test for single cell gene expression (18) (Fig. 2.14). In addition to the original four clusters, iterative clustering identified a clearly distinguishable fibroblast-like sub-type, FB2, which closely resembles pericytes as it is positive for *Mcam*, *Cspg4* (*Ng2*), and *Pdgfrb* (Fig. 2.15).

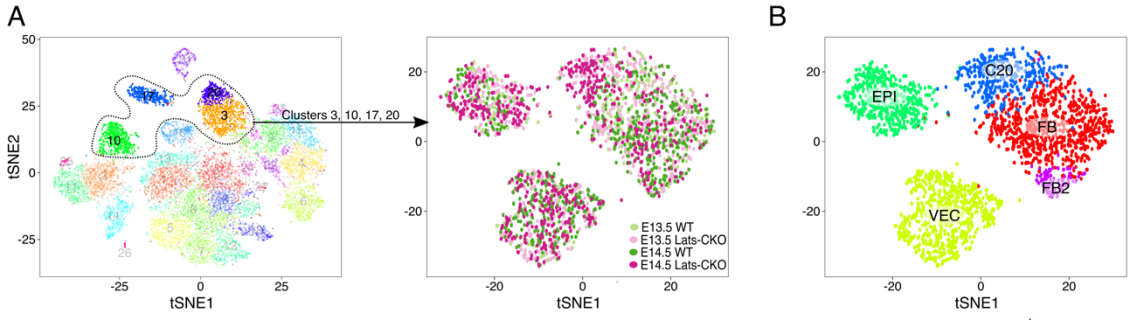

Figure 2.14. Subsetting and clustering of epicardial and putative epicardial-derived cells. (A)(Right) View of experimental identity for each single-cell in the data, colored as in Fig. 2.6A. (B) tSNE plot of *Lats1/2* CKO enriched clusters. Epicardial cells (EPI), fibroblasts (FB), cluster number 20 (C20), vascular endothelial cells (VEC), and fibroblast cluster 2 (FB2) which resemble pericytes.

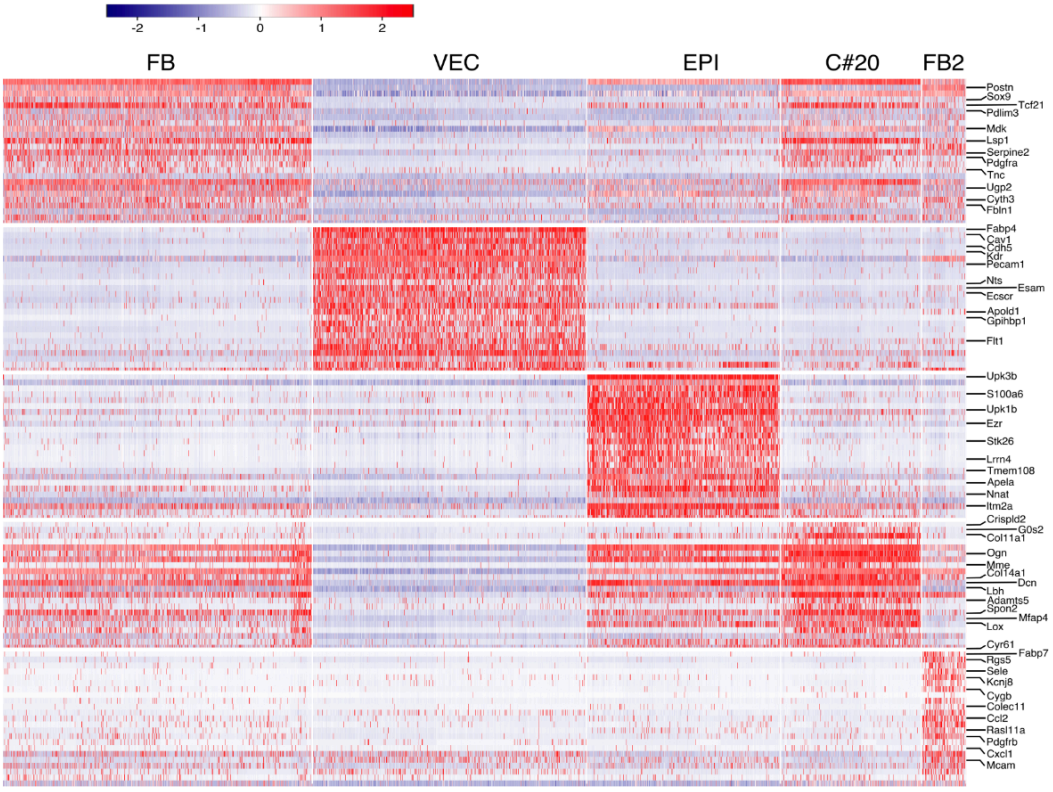

Figure 2.15. Heatmap of differentially expressed genes from FB, VEC, EPI, C20, and FB2 clusters. Rows are genes and columns represent single-cells. Red indicates high relative expression.

The C20 transcriptional signature resembled that of fibroblasts, while sharing epicardial features, but it was distinct from VECs (Fig. 2.15). C20 cells expressed a subset of fibroblast markers such as *Col1a1* and *Spon2*, yet was deficient for mature fibroblasts markers, such as *Postn and Sox9* (Fig. 2.15, Fig.2.16). C20 cells also expressed epicardial genes such as *Wt1* and *Aldh1a2*, as well as, *Dpp4, Smoc2*, and *Alcam,* but failed to express other mesothelial markers such as *Upk3a* and *Upk3b,* encoding integral membrane proteins (Fig. 2.15). Other genes that were not normally expressed in epicardium or fibroblasts were uniquely enriched in C20, such as *Ephb2* and *Vgll3*, indicating that C20 possesses its own distinctive signature, while sharing similarity with the epicardium and cardiac fibroblasts. Overall, the Drop-seq data showed accumulation of epicardial progenitor cells and C20 cells, with a concomitant reduction in differentiated cardiac fibroblasts in *Lats 1/2* mutant hearts. This suggests that *Lats1/2* is required for progression of epicardium to a fibroblast fate.

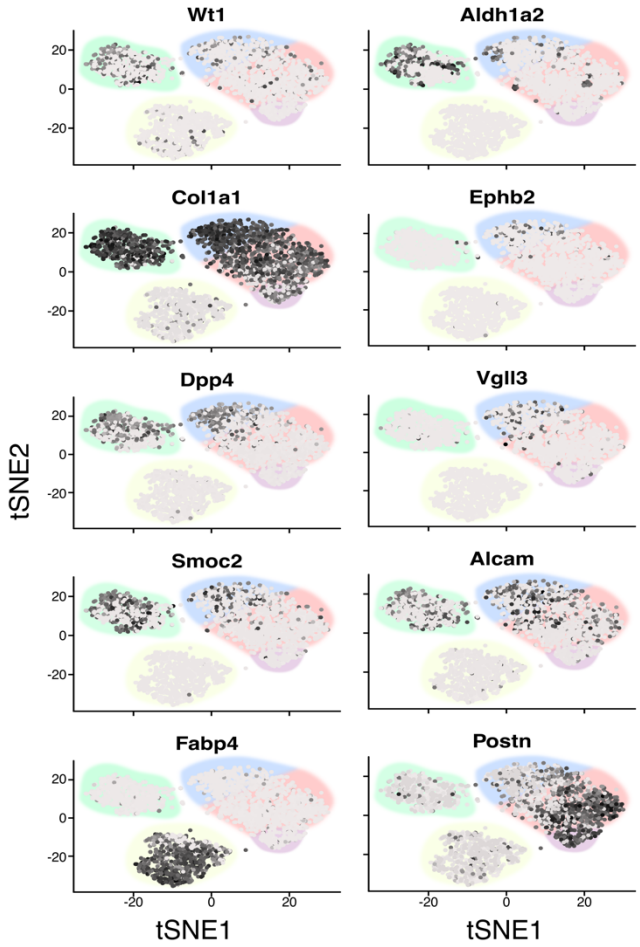

Figure 2.16. Gene expression projected across the tSNE. Black indicates high gene expression, and cluster identities and boundaries are set in the background and colored according to Figure 2.14B.

Pseudo-time analysis reveals that *Lats1/2* deficiency results in defective epicardial cell developmental transitions

Our data suggest that *Lats1/2* deficiency perturbed the normal epicardial developmental trajectory. To look at this question more carefully, we used the

Monocle2 algorithm to order cells along a developmental axis progressing from epicardial cells to cardiac fibroblasts (19). Importantly, the pseudo-time ordering matched closely with the graph-based clustering results, especially when projected across the tSNE (Fig. 2.3E,F). The left most portion of the epicardial cluster represents the most primitive cellular-state, while the bottom right section represents the most differentiated cellular state (Fig. 2.3E, bottom panel). C20 is isolated centrally along this differentiation axis supporting the notion that C20 is a transition state intermediate between epicardial progenitors and differentiated fibroblasts (Fig. 2.3E, top panel).

Cells diverging from the Monocle Minimum Spanning Tree (MST) are captured as alternative trajectories by their connection to the full MST path through a node (32). Nodes represent potential developmental junctions where cell-fate decisions are made. We identified a node (Fig. 2.3E, bottom, Node X) proximal to the final bifurcation of cardiac fibroblasts (Fig. 2.3E, Branch A) and the C20 population (Fig. 2.3E, Branch B) revealing two distinct EPDC differentiation paths. The “Branch A” trace, composed primarily of control cells, revealed the normal EPDC to fibroblast differentiation trajectory and the cellular transition from epicardium to mature fibroblast. In contrast, the “Branch B” trace, comprised predominantly of *Lats1/2* mutant cells, revealed an intermediate epicardial-fibroblast cell type, indicating that these *Lats1/2* mutant cells failed to progress to a fully differentiated cardiac fibroblast.

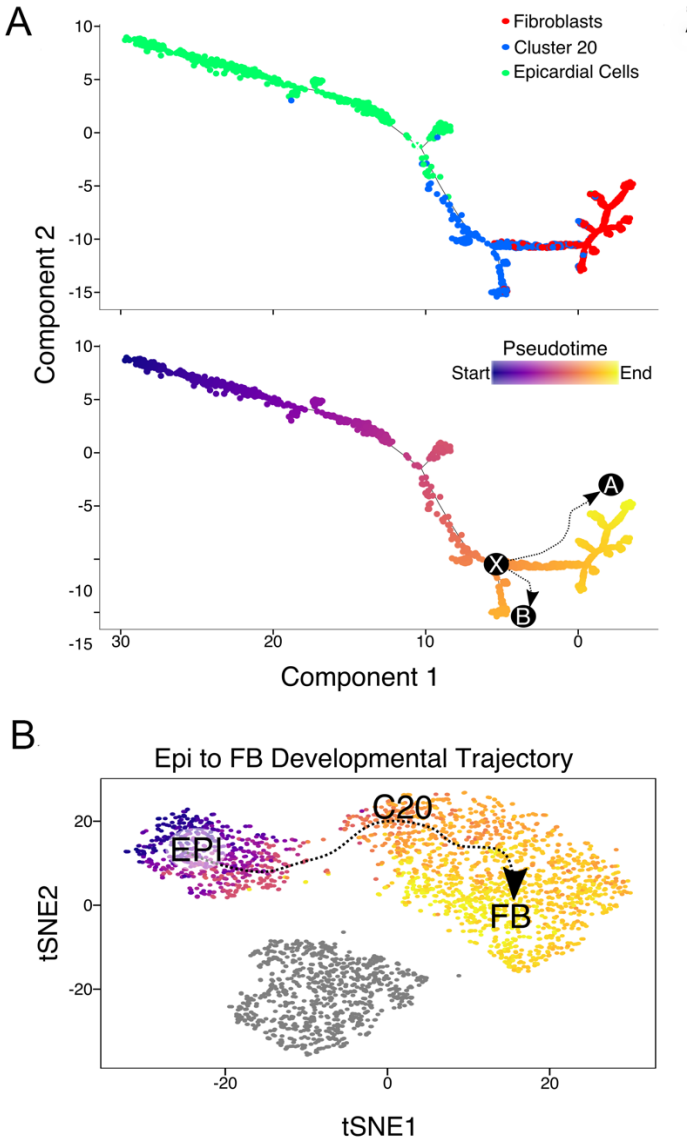

Figure 2.17. Pseudotime trajectory of epicardial cells, fibroblasts, and C20. Cells are colored by cluster across the epicardial to fibroblast differentiation axis(top). The pseudotime score is assigned to individual cells. Cells with a dark color and bright color represent the start and end of pseudotime respectively (bottom). The Monocle2 minimum spanning tree is the underlying black line, and the critical node is denoted as 'X' with dashed arrows representing the bifurcation of Branch A (fibroblast) and Branch B (C20).

To identify the genes associated with the Node X bifurcation, we examined gene expression patterns across pseudotime and uncovered several co-varying expression patterns. The first expression pattern, attributed to fibroblast differentiation, had a relatively higher expression level in differentiated fibroblasts (Fig. 2.18 A(B)). We focused on the genes associated with Branch B, and performed gene ontology (GO) analysis (Fig. 2.18 A(B) shading to Fig. 2.18 B). The enriched GO terms included extracellular matrix and vascular morphogenesis, suggesting that C20 contributed to the coronary vessel remodeling defects observed in *Lats1/2 CKO* hearts (Fig. 2.18 B). Further, the enriched GO term, regulation of cell migration, included several genes that have been shown to promote EMT, such as *Bmp4*, *Edn1* and *Ptn* (Fig.2.18B)(33-35) further supporting the idea that C20 cells efficiently progressed through EMT. This also agrees with the observation that the EMT marker, *Snai2*, was elevated in *Lats1/2* CKO embryos (Fig.2.19).

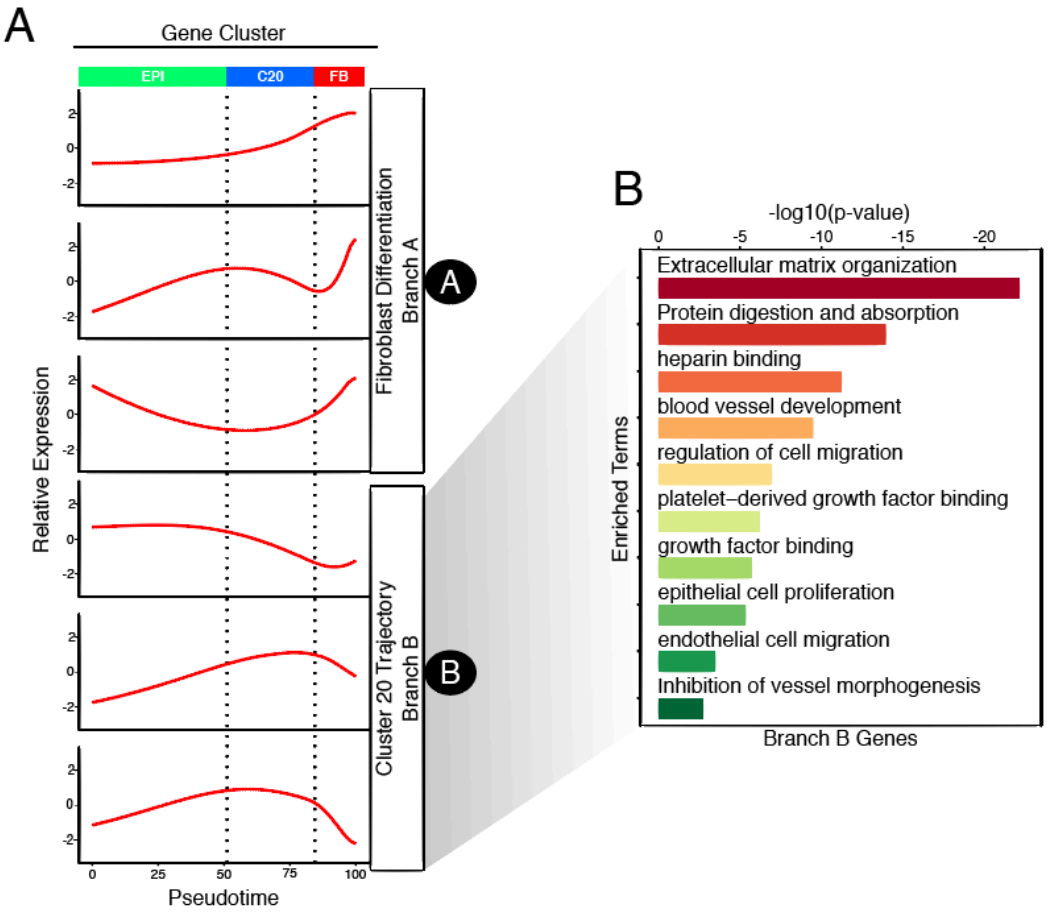

Figure 2.18. Gene expression pattern associated with pseudotime. (A) Hierarchical clustering of genes with branch-specific trends in gene expression across pseudotime. (top three: gene expression pattern enriched in Branch A; bottom three: gene expression pattern enriched in Branch B). (B) Gene ontology (GO) analysis of the genes identified from branch B, C20-specific, in Branch A.

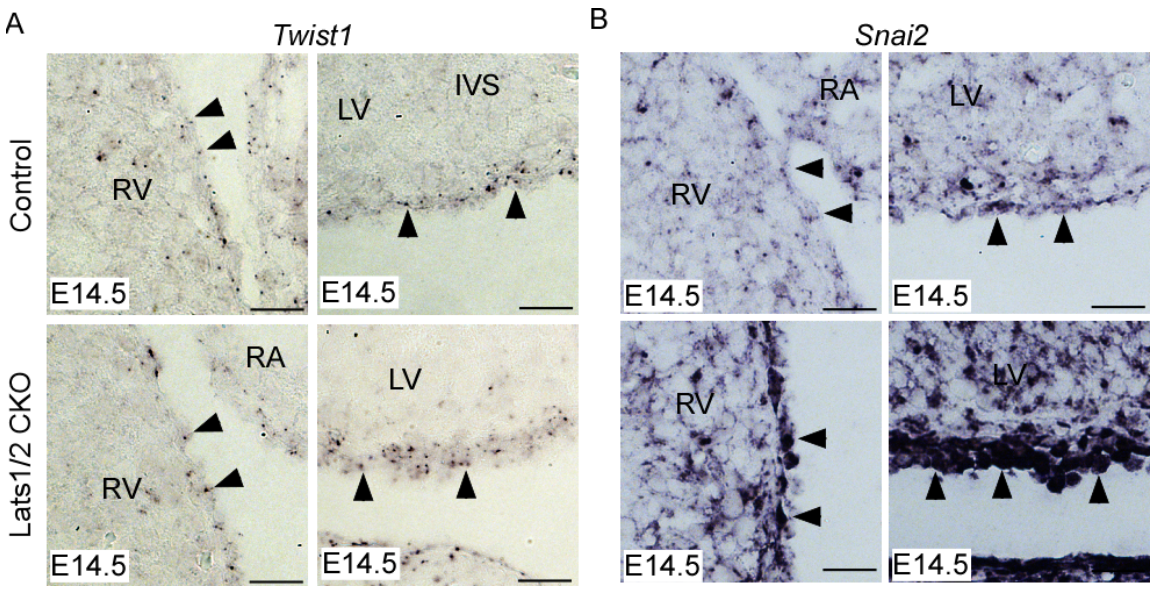

Figure 2.19. EMT factors expression in epicardium and EPDC. EMT factors *Twist1* and *Snai2* detected by *in situ* probe at E14.5. Scale bar: 25 μm.

The majority of Cluster 20-enriched genes are direct Yap-Tead targets

To identify the upstream regulators of C20 enriched genes, we performed transcription factor DNA-binding motif enrichment analysis across a 20 kb region centered on the Transcription Start Site (TSS) of each Branch B gene. Srf and Tead elements were the most enriched motifs in the Branch B gene set. While Tead was highly expressed in C20, Srf was present at low levels in C20, suggesting that most Branch B genes were directly regulated by Yap-Tead (Fig. 2.20A). Indeed, *Tead1* expression is enriched throughout C20 and its relative expression level decreases sharply moving across pseudotime from C20 toward

fibroblasts (Fig. 2.20B). Conversely, *Sox9* is low in epicardial and C20 cells but high in cardiac fibroblasts (Fig. 2.20B). Finally, we identified Tead1 motif enriched genes present in Branch B, and performed GO analysis specifically on these Yap-Tead target genes. We found several GO terms that were particularly well-represented among Branch B-specific Yap-Tead targets, including extracellular matrix organization, regulation of cell migration, and blood vessel development (Fig.2.18B, Fig. 2.20C). Additionally, we also uncovered other genes such as *Dhrs3*, not included in a specific GO category, that also are Yap-Tead target genes contained in C20 cluster (Fig. 2.20C).

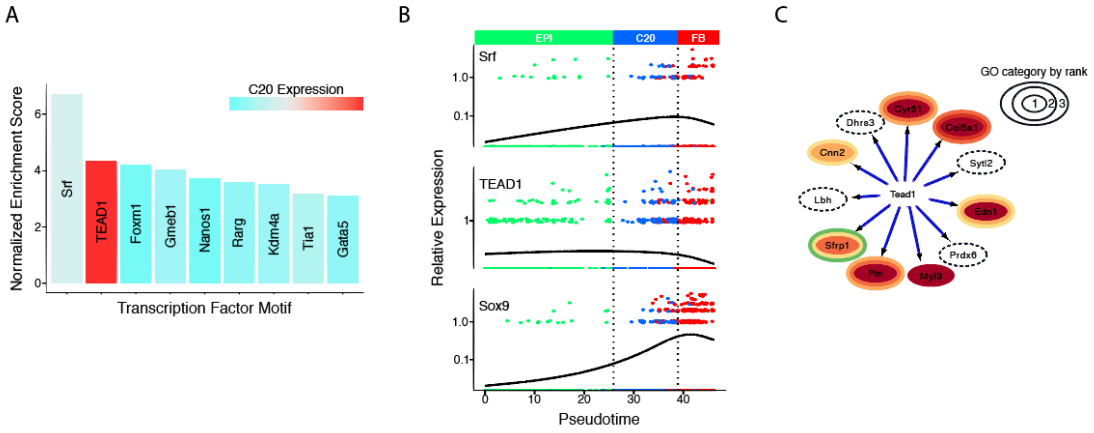

Figure 2.20. Cluster 20-enriched genes are direct Yap-Tead targets. (A)Motif enrichment analysis of Branch B, C20, specific genes. Expression of each transcription factor is in percent of cells above threshold within C20. Red indicates high expression. (B) Expression and cell density plots of key transcriptional regulators across pseudotime. Points are each colored by cluster identity from Figure 2.14 B, and 2.17A. (C) Tead1 target gene visualization and annotation. Gene ontology categories assigned and color coordinated based on Figure 2.18B.

The C20 cluster resides in subepicardium and *Lats1/2* deficiency results in subepicardial expansion

To validate our findings from pseudo time analysis and gain spatial information about C20, we performed IF experiments based on known epicardial-associated markers and newly identified genes expressed in C20. Expression of α-actinin outlined the division between myocardium and epicardium/subepicardium (Fig. 2.21 A,B). We investigated podoplanin expression, a marker of the single cell layer epicardium in control hearts and *Lats1/2* CKO hearts. As mentioned above, podoplanin expression expanded into subepicardium suggesting that the *Lats1/2* CKO mutant subepicardium still maintained some epicardial characteristics (Fig. 2.21 A,B).

We next investigated Pdgfrα expression, as it marks fibroblasts and the subepicardium. In control hearts, Pdgfrα was expressed in a single cell layer within subepicardium, while in *Lats1/2* CKO embryos Pdgfrα was expressed in a several layer thick subepicardium (Fig. 2.21 C, D). Likewise, Wt1, a marker for epicardium and subepicardium, was expressed in *Lats1/2* CKO epicardium and the expanded subepicardium (Fig. 2.21 E) (36). Similarly, Dpp4 and Col1a1, expressed in both epicardium and subepicardium, were expressed in epicardium and expanded subepicardium in *Lats1/2* CKO hearts (Fig. 2.21 F). Together, the IF data support the conclusion that the C20 population normally resides in subepicardium and that *Lats1/2* deficiency results in subepicardial expansion.

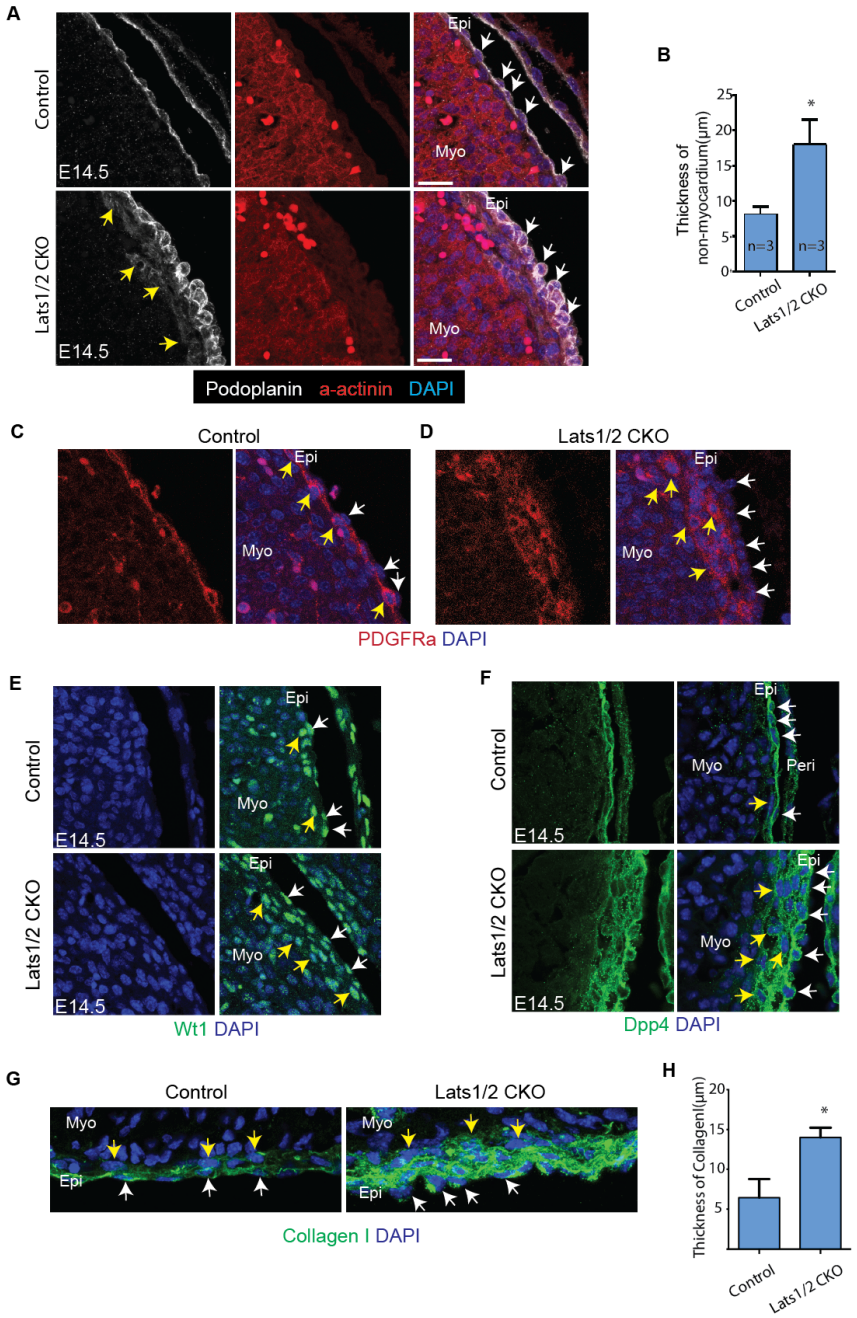

Figure 2.21. C20 is located in the subepicardium and expands in *Lats1/2* CKO hearts.(A-B) Podoplanin labels epicardium (white arrows) and α -actinin labels myocardium. The region in between of podoplanin and α -actinin delineated the subepicardium in control hearts. The expanded subepicardium in *Lats1/2* CKO were weakly stained by podoplanin (yellow arrows in *Lats1/2* CKO). Data in Fig.4B are means ± SD. **P*<0.1 was by Mann-Whitney U test. (C-D) PDGFR-α rarely labels epicardium(white arrows) and extensively labels subepicardium (yellow arrows). *Lats1/2* CKO hearts exhibited thickened PDGFR-α positive subepicardium. (E) Wt1 labels epicardium (white arrows) and subepicardium (yellow arrows) in *Lats1/2* CKO hearts. *Lats1/2* CKO hearts displayed expanded Wt1 positive subepicardium. (F) Dpp4 labels epicardium (white arrows) and subepicardium (yellow arrows). *Lats1/2* CKO hearts displayed expanded Dpp4 positive subepicardium. (G-H) Collagen I labels epicardium (white arrows) and subepicardium (yellow arrows). *Lats1/2* CKO hearts showed expanded Collagen I positive subepicardium. Data shown are means ± SD. **P*<0.1 was by Mann-Whitney U test.

Lats1/2 epicardial deficiency results in diminished cardiac fibroblast differentiation

Next, we investigated the cardiac fibroblast differentiation defect in more depth by performing lineage-tracing experiments using the *Rosa26*^{mTmG} genetic reporter to follow epicardial-derived lineages. EdU labeling indicated that in *Lats1/2* CKO embryos the *Wt1*^{CreERT2} lineage-derived epicardial cells and EPDCs were more proliferative than controls (Fig. 2.22 A-C). We noted that proliferation genes were not enriched on the Branch B GO analysis suggesting that proliferation was not the only distinguishing factor between C20 and cardiac fibroblasts (Fig. 2.18 B). Using the *Rosa26*^{mTmG} genetic reporter to label the *Wt1*^{CreERT2} lineage and PDGFRα to mark cardiac fibroblasts, we observed by IF and FACS a reduction in epicardial-derived fibroblasts from 44% to 32% in *Lats1/2* CKO mutants compared to controls (Fig. 2.23 A-C). IF, using another fibroblast marker Vimentin, further confirmed the reduction of epicardial-derived fibroblasts (Fig. 2.23 D-E). Taken together, the lineage tracing data further corroborated our previous Drop-seq results, demonstrating that inactivation of *Lats1/2* led to defective epicardial differentiation into mature cardiac fibroblasts.

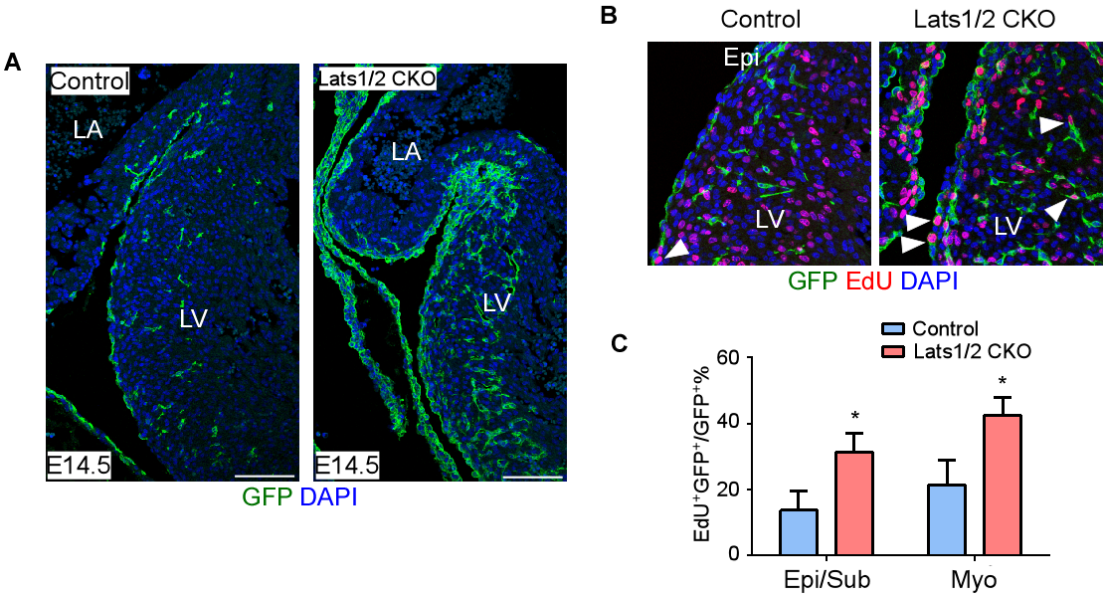

Figure 2.22. Increased epicardium and EPDC proliferation in *Lats1/2 CKO* hearts. (A) The *Wt1* lineage was traced by GFP expression, which includes epicardium and EPDC. An increased number of epicardium and EPDCs were observed in *Lats1/2* CKO hearts. (B-C) *Lats1/2* CKO exhibited significantly increased EdU labelling in GFP positive cells. Proliferating epicardial cells and EPDC were indicated as GFP^+ EdU^+ double positive cells(arrowheads). **P*<0.05, Mann-Whitney U test. Data shown are means ± SD. Scale bar: 50μm.

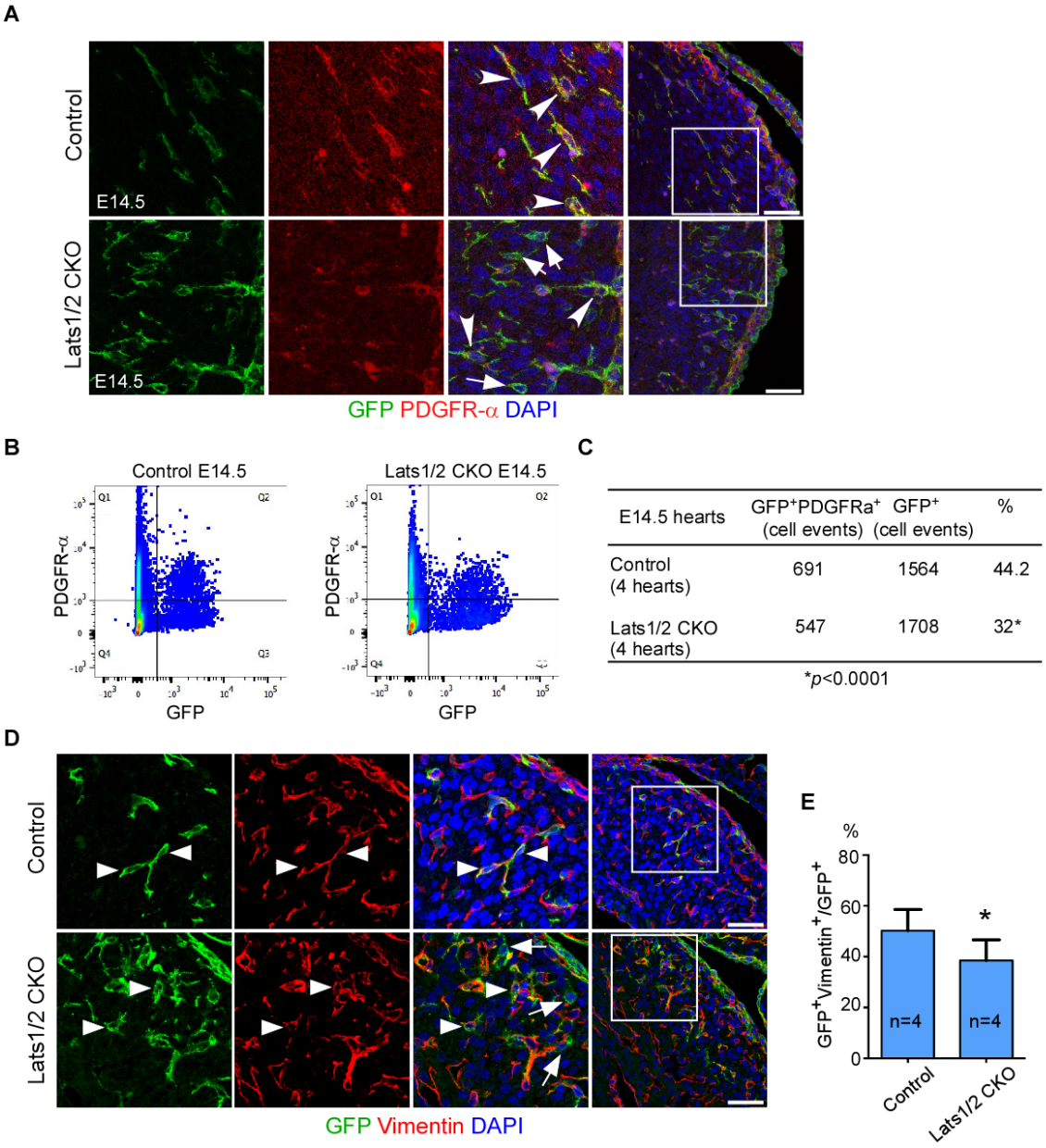

E14.5 hearts	GFP⁺PDGFRa⁺ (cell events)	GFP⁺ (cell events)	%
Control (4 hearts)	691	1564	44.2
Lats1/2 CKO (4 hearts)	547	1708	32*

*p<0.0001

Figure 2.23. Knocking out *Lats1/2* in epicardium leads to reduction of epicardial derived fibroblast. (A-B) The epicardial lineage was traced by GFP expression. Epicardial-derived fibroblasts are labelled (arrowheads) by GFP and PDGFR-α double positive staining. Other epicardial-derived lineages are indicated (arrows) by GFP single positive staining. A reduction of epicardial derived fibroblasts were observed in *Lats1/2 CKO* hearts. Panels on the left are a higher magnification view of the boxed area in the panels on the right. (B-C) FACS analysis quantification of the percentage of epicardial derived fibroblasts (*P<0.0001 was by Chi-square test). (D-E) Another fibroblast marker Vimentin also showed decreased epicardial derived fibroblasts in *Lats1/2 CKO* hearts (epicardial derived fibroblasts: arrowheads, epicardial derived other lineages: arrows). Panels on the left are the higher magnification of the boxed area in the panels on the right. Data shown are means ± SD. *P<0.1, Mann-Whitney U test. Scale bar: 50μm.

Yap controls fibroblast differentiation and coronary vessel patterning

Motif analysis showed enrichment of Tead motifs in C20-expressed genes (Fig. 2.20 A). Moreover, our genetic rescue experiment supported the conclusion that coronary vessel defects are mediated through Yap (Fig. 2.4). Next, we analyzed the TEAD motif-containing cis-regulatory regions in genes revealed by Drop-seq.

Several secreted intercellular factors associated with vascular morphogenesis were enriched in C20 including *Spon2*, *Ogn*, *Dpp4*, *Gpc3* and *Alcam* (Fig. 2.15, Fig.2.16), all of which have been suggested to regulate vasculogenesis and angiogenesis (26,37-41). *Dhrs3*, as shown above, was up-regulated in the differentiation arrested Branch B (Fig. 2.20), which may contribute to impaired epicardial-fibroblast differentiation by reducing retinoic acid signaling (42). To determine if the C20- expressed genes are directly regulated by Yap, we compared embryonic heart H3K27ac data with cardiac DNase-seq (DNase I hypersensitive site (DHS)) data and extracted TEAD motifs from the E14.5 H3K27ac peaks. Several consensus TEAD motifs, Yap binding sites, were identified at enhancer and promoter regions of genes enriched in Branch B, such as *Ogn*, *Spon2*, *Gpc3*, and *Alcam* (Fig. 2.24 A,B). Consensus Tead motifs were also found in *Dpp4* and *Dhrs3*. We further validated Yap-Tead regulation of *Dpp4* and *Dhrs3* by performing Yap ChIP-qPCR at the Tead motifs contained within H3K27ac and DHS peaks to determine if Yap directly bound to these loci. In both *Dpp4* and *Dhrs3*, Yap showed specific binding further supporting the notion that

Yap directly regulates genes that are essential for normal coronary vessel patterning and cardiac fibroblast differentiation (Fig.2.24 C).

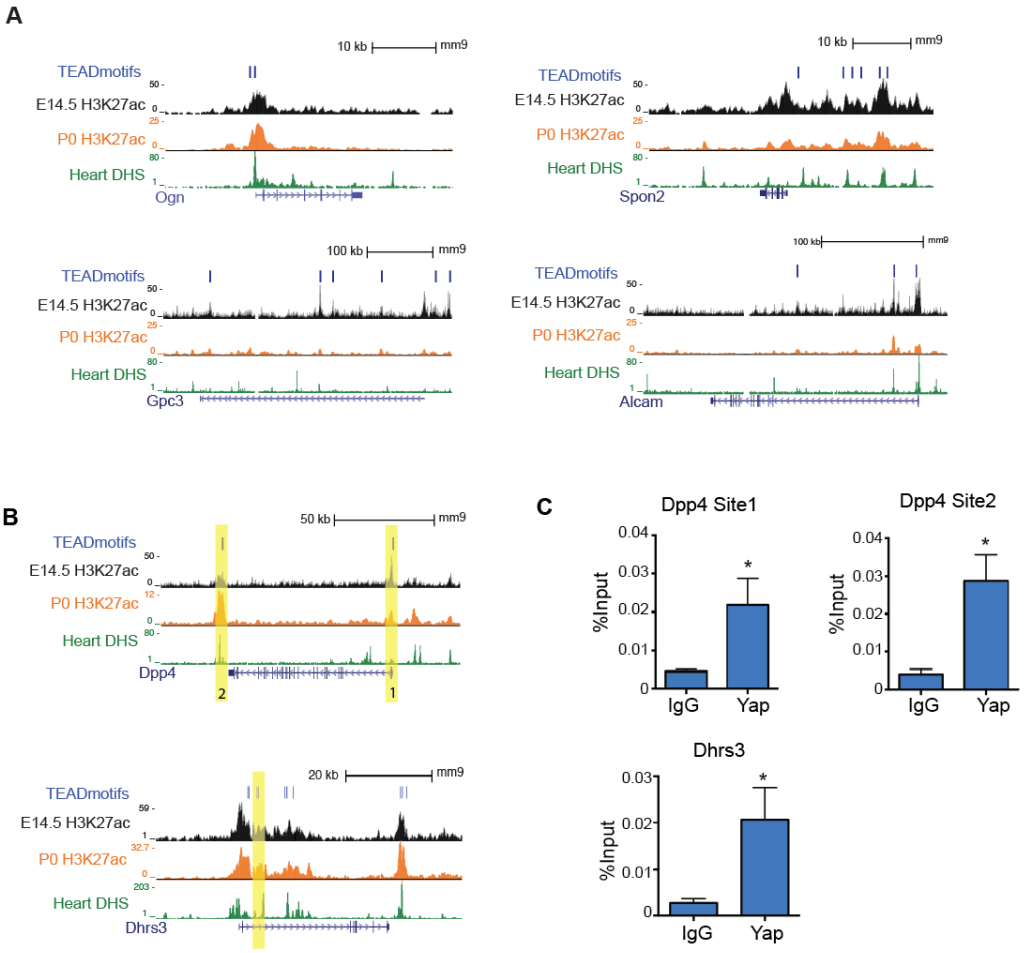

Figure 2.24. Direct Yap binding to the regulatory regions of the factors regulating extracellular milieu and cell differentiation in *Lats1/2* CKO hearts. (A) Numerous TEAD binding motifs were identified at the regulatory regions of genes encoding intercellular factors. (B-C) Yap-TEAD binding sites locates at the regulatory regions of Dpp4 and Dhrs3. Yap ChIP-qPCR, quantified in the bar graphs, demonstrated Yap binding at the yellow highlighted region in the corresponding gene tracks. Data are means ± SD. **P*<0.1 was by Mann-Whitney U test.

Discussion

Our study used high-throughput sc-RNA-seq to uncover an essential role of *Lats1/2* in orchestrating epicardial lineage differentiation into cardiac fibroblasts. Lats1/2 kinases function to restrain Yap transcriptional activity and regulate the transition from epicardium to subepicardial mesenchyme and mature cardiac fibroblasts. In addition, Lats1/2 function is required for a precise extracellular milieu to enhance coronary vascular development (Fig. 7). Our data provide new insight into cardiac cellular diversity at two different developmental stages, E13.5 and E14.5.

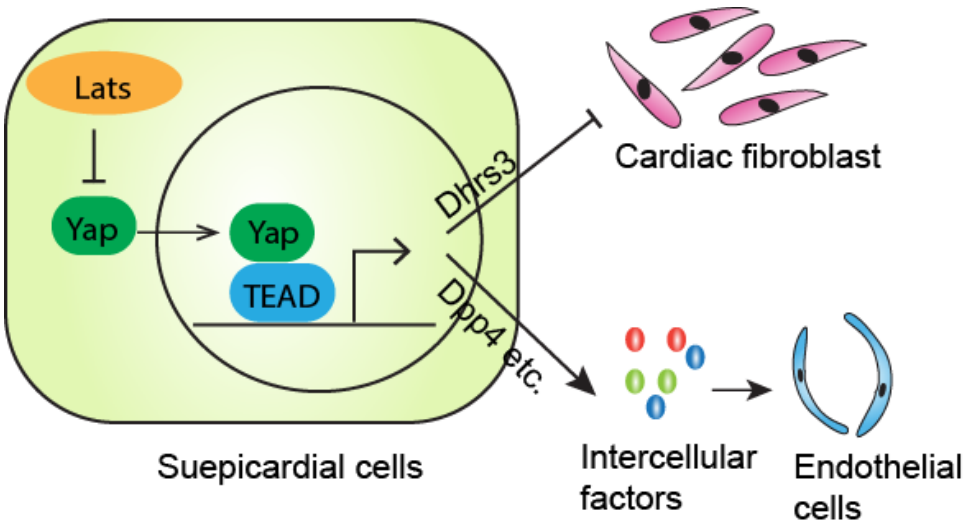

Figure 2.25. Working model. Lats kinase regulation of subepicardial cell differentiation to cardiac fibroblasts and coronary vessel patterning through controlling the composition of the extracellular milieu.

Using Drop-seq, we investigated cardiac cellular diversity during development at E13.5-14.5. Our data provide important insight into all major cardiac cell types, including rare cell types like macrophages and arterial endothelial cells. Interestingly, we also uncovered the transcriptional signatures of proliferating cardiomyocytes that will be useful for further studies in cardiomyocyte development and regeneration. Furthermore, we characterized many cell types that are required for valve development and we identified novel markers for cells that contribute to developing valves. Interestingly, distinctions between left and right ventricular cardiomyocytes identified by Li et. al at E10.5 were not appreciable in our data set, suggesting that these transcriptional distinctions are negligibly by E13.5 (43). It is likely that by E13.5 cardiomyocytes derived from both heart fields have differentiated to an extent that their molecular signatures become indistinguishable. Consistent with Li et. al, we detected signatures for AVC and trabecular cardiomyocytes.

Lats1/2 regulate epicardial progenitor differentiation into cardiac fibroblasts

By examining the relative proportion of cells from wild type and *Lats 1/2* mutant heart within each cluster, we found that epicardium and C20 are composed predominantly of *Lats1/2* mutant cells. C20, a cell type intermediate between epicardium and fibroblast is located in subepicardium. The characteristics of C20 indicate that in *Lats1/2* mutants there is a defect in the epicardial-to-cardiac fibroblast developmental trajectory. Consequently, we observed that the

epicardial-derived fibroblast cluster at E14.5 is reduced in *Lats1/2* mutant hearts. However, we did not find any differences in smooth muscle cells, the other major epicardial derivative, revealing a specific role for *Lats1/2* function in fibroblast differentiation.

Lats1/2 CKO hearts displayed subepicardial expansion and reduction of epicardial derived fibroblasts. Indeed, Lats kinases are inhibitors of cell proliferation and *Lats1/2* deficient subepicardium showed increased EdU incorporation, suggesting that up-regulated proliferation within this region contributed to the accumulation of C20 cells in subepicardium. Nonetheless, our pseudotime and sc-RNA-seq data provided the resolution to show that proliferation was not the major difference between C20 and cardiac fibroblasts. Rather, we identified Yap target genes such as *Dhrs3* that possibly inhibit fibroblast differentiation directly by down-regulating retinoic acid signaling.

Recent work showed that Yap/Taz in the AVC and epicardium is required for EMT (44), and in the epicardial context, led to subsequent decrease of all epicardial-derived lineages (27). In our study, excessive nuclear Yap activity in *Lats1/2* CKO did promote EMT supporting the role for Yap as an inducer of EMT. In contrast, we do not detect a smooth muscle phenotype in *Lats1/2* CKO suggesting that Yap/Taz are regulated through both Hippo-dependent and Hippo-independent mechanisms in epicardial development (45).

Hippo signaling coordinates vascular development with fibroblast differentiation

An important insight from our study, not previously appreciated, is the essential non-autonomous connection between cardiac fibroblast differentiation and vascular patterning. Our data suggest that the disorganized coronary vessel patterning in *Lats1/2* CKO hearts is due to aberrant signaling from *Lats1/2* mutant C20 cells. Cross talk mediated by growth factors between epicardium and myocardium is critical for coronary vessel angiogenesis and myocardium growth during heart development (46,47). Our data show that developing fibroblasts express growth factors and factors that modulate extracellular matrix composition that controls signaling to the developing vasculature.

The genes enriched in C20 cells (Branch B, Fig. 3E) indicate that extracellular matrix organization and growth factor binding was disrupted in *Lats 1/2* mutant hearts. Several intercellular factors such as Smoc2, Spon2 and Ogn are proteins embedded in the extracellular matrix that modulate growth factor activity to control angiogenesis. In addition to extracellular proteins, the cell surface serine protease, Dpp4, and its direct inhibitor Gpc3 regulate multiple, essential signaling events in coronary vascular development (39,48). Dpp4 controls the functional activity of chemokines and cytokines that contain Dpp4 proteolytic motifs including members of the FGF, BMP/TGF β, IGF, CXCL, and CCL family. Importantly, many of these signaling factors have been implicated in coronary vasculature development (26,38,40). Multiple TEAD motif were found in

the regulatory regions of these genes suggesting that they are direct Yap target genes. In particular, *Dpp4* was validated as a direct target of Yap. These data are consistent with our genetic evidence showing that reduced Yap/Taz dosage in *Lats1/2* mutant epicardium suppressed the vascular phenotype of *Lats 1/2* CKO hearts.

During normal heart development, organ vascularization is coordinated with overall heart size to meet the growing metabolic needs of the heart. Our data suggest that the epicardium and subepicardium are important for coordinating organ vascularity with organ size. In other contexts, it has been shown that in addition to Hippo pathway kinases, mechanical tension acts as another mode of regulation of nuclear Yap activity (49). Thus, a tempting model would be that an increase in tissue surface tension gradually activates Yap in epicardium/subepicardium as heart size increases. With heart growth, a gradual tension increase on epicardium and subepicardium may transiently promote nuclear Yap activity and EMT with subepicardial cell proliferation. In this scenario, Hippo kinase activity may modify the influence of mechanical tension on EMT and proliferation so that the correct number of subepicardial cells are formed.

Within subepicardial cells, Lats1/2 kinases are important for enhancing differentiation into cardiac fibroblast. In addition, our study suggested that subepicardial cells provide a permissive extracellular matrix environment that is essential for coronary vascular development and maturation. The subepicardium, a transient and rare population, is difficult to study. In *Lats1/2* mutants this

population is expanded and by performing transcriptomics at single cell resolution, we were able to study this population in greater depth. Our findings suggest that as endothelial progenitors invade the heart they require an ECM provided by subepicardial cells to develop normally.

CHAPTER III

HIPPO AND MECHANICAL SIGNALING COOPERATIVELY DETERMINE EPICARDIAL CELL SPECIFICATION

Introduction

Coronary artery disease is a major cause of heart failure and death worldwide (7,50). It is imperative to identify effective therapies to restore coronary circulation and heart function. Recent findings indicated that adult epicardium and epicardial derived cells (EPDCs) reexpress embryonic genes, resume embryonic plasticity, and facilitate cardiovascular repair following injury (46,51-53). Understanding the molecular mechanisms regulating epicardial development would be expected to offer new therapeutic targets for cardiac repair after injury.

In mammals, EPDC derived from Wt1 expressing lineage mainly give rise to vascular smooth muscle cells and fibroblasts. A second epicardial lineage, expressing *Scx* and *Sema3D* contribute to endothelial cells (54). A small percentage of epicardial cells are positive for both *Wt1* and *Scx* and *Sema3D* (54). In addition to its cellular contribution, EPDC secrete growth factors that promote vasculogenesis and angiogenesis and enhance cardiomyocyte proliferation (51).

Mechanical signaling and cell shape changes, driven by mechanical forces, influence cell fate determination in cultured cells (55,56). In mechanical signaling, the cell transduces extracellular mechanical cues into a biochemical output. The activity of Hippo pathway components Mst1/2, Lats1/2, and Yap both influence and are influenced by cytoskeletal organization that adjusts to mechanical input

from external forces (57). For example, cells grown on hard substrates or low density have more F-actin polymerization with preferentially nuclear localized Yap. In contrast, soft substrates or high cell density reduces F-actin polymerization and sequesters p-Yap in the cytoplasm. The mechanical cues inducing Yap translocation or activation/inactivation have been proposed to be both Lats1/2 dependent and independent (49,58). However, in the epicardium, whether Hippo signaling is involved in mechanical signaling to influence cell differentiation is unknown.

Here, by deleting Lats1/2 kinases in the Wt1 epicardial lineage, we find that Hippo mutant epicardium preferentially generates a highly proliferative endothelium. Furthermore, *Lats1/2* mutant epicardium had mechanical properties and cytoskeletal organization characteristic of cells in a stiff matrix environment that also promotes the endothelial fate. Our data reveal that mechanical signaling and the Hippo pathway cooperatively determine epicardial specification.

Materials and Methods

Mice

Wt1^{CreERT2} (9), *Lats1/2*$^{flox/flox}$ (3), *Rosa26*^{mTmG} (11) alleles have been described previously. Mice were on a mixed genetic background of C57BL/6 and 129SV. Tamoxifen was dissolved in peanut oil with 5% ethanol at 10mg/ml. For Wt1 ^{CreERT2},0.1mg/g body weight tamoxifen was administrated to plugged female by intraperitoneal injection at embryonic (E) day11.5.

Immunofluorescent staining

Epicardium-restricted-Lats1/2 mutant embryos (Lats1/2 CKO) were generated by crossing *Wt1*^{CreERT2} with *Lats1/2*$^{flox/flox}$; *Rosa26*^{mTmG}. Control embryos were generated by crossing Wt1^{CreERT2} with *Rosa26*^{mTmG}. Embryos were collected at E13.5 or E14.5. For immunofluorescence staining, antibodies used were as follows: GFP(1:200, Abcam ab290, ab6673), PECAM-1(1:200, BD Pharmingen 550274), PDGFR-β (1:100, Cell Signaling Technology, 3169),Wt1(1:200, Santa Cruz, SC-192), Phalloidin (1:200, Thermo Fisher Scientific ,A22287). To visualize specific antigen, far red 647 fluorophor was applied. When applications were necessary for green and red spectrum, sections were pre-treated with 0.3% H_2O_2 in PBS for 20min at room temperature to quench the endogenous GFP and Tomato signals, which come from reporter line Rosa26^{mTmG}. In some cases, Tyramide Signal Amplification Systems (1:100, Perkin Elmer) were applied to amplify signal. Alexa Fluor 647 conjugated Wheat Germ Agglutinin (1:200, Life Technologies, W32466) were used for WGA staining. Immunofluorescence images were captured on a Leica TCS SP5 confocal microscope, N-SIM Super-Resolution Microscope System (Nikon). 3D reconstructed images were process by Imaris software provided in Baylor College of Medicine Optical Imaging and Vital Microscopy Core. Sample size labeled on corresponding bar graph was number of hearts being analyzed. Three field of views were analyzed in each heart.

Isolation of embryonic epicardial cells

Embryonic hearts were harvested at E11.5 or E13.5. Whole ventricle was placed on culture dishes coated with 1% Type I rat tail collagen (Corning). Epicardial cell monolayer was formed after 24 hr and hearts were removed. For RNA-seq experiment, explants isolated at E13.5 were cultured for 2 days.

EdU incorporation assay

To study cell proliferation, pregnant females were injected with EdU (0.5mg) 2hr before harvesting embryos. Hearts were processed as described above. EdU incorporation was assayed by Click-it EdU imaging kit (Life Technologies).

Western Blotting

Protein level was detected by Western Blotting, which was performed as previously described(3). Epicardial cell line MEC1 was used for western blotting(59). siRNA used were as follows: Non-targeting siRNA(siNC) (Dharmacon, D-001810-02-05), Mouse Lats1 (siLats1) (Dharmacon,L-063467-00),Mouse Lats2 (siLats2)(Dharmacon,L-044602-00) . RNAiMAX (Thermo Fisher Scientific) was used for transfection. Cells were treated with siRNA for 48 hours and harvest for protein detection. Antibody used for Western Blotting were as follows: anti-pYap, anti-MLC, anti-pMLC and anti-Lats1 (Cell Signaling Technology), anti-a-tubulin(Sigma).

FACS analysis

To determine the percentage of endothelial cell of initial labeling, pregnant females were injected with tamoxifen at E11.5 and embryonic hearts were harvested at E12.5 or E14.5. Cells were dissociated as previously described (12). Hearts were chopped into several pieces and digested by 1mg/ml collagenase I for 20 min at 37 degree. Every 10min, gently pipette sample up and down to mechanically dissociate the cells. 10% FBS in DMEM was applied to stop the digestion and samples were passed through 100μm strainer. After washed twice with 1% FBS in PBS, cells were stained with PECAM-1 (eBioscience 17-0311-80) or isotype (eBioscience 17-4321-41) conjugated with APC. Cells were analyzed using BD Biosciences SORP Aria I and BD Biosciences LSRII and images were processed with FlowJo software.

RNA sequencing

Pregnant females were injected with Tamoxifen at E11.5 and epicardial explant culture was performed at E13.5. *Wt1*Cre^{ERT2}; *Rosa26*^{mTmG}/+ embryos were used as controls and *Wt1*Cre^{ERT2}; *Lats1/2* $^{f/f}$; *Rosa26*^{mTmG}/+ embryos were used as mutant. Two litters of embryos were pooled as one sample. Three different samples were collected for each genotype and subjected to RNA sequencing. Total RNA was extracted using Qiagen RNeasy micro kit according to the manufacturer's protocol. mRNA was purified by Dynabeads mRNA DIRECT Micro Kit(Life Technologies) and then converted to barcoded cDNA libraries for RNA sequencing on the Ion Proton System using Ion Total RNA-Seq Kit v2.0(Life

Technologies) and RNA-Seq Barcode 01-16 Kit(Life Technologies). RNA-seq was performed on Ion Proton. Around 35 million reads were generated for transcripts quantification in each sample. Paired-end RNA Seq reads were aligned to mm9 (*Mus musculus* assembly July 2007). Raw read counts were normalized and analyzed for differential gene expression by DESeq2. GO-seq was used for Gene Ontology (GO) analysis to extract the information on gene set and gene network.

Atomic force microscopy

Pregnant female were injected with Tamoxifen at E11.5 and hearts were isolated at E13.5. *Wt1*Cre^{ERT2}; *Rosa26*^{mTmG}/+ embryos were used as controls and *Wt1*Cre^{ERT2}; *Lats1/2* $^{f/f}$; *Rosa26*^{mTmG}/+ embryos were used as mutant. Freshly isolated hearts were mounted on poly-l-lysine coated coverslip. All AFM images and measurements were taken by Bioscope Catalyst AFM (BRUKER) and Olympus IX81 inverted optical microscope located at Houston Methodist Research Institute Microscopy-SEM/AFM core. A spherical AFM tip was made by attaching a silicon particle with 5μm diameter (Hamilton Company) to a silicon nitride cantilever (MLCT, BRUKER) with tip half angle 18º (60) . Spring constant was at 0.02N/m calibrated by thermal vibration in air. Deflection sensitivity was at 77.9nm/V obtained by a standard force-displacement curve in PBS on a silicon wafer. Contact mode was conducted and the probe was engaged onto the surface of the heart at ramp rate 1Hz without X-Y axis scanning. Each single measurement was acquired by the average of 50-100 times of indentation force engagement. For each heart tissue, 10 different measurements were performed

and 3-4 hearts were measured in control and *Lats1/2* CKO hearts. 30-40 measurements were pooled in each group. Young's modulus was calculated from force displacement curve using Nanoscope analysis software v1.40r2.

Epicardial cell differentiation assay on tunable stiffness hydrogel

Epicardial cells were isolated at E11.5 from *Lats1/2*$^{f/f}$; *Rosa26*^{mTmG}/*Rosa26*^{mTmG} embryonic hearts. Tissue was removed after 24hr and outgrowth was trypsinized and replated on tunable stiffness hydrogel, which was prepared as previously described (61). Stiffness was adjusted based on the relative concentration of acrylamide and bis-acrylamide. Hydrogel were coated with type I rat tail collagen (0.5mg/ml) before epicardial explant culture. 1hr after seeding cells on hydrogel or plastic dish, cell were either infected with the adenovirus packaged by Ad5 empty vector or Ad5-CMV-Cre vector for 48hr. Virus was generated by Baylor College of Medicine Vector Development Core Lab. Cells were continuously cultured in Endothelial Cell Growth Medium (Lonza) supplemented with 50ng/ml b-Fgf (R&D Systems) and 50ng/ml VEGF (R&D Systems) for 11 days and medium was changed every two days. Endothelial cells were detected by PECAM-1(1:200) immunofluorescence staining.

Results

Lats1/2 epicardial deficiency results in elevated proliferation with altered epicardial cell diversification

Our above study has shown *Lats1/2* deficiency led to coronary vessel defects and reduction of epicardial derived cardiac fibroblast differentiation. To investigate how EPDC fate associates with coronary vessel phenotype in more depth, we performed lineage tracing using $Rosa26^{mTmG}$ reporter line. GFP immunofluorescence staining was used to co-label epicardial lineage with PECAM-1, PDGFRα and PDGFRβ that are markers for endothelial cells, fibroblasts and smooth muscle cells respectively. Paraffin tissue sections were bleached by 0.3% H_2O_2 to quench the fluorescence signal from the $Rosa26^{mTmG}$ reporter, and the cell lineage specific markers were visualized in far-red spectrum to avoid interference from tdTomato (see methods). Unexpectedly, the percentage of endothelial cells derived from EPDC was increased from 2.6% in control to 12.5% of EPDC in *Lats1/2* CKO based on immunofluorescent staining and FACS quantification (Figure 3.1 A-B). The increase in endothelial cell number came at the expense of fibroblasts and smooth muscle cells, the major Wt1-expressing epicardially-derived cell types in control hearts. In *Lats1/2* CKO mutants, fibroblast contribution was reduced as shown in previous study (Figure 2.23), while smooth muscle cells decreased from 40% to 25% of EPDCs (Figure 3.2 A-B).

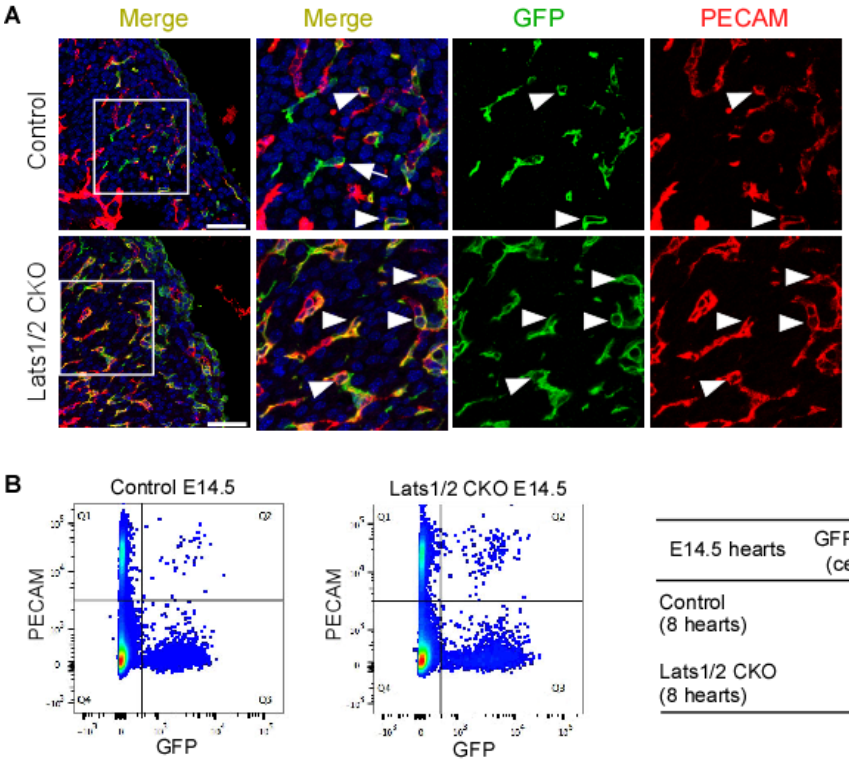

E14.5 hearts	GFP⁺PECAM⁺ (cell events)	GFP⁺ (cell events)	%
Control (8 hearts)	38	1416	2.6
Lats1/2 CKO (8 hearts)	201	1603	12.5*

*p<0.0001

Figure 3.1 Knocking out *Lats1/2* in epicardium leads preferential differentiation into endothelial cells. (A) *Wt1* lineage was traced by GFP expression. Endothelial cell was examined by PECAM-1 immunofluorescence staining. (B) FACS analysis quantification of the percentage of epicardial derived endothelial cells (*P<0.0001 was by Chi-square test).

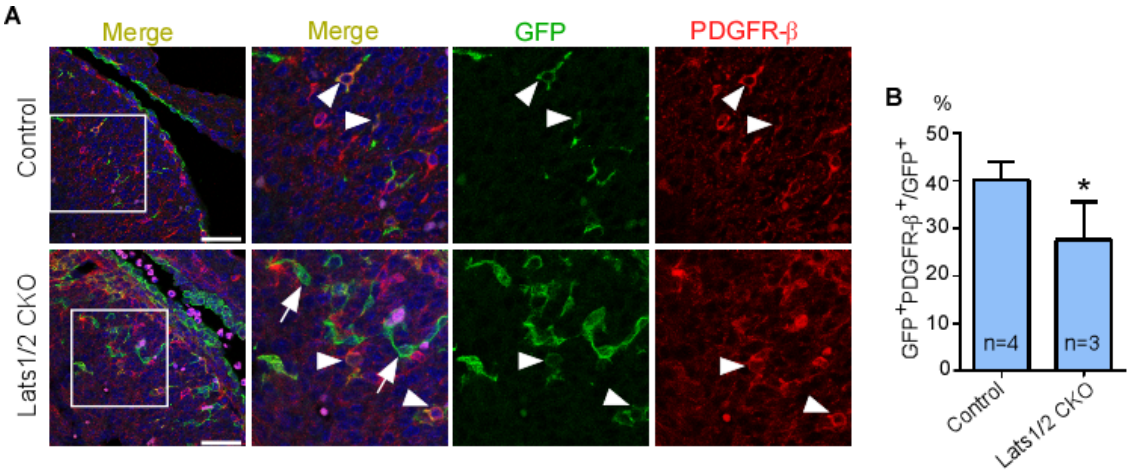

Figure 3.2. *Lats1/2* deficiency in epicardium results in reduction of smooth muscle cell differentiation from epicardial cell. (A) *Wt1* lineage was traced by GFP expression. Smooth muscle cell was examined by PDGFR-β immunofluorescence staining. (B) Quantification of the percentage of epicardial derived endothelial cells (*P<0.1 was by Mann-Whitney U test).

Endogenous Wt1 expression has been reported in E14.5 endothelial cells, which is at a relative late stage (36). Other work indicated that tamoxifen injections in Wt1creert2 mice at E10.5 labeled only a very small percentage of endothelial cells (62). To investigate the source of increased endothelial cells in our study, we performed fluorescence-activated cell sorting (FACS) to examine

the endothelial cell labeling 24-hours after tamoxifen induction when nuclear Cre activity is maximum (63). In controls, only 0.68% of GFP positive cells were PECAM positive, but in *Lats1/2* CKO hearts 2.67% of GFP positive cells were PECAM positive (Figure 3.3 A-B). This indicates that a minimal number of endothelial cells are included in the initial labeling as shown by less than 1% of control GFP positive endothelial cells and that Lats 1/2 deletion causes a rapid endothelial cell expansion within 24 hours of tamoxifen injection.

We next examined the proliferation rate in each type of EPDC in more depth. In E14.5 control, fibroblasts, smooth muscle cells, and endothelial cells had equivalent rates of EdU incorporation (Fig.3.3 C-D). In contrast, *Lats1/2* CKO endothelial cells had significantly increased EdU incorporation while fibroblasts and smooth muscle had similar EdU incorporation rates as the control. Together, these data indicate that *Lats1/2* deletion in Wt1-expressing epicardium causes a rapid increase in endothelial cell proliferation but not fibroblasts or smooth muscle.

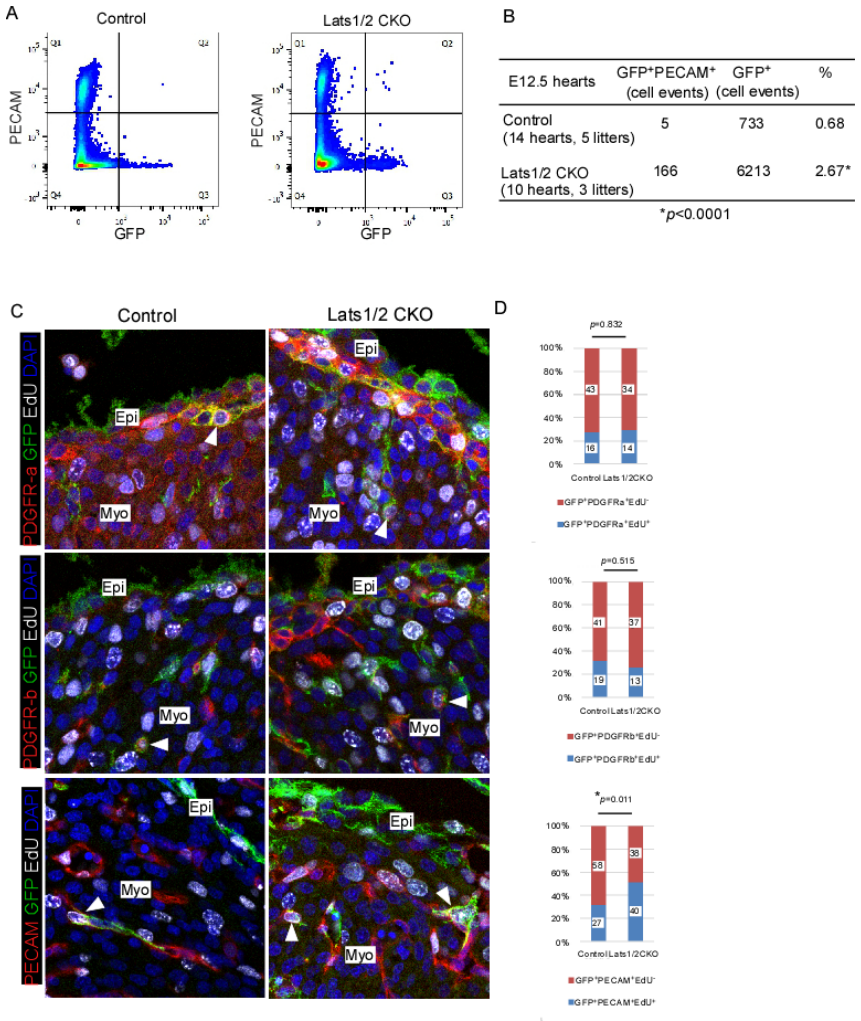

E12.5 hearts	GFP⁺PECAM⁺ (cell events)	GFP⁺ (cell events)	%
Control (14 hearts, 5 litters)	5	733	0.68
Lats1/2 CKO (10 hearts, 3 litters)	166	6213	2.67*

*p<0.0001

Figure 3.3. Initial labeling of endothelial cells and proliferation in different EPDC.(A-B) FACS analyses at E12.5 to examine endothelial cell labelling by Wt1CreERT2 after 24-hour tamoxifen induction. In *Lats1/2* CKO hearts, 2.67% of GFP+ cells was endothelial cell, which was significantly higher than 0.68% in the controls (*P<0.0001 was by Chi-square). (C-D) EdU incorporation rate in three different types of EPDC at E14.5. Triple positive cells (PDGFRa+GFP+EdU+; PDGFRb+GFP+EdU+;PECAM+GFP+EdU+) were indicated by arrowheads in C. *Lats1/2* CKO hearts showed preferentially increased EdU incorporation rate in endothelial cells (*P=0.011 in D was by Chi-square) but not in fibroblasts and smooth muscle cells. In control, fibroblasts(GFP+PDGFRa+), smooth muscle cells(PDGFRb+) and endothelial cells(PECAM+) maintain the same EdU incorporation rate, but in the *Lats1/2* CKO heart, EdU incorporation was significantly higher in endothelial cells than other two cell types(*P=0.015 and 0.005 in E were by Chi-square). Numbers labelled on each bar graph are the actual observed cell numbers and they are proportioned to 100%. Epi, epicardium; Myo, myocardium.

Lats1/2 inactivation resulted in increased cell stiffness

To gain deeper insight into molecular mechanisms underlying the vascular defects in the *Lats1/2* CKO mutants, we performed RNA-sequence (seq) using primary epicardial explant cells at E13.5(Fig.3.4A) (64). Before subjecting cultured cells to RNA-seq and to validate that explants maintained epicardial characteristics, explanted cell composition was studied by Wt1 immunofluoresence that showed the great majority of explanted cells were Wt1 positive (Fig.3.4B). Moreover, RNA-seq showed that the epicardial marker Wt1 was highly enriched while the fetal myocardial marker Myh7 was depleted (Fig.3.4C). In addition, the LoxP flanked exons of Lats1 and Lats2 were strongly reduced in the Cre treated samples (Fig.3.4 C).

RNA-seq showed that in *Lats1/2* CKO epicardial explants, 167 genes were up-regulated and 275 genes were downregulated when compared to wild type explants (Fig.3.5A). Subjecting genes with significant expression changes to gene ontology analysis revealed that signaling pathways related to vasculogenesis and angiogenesis were enriched in the up-regulated gene set. In particular, we noted that the FGF, Angiopoietin, and PDGF pathways were upregulated (Figure 3.5 B-C). These gene expression changes were consistent with the increase in endothelial cells that we observed in the *Lats1/2* CKO hearts.

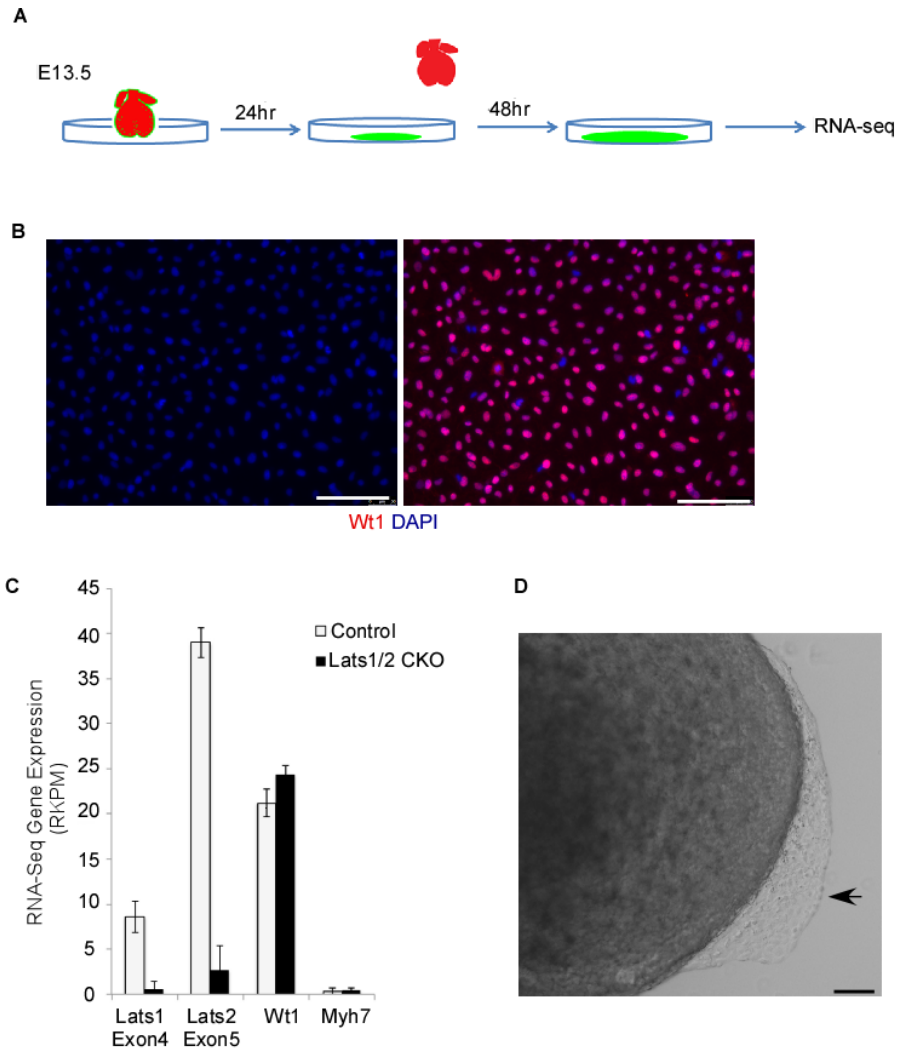

Figure 3.4. RNA-seq experiment design and quality control. (A)Schematic of epicardial cells isolation. (B) Cell identity after 3-day culture. The majority of explant culture expressed epicardial cell marker Wt1. (C) Knockout efficiency and purity of isolated cells. Gene expression level was represented by normalized reads number, RPKM (reads per kilobase per million). The expression level of exon4 of *Lats1* and exon5 of *Lats2*. (D)Relative position of explant cells and heart in culture. Scale bar 100um.

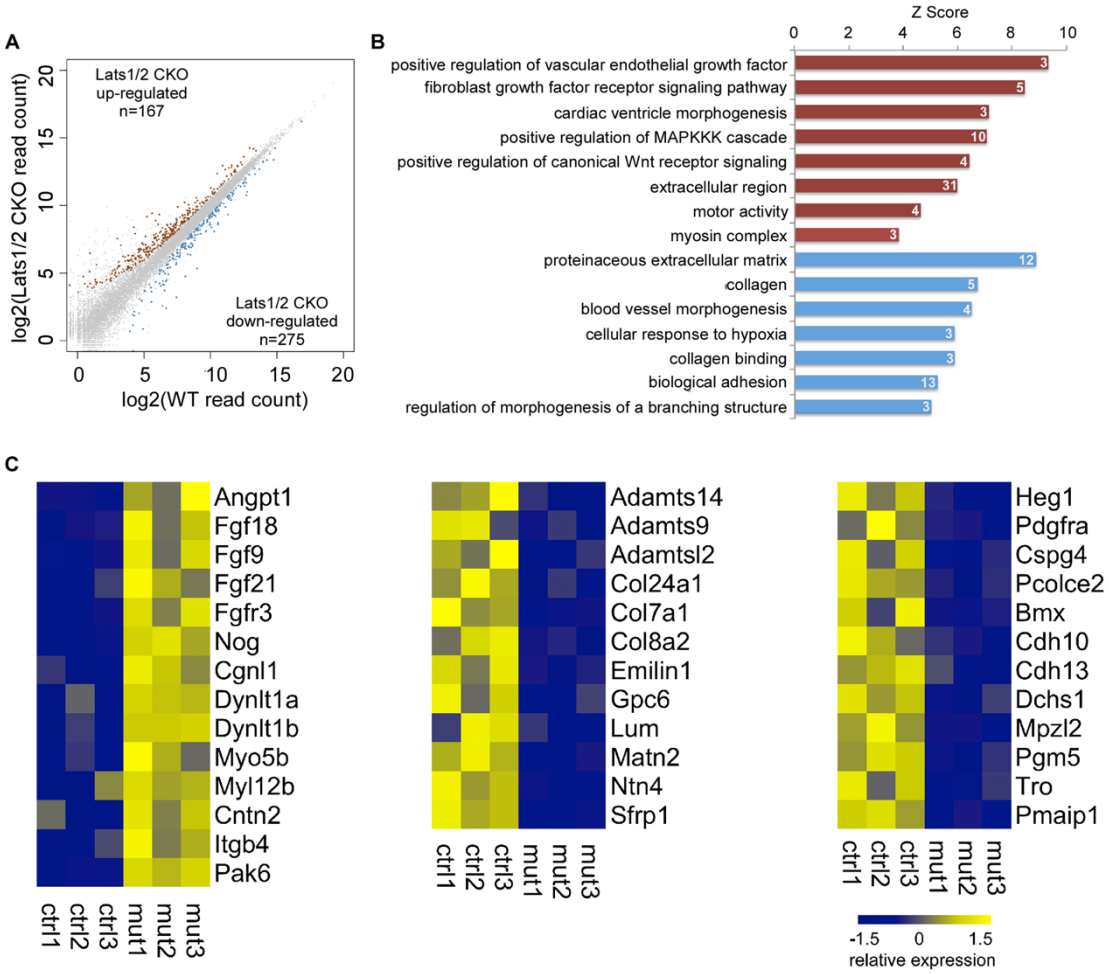

Figure 3.5. Differential gene expression and GO analysis.(A) Differential gene expression. In *Lats1/2* CKO primary epicardial cells, 167 genes were upregulated and 275 genes were downregulated. (B) GO analysis. Enriched GO terms of up-regulated genes (upper red bars) and down-regulated genes (bottom blue bars). Number on each bar represented the number of genes changed in its corresponding term. (C) Heat map of selected differentially expressed genes based on the GO terms of interest. Color key represents log-transformed relative gene expression level between control and mutant with three biological replicates in each group.

Gene categories in the down-regulated gene set included collagen and extracellular matrix, as well as, blood vessel morphogenesis and branching morphogenesis. For example, genes such as *Adamts14, Adamts9, Adamtsl2, Col7a1, Col8a2,* and *Emilin* that regulate collagen processing and extracellular matrix deposition were downregulated. Other genes that promote blood vessel morphogenesis such as *Heg-1* and *Bmx* were also downregulated (65,66). These changes in gene expression are consistent with the defective vascular morphogenesis phenotype with reduced numbers of fibroblasts and smooth muscle cells that we observed in *Lats1/2* CKO mutant hearts.

We also noted that genes involved in motor activity, myosin complex, and Rho GTPase activity were enriched in the up-regulated data set. Included in these categories were dyneins *Dynlt-1a* and *Dynlt-1b* that are important in intracellular trafficking (67). We noted upregulation of Myo5b encoding a non-muscle myosin and a regulatory myosin light chain, *Myl12b*. Moreover, *Cgnl1*was upregulated and encodes a protein that links actin cytoskeleton to adherens and tight junctions (68). We also saw increased expression of the integrin, *Itgb4* that encodes a protein linking the actin cytoskeleton to the extracellular matrix. As a readout of cytoskeleton contractility, we examined the phosphorylation level of myosin light chain(p-MLC). Using siRNA against *Lats1/2* efficiently to knock down the expression of *Lats1/2* in epicardial cell line MEC1 cells, we found p-MLC was up-regulated(Fig.3.6). Together, these findings support the notion that epicardial

deletion of *Lats1/2* resulted in up-regulated actin and myosin cytoskeletal proteins and a more rigid cytoskeleton.

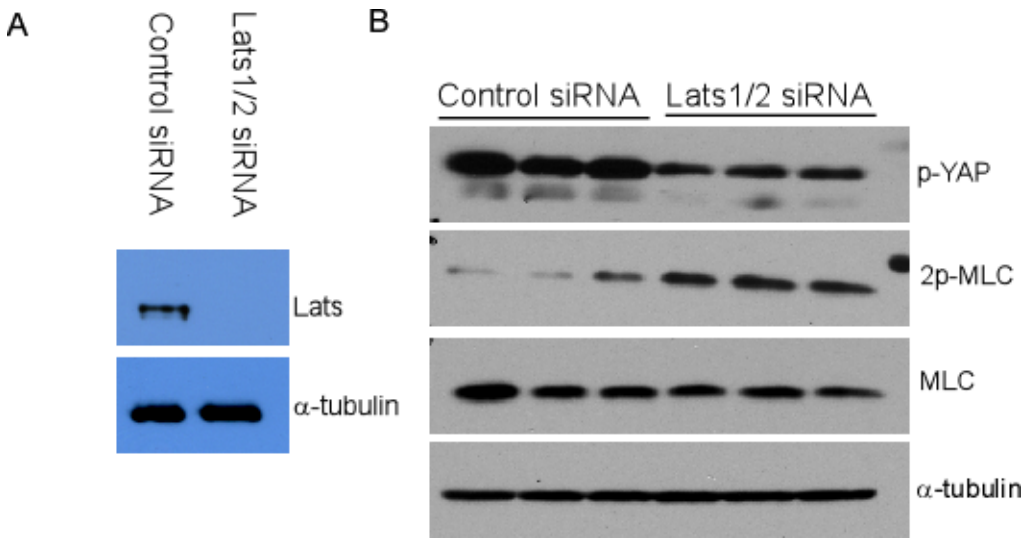

Figure 3.6. Phosphorylation level of MLC is up-regulated in *Lats1/2* knockdown cells.

To test the idea that *Lats1/2* CKO epicardial cells were more rigid than control epicardial cells, we directly measured epicardial stiffness in situ in *Lats1/2* CKO and control E13.5 hearts by atomic force microscopy (AFM). A spherical AFM cantilever (Fig.3.7 A-B) was pointed to the surface of embryonic heart (Fig.3.7 C) and Young's modulus was generated by force-displacement curve with an indentation depth of 1.5μm that reflects the stiffness of cells with negligible

effects of the substrate (69,70). We found the stiffness was significantly increased in *Lats1/2* CKO hearts (Fig.3.7 D).

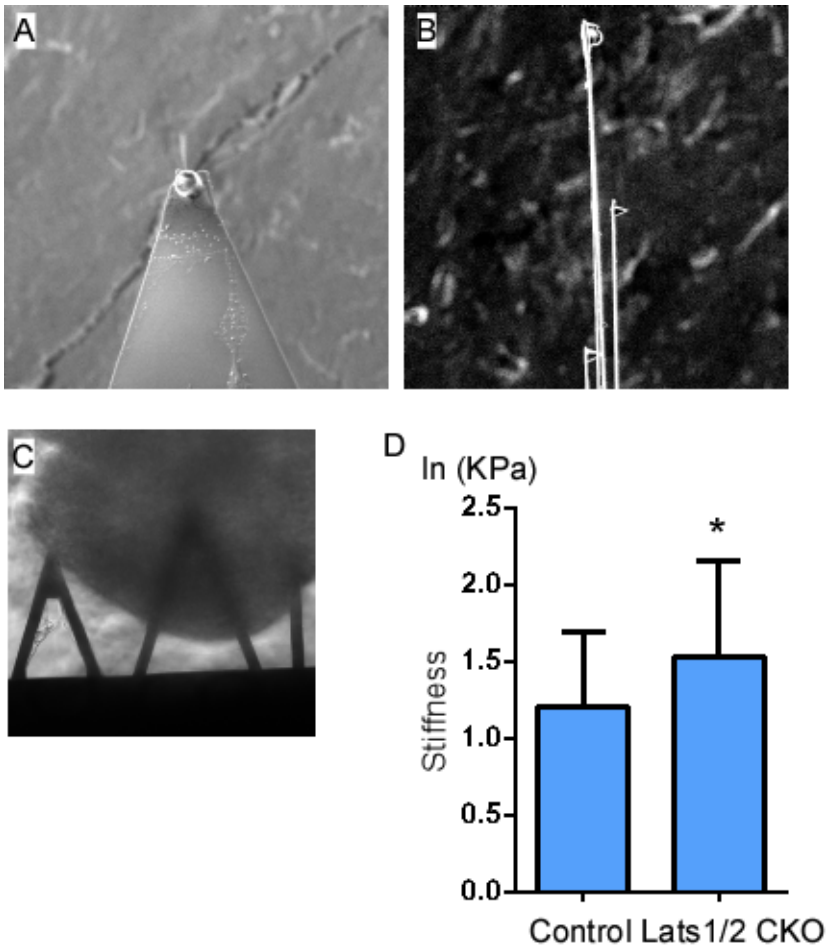

Figure 3.7. Aberrant stiffness in *Lats1/2* CKO hearts. (A-B) Images of AFM cantilever after attaching a 5μm silicon particle. (C) Epicardial cell stiffness was measured by AFM. (D) Increased cell stiffness in *Lats1/2* CKO. Original data was transformed by Ln to fit normal distribution.

Since the state of the cytoskeleton is closely related to cell shape, we examined cell shape used wheat germ agglutinin (WGA) staining. Control epicardial cells had a flat and compact morphology while the *Lats1/2* CKO mutant epicardial cells had a spherical shaped (Fig.3.8A). We next stained F-actin by phalloidin and reconstructed our confocal images into 3D and used super resolution microscopy to further evaluate cell morphology. While the control epicardial cells had a flat morphology with F-actin distributed with a slight preference for the basal aspect of the cell the spherical *Lats1/2* CKO epicardial cells contained a large amount of basal F-actin with nuclei pushed to one side of the cell (Fig.3.8 B). The change of F-actin was further validated by FACS analysis to examine intensity phalloidin dye which stains F-actin in epicardial cells. *Lats1/2* CKO cells showed enhanced phalloidin intensity(Fig.3.9). Taken together, these findings indicate that *Lats1/2* deletion in epicardium results in a more rigid cytoskeleton with excessive F-actin.

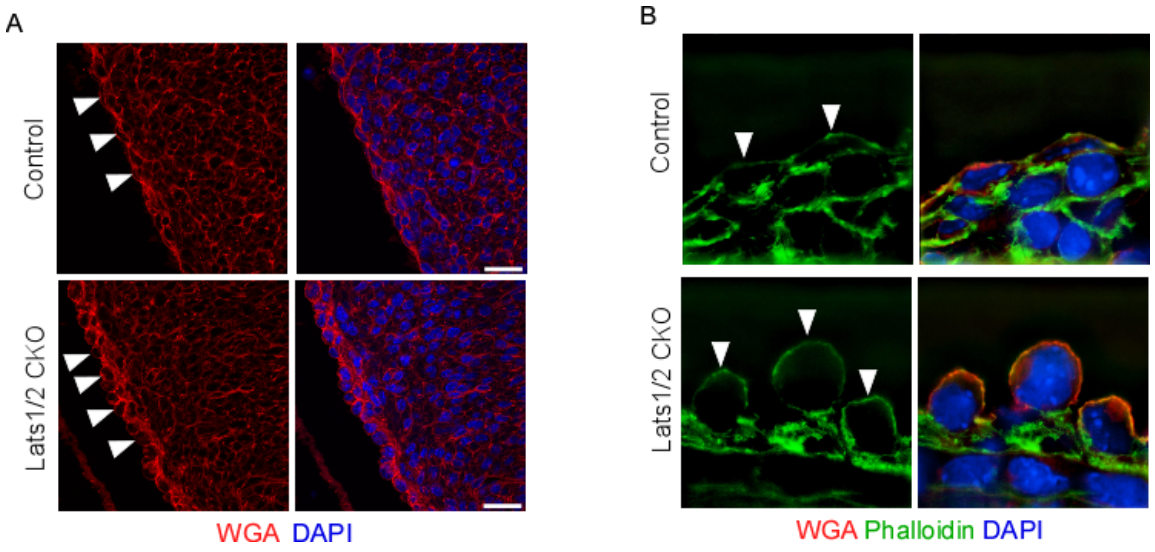

Figure 3.8. Disorganized F-actin and rounded cell shape in *Lats1/2* CKO epicardial cells. (A-B) Cell boundary was delineated by WGA staining. In *Lats1/2* CKO, epicardial cell shape became rounded compared with control (arrows). (E-F) Images of super-resolution microscopy found rounded cell shape and accumulation of F-actin in *Lats1/2* CKO epicardial cells.

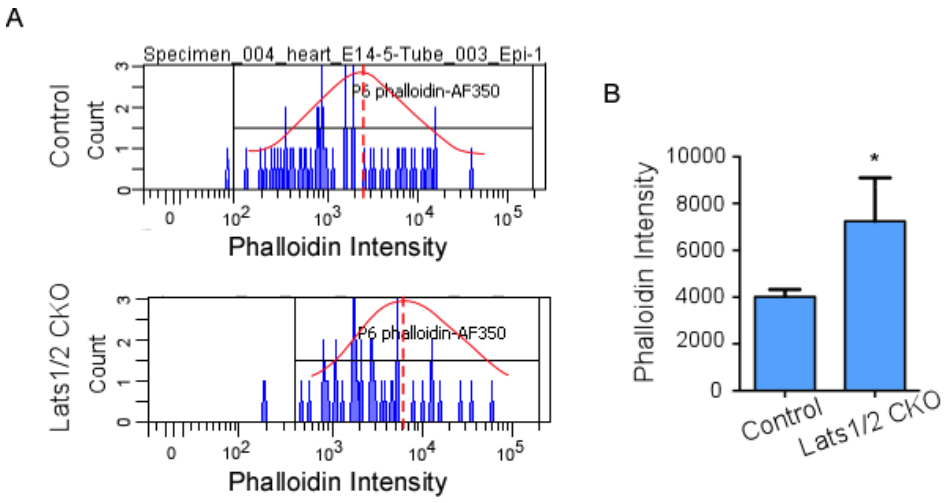

Figure 3.9. Enhanced F-actin intensity in *Lats1/2* CKO epicardial cells by FACS analysis.

Hippo pathway and mechanical signaling coordinately determine EPDC diversification

Up to this point, our data suggest that *Lats1/2* CKO mutant epicardial cells have a stiffer cytoskeleton that promotes endothelial cell expansion. The *Lats1/2* CKO mutant cells with their stiffer cytoskeleton have characteristics of cells found on a stiff extracellular matrix since cells respond to stiff matrix by making a more rigid cytoskeleton. The prediction from this would be that epicardial cells cultured on a stiff matrix will form endothelial cells at a higher frequency than cells on a softer, more physiologic matrix. Also since *Lats1/2* CKO cells already have a rigid cytoskeleton they should form endothelial cells on a softer matrix.

To test these predictions, we plated epicardial cells on a tunable stiffness matrix. We isolated epicardial cells from *Lats1/2* $^{flox/flox}$*; Rosa26*^{mTmG} embryos and infected them with an Adenovirus (Ad5) empty vector as control or Ad5-CMV-Cre to delete *Lats1/2* in vitro. Cells were grown on the stiff plastic substrate or the softer, physiologic-relevant 4 kilopascal (KPa) matrix to compare the influence of matrix stiffness on cell fate (Fig.3.10 A). When cells were grown on the plastic substrate both control and *Lats1/2* mutant epicardial cells were equivalently driven to become endothelial cells regardless of Lats kinase activity (Fig.3.10 B, C, F). In contrast, for cells grown on 4KPa that approximates physiologic stiffness in vivo, *Lats1/2* mutant cells but not control cells more frequently acquired the endothelial phenotype (Fig.3.10 D-F). Together, these findings indicate that biomechanical properties of the extracellular matrix are a major determinant of

epicardial cell diversification and that Hippo signaling acts to reduce cytoskeletal rigidity to inhibit endothelial cell proliferation.

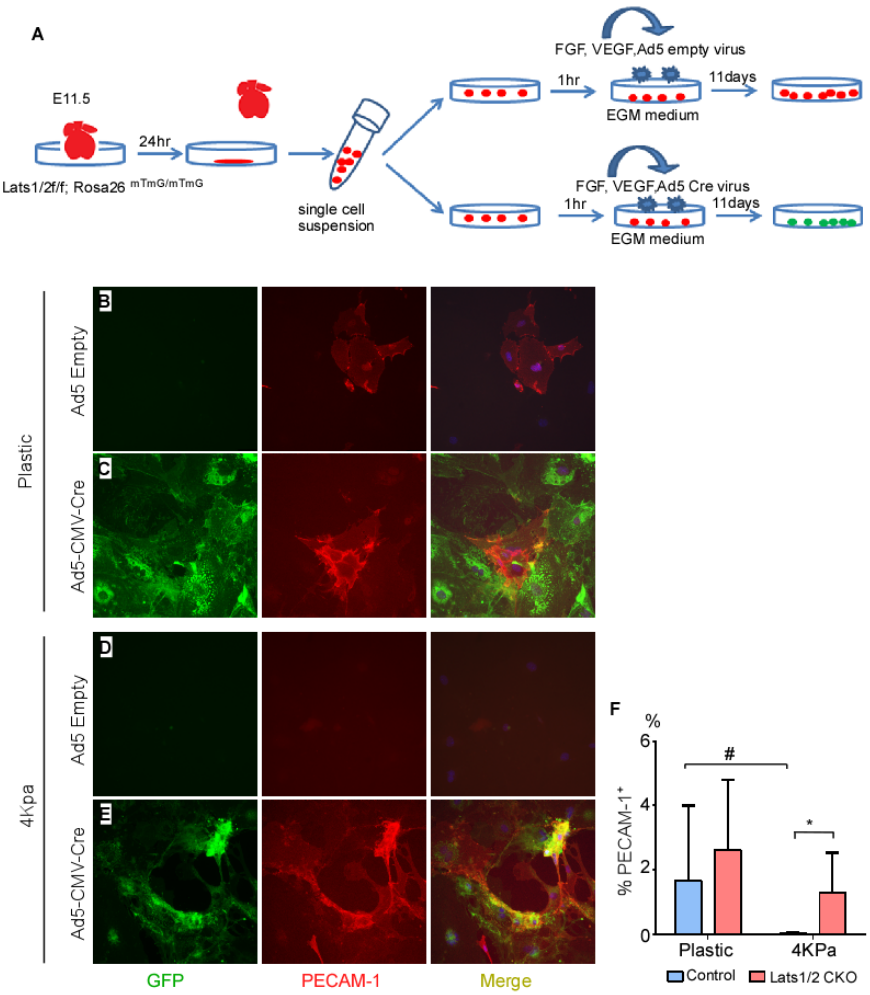

Figure 3.10. Lats kinase cooperates with matrix stiffness to regulate EPDC fate. (A) Workflow of inducing epicardial cell into endothelial cell. (B-F) GFP represented *Lats1/2* deficient cells. Endothelial cells identity were observed using PECAM-1 after 11-day culture. On plastic substrate, control and *Lats1/2* deficient epicardial cells both equivalently gave rise to endothelial cells. On 4KPa, increased endothelial cells derive from epicardial cells after knocking out *Lats1/2*. Sample size=5. Data are means ± SD. **P*=0.034 and $^{\#}P$= 0.007 were by Mann-Whitney U test.

Discussion

Mechanical signaling affects cell morphology and cell fate in mesenchymal stem cells in vitro (71). Here, we show that diversification of epicardial progenitor cells are sensitive to mechanical signaling. Lats kinase activity inhibits proliferation of endothelial cells depending upon the state of the actin cytoskeleton. At physiologic mechanical stress, Lats represses endothelial cell expansion but loses its inhibitory activity under high mechanical stress.

Mechanical signaling determines epicardial diversification

Our findings indicate that at E10.5-E11.5, after epicardial cells attach onto the myocardium and undergo EMT, Lats1/2 maintain epicardial cells in a specific mechanical state that determines their flat compact shape that is critical to promote smooth muscle and fibroblast development (Figure 3.11). In *Lats1/2* mutants, epicardial cells have a more rigid cytoskeleton as directly measured by AFM. The super-resolution images further support the notion that *Lats1/2* mutant epicardial cells had a stiffer cytoskeleton since mutant epicardial cells expressed excessive intracellular actin bundles and the nucleus was pushed to one side.

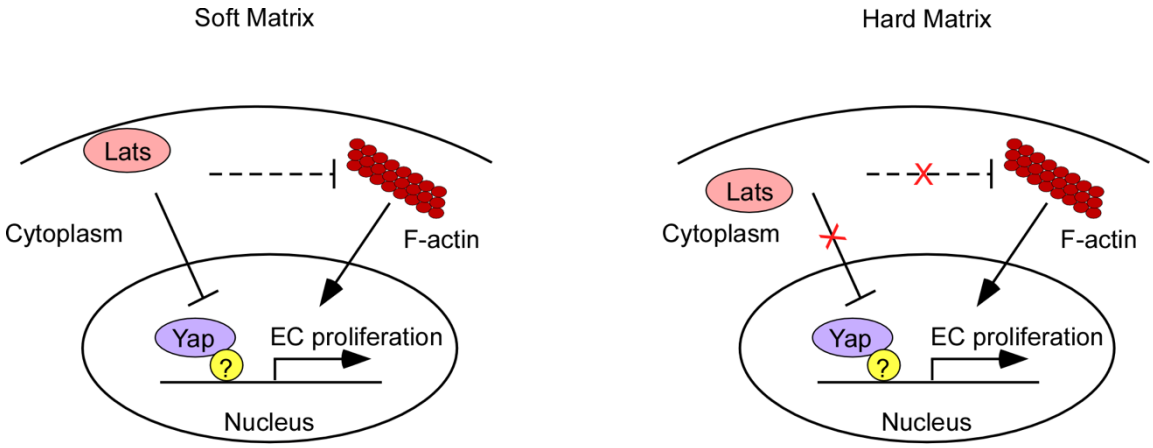

Figure 3.11. Schematic model of Hippo-mechanical dependent epicardial cell proliferation regulation. On soft matrix or physical relevant stiffness, Lats is recruited to the plasma membrane to inhibit Yap nuclear activity, which is speculated to initiate endothelial cell (EC) expansion with assistance of unknown transcription factor(s). Lats also exerts its inhibitory effect on F-actin polymerization, which is known to promote Yap nuclear activity. On hard matrix, Lats dissociates from plasma membrane and loses its inhibition on Yap and F-actin polymerization. Therefore, Lats kinase inhibitory activity on EC proliferation becomes dispensable.

The change in epicardial development observed in *Lats1/2* mutants resulted in fewer fibroblasts and smooth muscle cells that are important supporting cells for myocardium and vasculature. The lack of these essential supporting cells likely contributes to the failure of myocardial development with smaller hearts and embryonic lethality. Moreover, endothelial cells in *Lats1/2* mutants fail to complete tubulogenesis and branching morphogenesis. In addition to the reduction in the number of smooth muscle cells, our RNA-seq data showed that *Lats1/2* mutant epicardium expressed elevated levels of genes encoding components of the pro-vasculogenic FGF, Angiopoietin and PDGF pathways. Despite this, other genes

that are important for vascular morphogenesis, such as *Heg-1* and *Bmx*, were reduced and this undoubtedly contributed to failure of normal vascular morphogenesis.

Hippo pathway intersects with mechanical signaling in epicardial cells

Mechanical cues and actin cytoskeletal status have been identified as upstream inputs into Hippo signaling and/or Yap subcellular localization (57). With the exception of one study investigating Yap subcellular localization in a mixed cardiac cell population, there is little known about the interplay of mechanical signaling and Hippo signaling in the heart (72). Our findings suggest that in epicardial progenitors, the status of the cytoskeleton determines whether Lats inhibits endothelial cell proliferation. On a soft substrate of 4 KPa, Lats kinases inhibit endothelial development. In contrast, when epicardial explants were cultured on plastic, modeling a stiff matrix, endothelial markers were expressed whether or not Lats activity was present. These data suggest that Lats activity is dispensable when cells are cultured on stiff matrix and express large amounts of polymerized actin.

Based on experiments performed in Drosophila, one possible explanation is that Lats is recruited to the plasma membrane and activated, perhaps by Neurofibromatosis 2 (Nf2), in cells that have less polymerized actin (73). Actin cytoskeletal disruption using the actin polymerization inhibitor Latrunculin B promotes recruitment of Lats by Nf2 to the plasma membrane with activation of Lats kinase activity. In epicardial cells on a softer, physiologic substrate, Lats

inhibits endothelial cell proliferation while promoting a less rigid cytoskeletal organization and Yap cytosolic localization (Figure 7). Further work is required to determine if Nf2 recruits Lats kinases in the epicardium. An alternative possibility is that polymerized F-actin induces a Lats kinase inhibitory activity. In conditions, such as a soft extracellular matrix where there is less polymerized actin within the cell, the repressive activity inhibiting Lats kinase is lost (74).

It is also notable that inactivation of the serum response factor (SRF) cofactor myocardin related transcription factor (MRTF) in epicardium results in a strong phenotype that has some similarities to what we observe in the *Lats1/2* epicardial mutants (75). Like Yap and Taz, the SRF-MRTF factors respond to mechanical signaling and have been reported to have overlapping target genes to that of Yap and Taz (76). It will be interesting to investigate potential functional overlap between Yap/Taz and MRTF in more depth.

Hippo signaling regulates the cellular mechanical state

Our study highlights the notion that in addition to being regulated by cytoskeleton, Hippo signaling can also affect cytoskeleton organization and cellular mechanical properties. It has been shown that loss of function mutations in Hippo core kinases leads to increased F-actin accumulation in the Drosophila wing disc (77). In our study, we found that the transcripts of genes associated with actin are upregulated, such as genes encoding Dynein motor proteins, the actin-contractility regulators Pak6 and Myl12b, and the Cgnl1 actin binding protein that links actin to adherens and tight junctions. Recent data indicate that Yap can

directly regulate genes that promote actin polymerization in the myocardium (2). It is conceivable that in the epicardium Yap also promotes expression of genes that enhance actin polymerization and promote cellular protrusions.

Epicardial plasticity and contribution to coronary endothelium

Under physiologic conditions, Wt1-lineage epicardial precursors contribute very few cells to coronary endothelial cells (reviewed in (78)). Our findings indicate that the Wt1-lineage epicardium does have the potential to generate coronary endothelial cells but that the Hippo pathway represses endothelial cell proliferation. Interestingly, our findings support the notion that Hippo pathway repression can be released by increases in mechanical signaling. Therefore, the Hippo pathway, cytoskeleton and perhaps extracellular matrix strike a balance to maintain the epicardial development into smooth muscle and fibroblasts.

CHAPTER IV

HIPPO KINASE LATS IS REQUIRED IN ADULT HEART HOMEOSTASIS MAINTENANCE AND INJURY RESPONSE

Introduction

Unlike lower vertebrates, adult mammalian heart has very limited regeneration capacity. Once heart is injured, myocardium will be replaced with fibrotic scar and heart function will be deteriorating with disease progressing. Currently, most studies have been focusing on cardiomyocytes. However, cardiac fibroblasts, which contribute to fibrosis *per se*, is under studied. As one of most prevalent cell types in heart, except its role in producing extracellular matrix to support heart structure, the cross-talk of cardiac fibroblast with other cell types during homeostasis and injury response is not well recognized.

Hippo signaling is a highly conserved pathway in limiting organ size through regulating cell proliferation and apoptosis. Here is our study, under non-injury condition, we inactivated potent Hippo signaling kinases Lats1/2 specifically in cardiac fibroblast. The homeostatic balance between fibroblasts and other cell types was disrupted by pronounced expansion of *Lats1/2* deficient fibroblasts. By this genetic model, we disclosed an interaction between fibroblasts and immune cells. Additionally, we found Lats1/2 kinases are required to suppress Myc expression to prevent elimination of less competitive neighboring cells. Under ischemia stress, the effect of loss of *Lats1/2* was augmented. Collectively, our

data revealed an essential function of Lats1/2 kinase in cardiac fibroblast under homeostasis, which also prepare fibroblasts for injury response.

Materials and Methods

Mice

Tcf21^{iCre}*(31)*, *Lats1/2*$^{flox/flox}$ (3), *Yap/Taz* $^{flox/flox}$(10),*Rosa26*^{mTmG} (11) alleles have been described previously. Mice were on a mixed genetic background of C57BL/6 and 129SV. Tamoxifen was dissolved in peanut oil with 5% ethanol at 10mg/ml. 3mg tamoxifen was administrated to 6-8 week old mice by intraperitoneal injection for 6 days.

Echocardiography

Cardiac function was analyzed by echocardiography every week post surgery. Imaging were performed on VisualSonics Vevo 2100 system with 550-s probe. B-mode images and M-mode images were captured on short-axis projection. Ejection fraction, fraction shortening, and cardiac output were calculated using cardiac measurement package installed in Vevo2100 system.

Histology and immunofluorescence

Fibroblast-specific-*Lats1/2* mutant mice (*Lats1/2* CKO) were generated by crossing *Tcf21*^{iCre} with *Lats1/2*$^{flox/flox}$; *Rosa26*^{mTmG}. Control were generated by crossing *Tcf21*^{iCre} with *Rosa26*^{mTmG}. For histology and immunofluorescence staining, hearts were fixed in 4% PFA overnight at 4°C and dehydrated in a serial ethanol, xylene and embedded in paraffin. Sections of 7μm thick sections were prepared for staining. Masson's Trichrome staining was performed according to

manufacture's instruction (Sigma, HT15). Antibodies used for immunofluorescence staining were as follows: GFP (1:200, Abcam ab290, ab6673), PECAM-1(1:100-1:200, BD Pharmingen 550274), c-Myc [Y69](Abcam, ab32072). To visualize some antigens, Alexa-647 was employed. When applications required green and red co-staining, sections were pre-treated with 0.3% H_2O_2 in PBS for 20min at room temperature to quench the endogenous GFP and Tomato signals, which come from the *Rosa26*^{mTmG} reporter line. In some cases, Tyramide Signal Amplification Systems (1:100, Perkin Elmer) were used to amplify signal. TUNEL assay was performed according to manufacture's instruction (Progema, G3250). Immunofluorescence images were captured on a Leica TCS SP5 confocal microscope.

EdU incorporation assay

Mice after MI were injected with EdU (0.5mg) 24hr before collecting heart tissue. Hearts were processed as described above. EdU incorporation was assayed by Click-it EdU imaging kit (Life Technologies).

Western Blotting

Protein level was detected by Western Blotting, which was performed as previously described(3). Mouse fibroblast cells line NIH3T3 was used for western blotting(ATCC®CRL-1658). siRNA used were as follows: Non-targeting siRNA(siNC) (Dharmacon, D-001810-02-05), Mouse Lats1 (siLats1) (Dharmacon,L-063467-00),mouse Lats2 (siLats2)(Dharmacon,L-044602-00) and mouse Myc (Dharmacon). RNAiMAX (Thermo Fisher Scientific) was used for

transfection. Cells were treated with siRNA for 48 hours and harvest for protein detection. Antibody used for Western Blotting were as follows: anti-Myc(Abcam), anti-Lats1 (Cell Signaling Technology), Gapdh(Abcam).

FACS analysis for cell cycle

Cardiac fibroblasts were isolated from hearts at 1 week post MI by langendorff perfusion. GFP positive cells were gated for analysis and DAPI were used for analyzing DNA content. FACS were performed on BD Biosciences SORP Aria I and BD Biosciences LSRII and cell cycle modelling were processed with FlowJo software.

RNA sequencing

For TRAP/Ribosome-associated RNA-seq, RNA pull-down from 1week post MI herats were performed according to McKnight Lab protocol (http://depts.washington.edu/mcklab/RiboTag.html). Anti-HA antibody (Cell signaling technologies) were used for pull-down. Ribosome-associated mRNA were extracted using RNeasy Plus Micro Kit(Qiagen). mRNA were further purified by Dynabeads mRNA DIRECT Micro Kit (Life Technologies) and then converted to barcoded cDNA libraries for RNA sequencing on the Ion Proton System using Ion Total RNA-Seq Kit v2.0(Life Technologies) and RNA-Seq Barcode 01-16 Kit(Life Technologies). RNA-seq was performed on Ion Proton. Around 12 million reads were generated for transcripts quantification in each sample. Paired-end RNA Seq reads were aligned to mm9 (*Mus musculus* assembly July 2007). Raw read counts were normalized and analyzed for differential gene expression by

DESeq2. Metascape (http://metascape.org/) was used for Gene Ontology (GO) analysis to extract the information on gene set and gene network. R and RStudio were used for generating heatmap.

For FACS-sorted RNA-seq, GFP positive cells were isolated using Langendorff perfusion of heart 3 days after 6-dose tamoxifen injection. Because of limited GFP cells, sorted cells were directly collected in RLT lysis buffer from RNeasy Plus Micro Kit (Qiagen) and SMART-Seq Ultra Low Input RNA Kit to prepare RNA-seq library (Clonetech Laboratories). Sequencing and analysis procedures were same as above for TRAP RNA-seq.

Results

Deficiency of *Lats1/2* in adult cardiac fibroblast results in abnormal tissue accumulation and injury response

To investigate the function of Lats1/2 kinases in adult cardiac fibroblast, we used Tcf21iCre to inactivate *Lats1/2* in cardiac fibroblast at adult stage. Cre activity was induced by tamoxifen injection. We subjected these animals for either sham or myocardial infarction surgery to examine the role of Lats1/2 in homeostasis and injury response (Fig.4.1 A). In sham group, majority of *Lats1/2* CKO mice maintained alive until 3 weeks after surgery. However, in MI group by occluding left descending artery (LAD-O), all mutant mice died by 3 weeks after ischemia (Fig.4.1 B). Gross heart morphology of sham mutant heart at end stage (3 weeks after surgery) (Fig.4.2 A, left) showed aberrant patch-pattern like white tissue in ventricles(star), and atria were pale, enlarged and stiffened. Right atrium

displayed much more severe abnormality(star). Surprisingly, MI mutant significantly exacerbated this phenotype in sham hearts (Fig.4.2, right), abnormal tissue accumulation expanded to the most region below the suture where artery occlusion performed(star). Atria in MI heart also had similar stiffened and enlarged morphology as in sham especially right atrium(star).

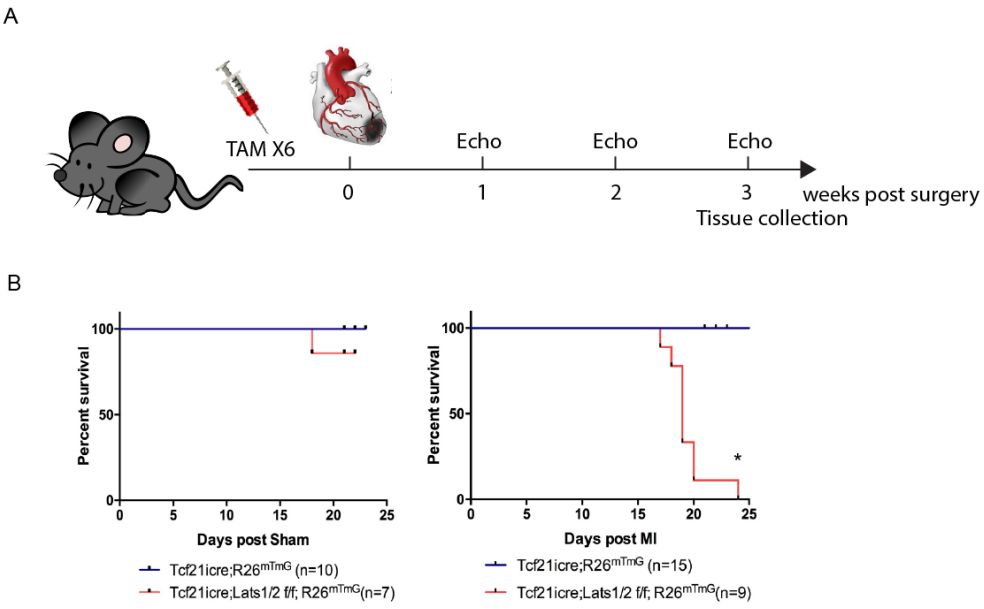

Figure 4.1 Experiment design and survival rate. (A) Adult mice at 6-8 week old were subjected to 6 consecutive dose of tamoxifen. Sham or MI surgery was performed after. Heart function was monitored by echocardiography every wek after surgery and tissues were collected at 3 weeks post surgery. (B) Survival rate of control (blue line) and *Lats1/2* CKO mice (red line) in sham group (left) and MI group(right) (*p<0.01 by Kaplan-Meier survival curve analysis).

We sectioned these hearts and examined histology by Masson's Trichrome staining. In sham group (Fig.4.2 left), the aberrant tissue accumulation in *Lats1/2* CKO hearts, mainly located at outer and inner surface of ventricular wall(stars). The accumulation at latter spot resulted in significant cardiac lumen restriction. These abnormal spots are not stained red compared with sham control, suggesting they are lack of muscle features. More profoundly, in MI group (Fig.4.2 right), instead of a compact scar formation after MI in control hearts(arrow), the region below the ligation was almost completely replaced with this aberrant type of tissue(star), and little myocardium and cardiac lumen were maintained. We reduced the activity of Lats1/2 downstream effector Yap/Taz by creating heterozygous alleles Yap and Taz and found the phenotype was partially rescued and some myocardium were maintained. This suggests Yap/Taz mediated the effect of *Lats1/2* deficiency. Moreover, within this abnormal tissue, we did not detect obvious collagen deposition, which results from injury response and scar formation, as blue stained in control MI hearts. Cardiac function monitored by ultrasound also showed consistent change. In Sham group(Fig.4.3 upper row), ejection fraction and fraction shortening were enhanced in mutant hearts, which probably are attributed to ventricular wall thickening and increase of contractility to compensate lumen restriction. Nonetheless, cardiac output, which is an index reflecting overall volume of blood pumped by heart per minutes, was significantly reduced in both sham (Fig.4.3 upper row) and MI groups (Fig.4.3 bottom row).

Taken together these data elucidate that Lats1/2 in adult cardiac fibroblast is required for maintaining tissue homeostasis and normal response to ischemia.

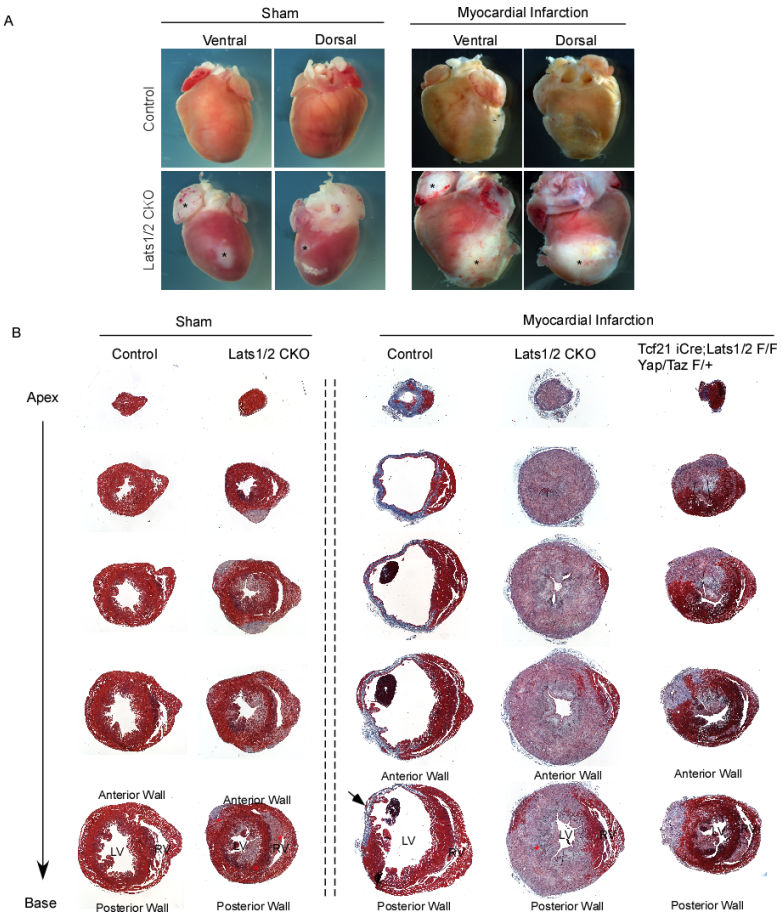

Figure 4.2. Gross heart morphology and histology. (A) Gross heart morphology at 3 weeks post surgery. *Lats1/2* CKO hearts in sham group (left) showed abnormal tissue accumulation. Atria were stiffened and enlarged(stars). *Lats1/2* CKO hearts in MI group (right) had a more profound phenotype with aberrant tissue expansion below the artery ligation(starts). Atria also appeared loss of compliance. (B) Histology was examined by Masson's Trichrome Staining. Red stains muscle and blue stains collagen. In sham group(left), abnormal tissue located at outer and inner surface of heart and resulted in cardiac lumen restriction. In MI group, control hearts were with compact scar (arrowheads), but mutant hearts displayed significant aberrant tissue expansion which resulted in disappearance of cardiac lumen(stars). Reducing activity of Yap/Taz seemed to partially rescue severity of phenotype of *Lats1/2* CKO hearts. Some myocardium was maintained.

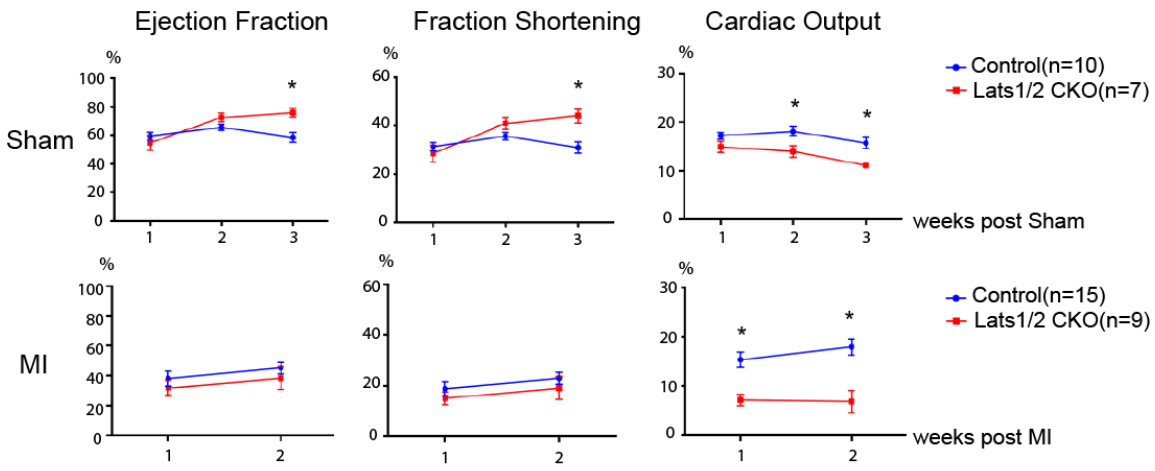

Figure 4.3. Cardiac function monitored by echocardiography. In sham group (upper row), ejection fraction and fraction shortening were enhanced but cardiac output was reduced in *Lats1/2* CKO (red lines) compared with control (blue lines). MI group (bottom row) mutant showed reduction of cardiac output since first week after surgery (t-test, *p<0.01).

Deficiency of *Lats1/2* unleashes cardiac fibroblast proliferation capacity and defective collagen deposition

To gain the insight of molecular mechanism of *Lats1/2* CKO heart phenotype, we performed Translating Ribosome Affinity Purification (TRAP)/RiboTag RNA-seq. At 1 week after MI, RNA associated with translating ribosome was purified and subjected to RNA-seq (Fig. 4.4 A). Gene Ontology(GO) analysis of differential

expressed genes showed gene associated with cell cycle, DNA metabolic process and ribosomal biogenesis were significantly up-regulated. Meanwhile, extracellular matrix organization, and actin filament-based process, and blood circulation associated genes, which are the key process of injury response, were greatly down-regulated (Fig.4.4 B). To validate our findings in RNA-seq, we examined DNA synthesis and cell cycle in *Lats1/2* deficient cells. EdU incorporation was performed 1day, 3days, 5 days and 7 days post MI(Fig.4.5). GFP from Rosa26^{mTmG} allele was used to trace fibroblast upon cre activation. We found in control hearts, at Day3, fibroblasts reached the peak of active DNA synthesis, and gradually tapered off at Day5. Interestingly, *Lats1/2* CKO showed similar DNA synthesis rate until Day3, but kept elevating at Day5 and maintained high at Day7. In addition, great amount of GFP positive cells distributed in patch pattern in mutant heart (Fig.4.5A Day7 *Lats1/2* CKO), corresponding to the the area of aberrant tissue we observed in histology, which suggests the origin of the tissue is mutant cardiac fibroblast.

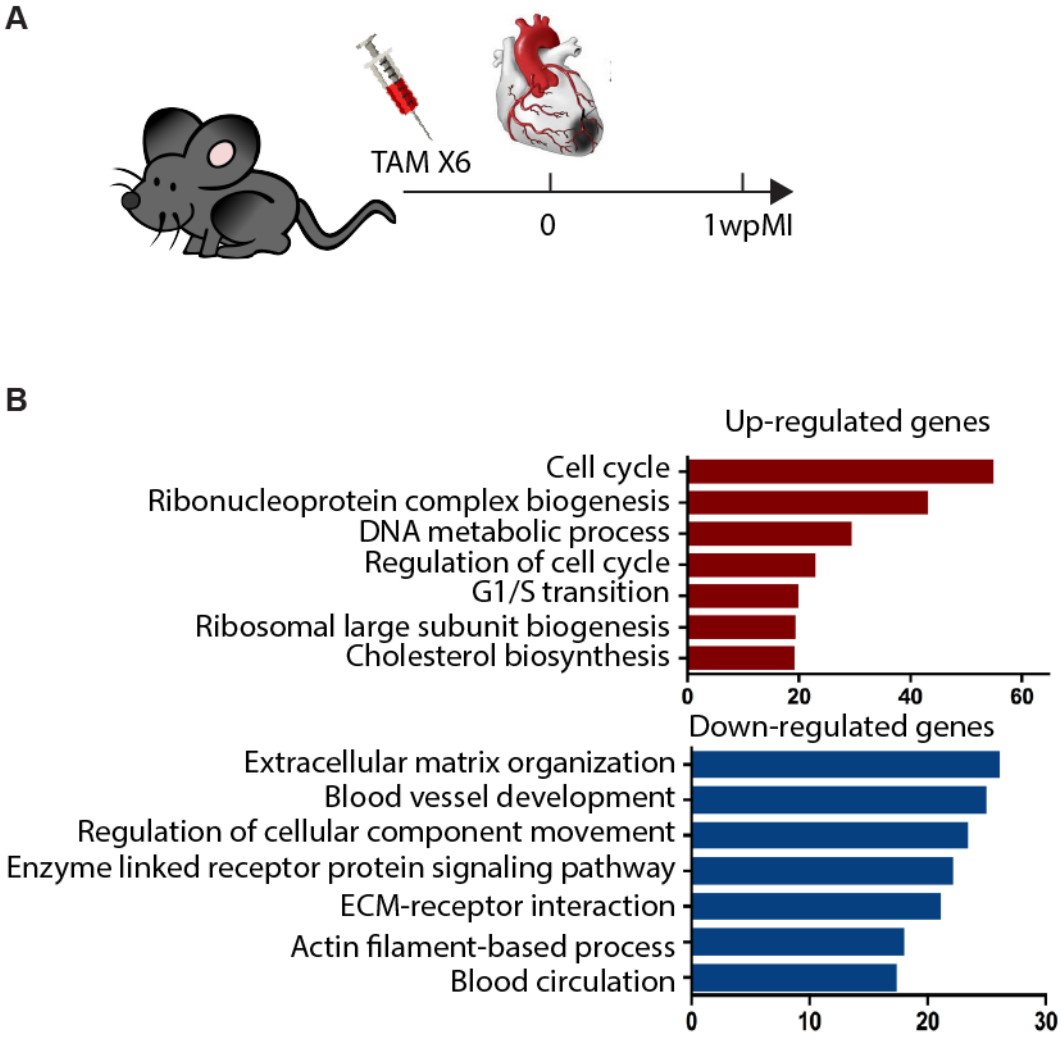

Figure 4.4. Translating Ribosome Affinity Purification (TRAP)/RiboTag RNA-seq. (A)Working flow of TRAP RNA-seq. (B) GO analysis of differentially expressed genes from TRAP RNA-seq.

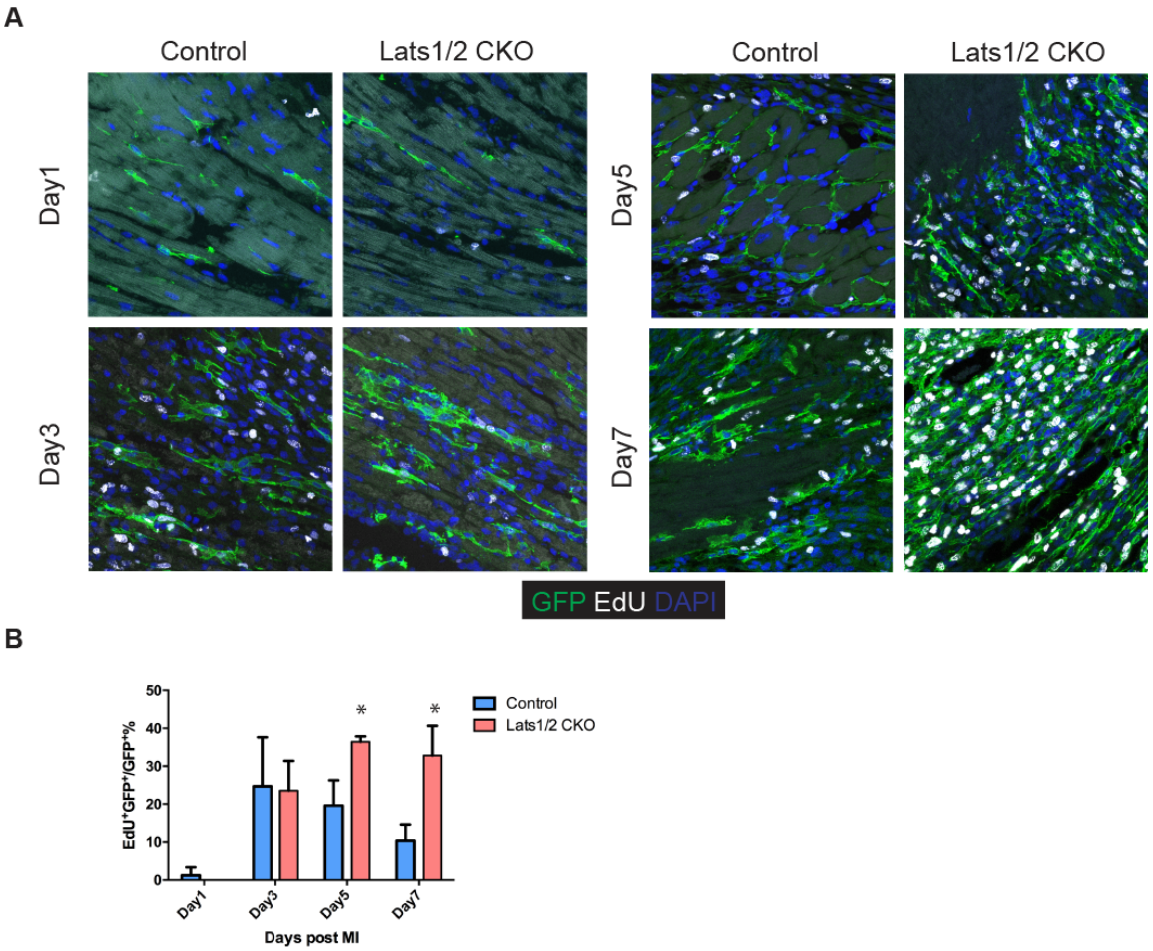

Figure 4.5. EdU incorporation assay. (A)EdU was inject 24 hours before tissue collection. Heart at 1 day, 3 days, 5 days and 7 days post MI were harvested. GFP labels Tcf21 derived cardiac fibroblasts and co-stained with EdU. (B) Quantification of EdU positive cardiac fibroblast over time.

We also analyzed cardiac fibroblast cell cycle by FACS at 7 days post MI (Fig.4.6). According to DNA content, we assigned cells with 2N and 4N into G1 and G2/M phase respectively, cells with DAPI intensity in between 2N and 4N to S phase, and cell with DNA content more than 4N to super G2 phase. In the *Lats1/2* CKO hearts, more cardiac fibroblast distributed at S phase and less in G1 phase, which suggest more cells involve in active cell cycle. To be noted, for the portion of cell in super G2, which is a readout of polyploidy and genome instability of malignant tumor, differences were not significant between control and mutant. Indeed, inactivation of Hippo components Lats1/2 has been reported in several tumor model, while here the data suggests removing *Lats1/2* in cardiac fibroblast results in fibroblast hyperproliferation but has not yet to become cancer cell. Another finding from RNA-seq was loss of collagen deposition in mutant heart, and Masson's Trichrome staining further corroborated this(Fig.4.7). Taken together, we concluded that inactivating *Lats1/2* tremendously unleashes cardiac fibroblast proliferation capacity and impaired ischemia induced collagen deposition.

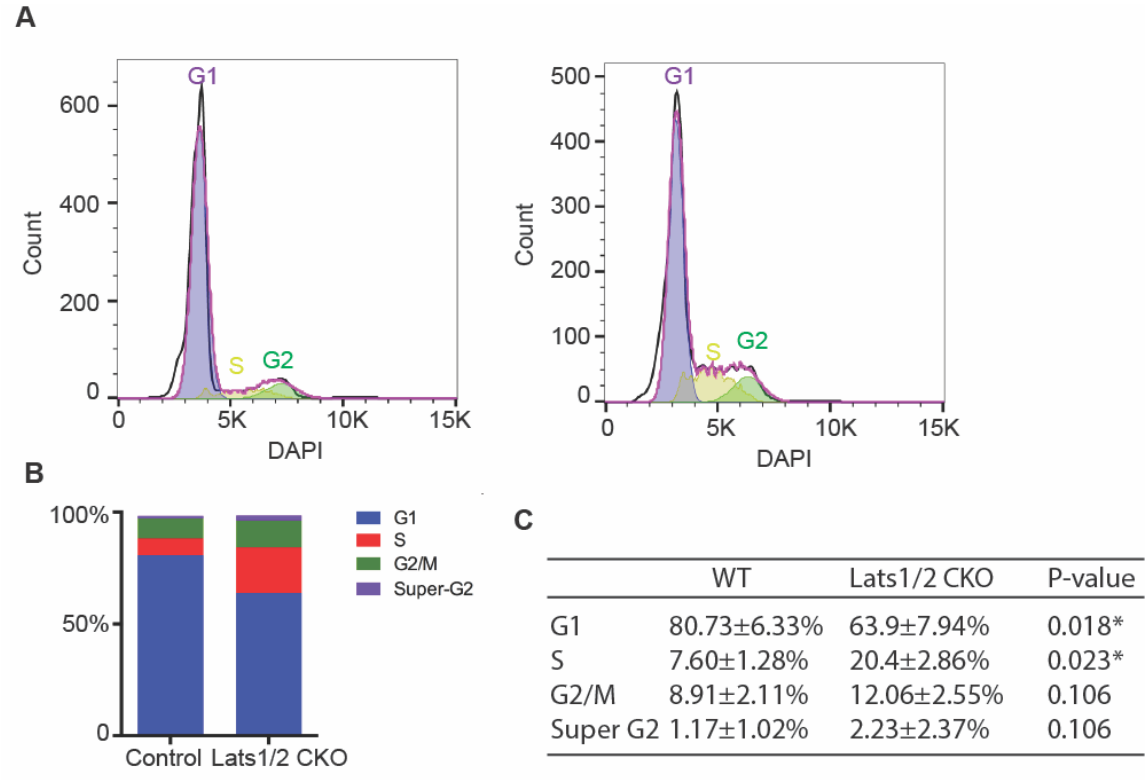

	WT	Lats1/2 CKO	P-value
G1	80.73±6.33%	63.9±7.94%	0.018*
S	7.60±1.28%	20.4±2.86%	0.023*
G2/M	8.91±2.11%	12.06±2.55%	0.106
Super G2	1.17±1.02%	2.23±2.37%	0.106

Figure 4.6. FACS analysis of caridiac fibroblast 1 week post MI. (A) GFP positive cells different cell phase distribution. (B-C) Composition of cells at different cell cycle phases. *p<0.05 by Chi-square test.

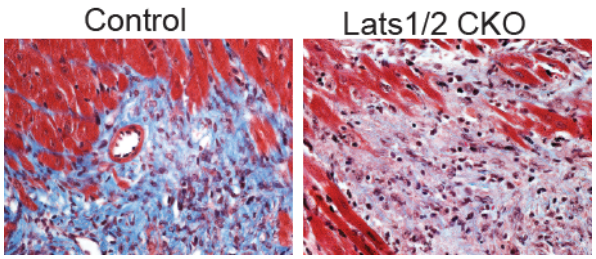

Figure 4.7. Masson's Trichrome staining of heart 3 week post MI. Red stains cardiac muscle and blue stains collagen deposition.

Lats1/2 inactivation leads to Myc activation and death of non-cardiac fibroblast

To capture early molecular event and dissect *Lats1/2* inactivation from MI induced phenotype, we focused on 3 days post tamoxifen injected heart. GFP positive cells were sorted and subjected to RNA-seq analysis. Consistent with TRAP RNA-seq, whose cells were collected at 1 week after MI, *Lats1/2* CKO cells showed significant increase of cell cycle genes. Notably, this dataset also revealed Myc target genes were up-regulated, suggesting Myc is an immediate effector of *Lats1/2* deficiency (Fig.4.8, upper panel). Interestingly, in the down-regulated genes, we uncovered interferon responding genes and innate immune response genes, and genes associated with T cell activation (Fig.4.8, lower panel, Fig.4.9), which suggests a regulatory role of fibroblast on immune cells and cross-talk between these two cell types.

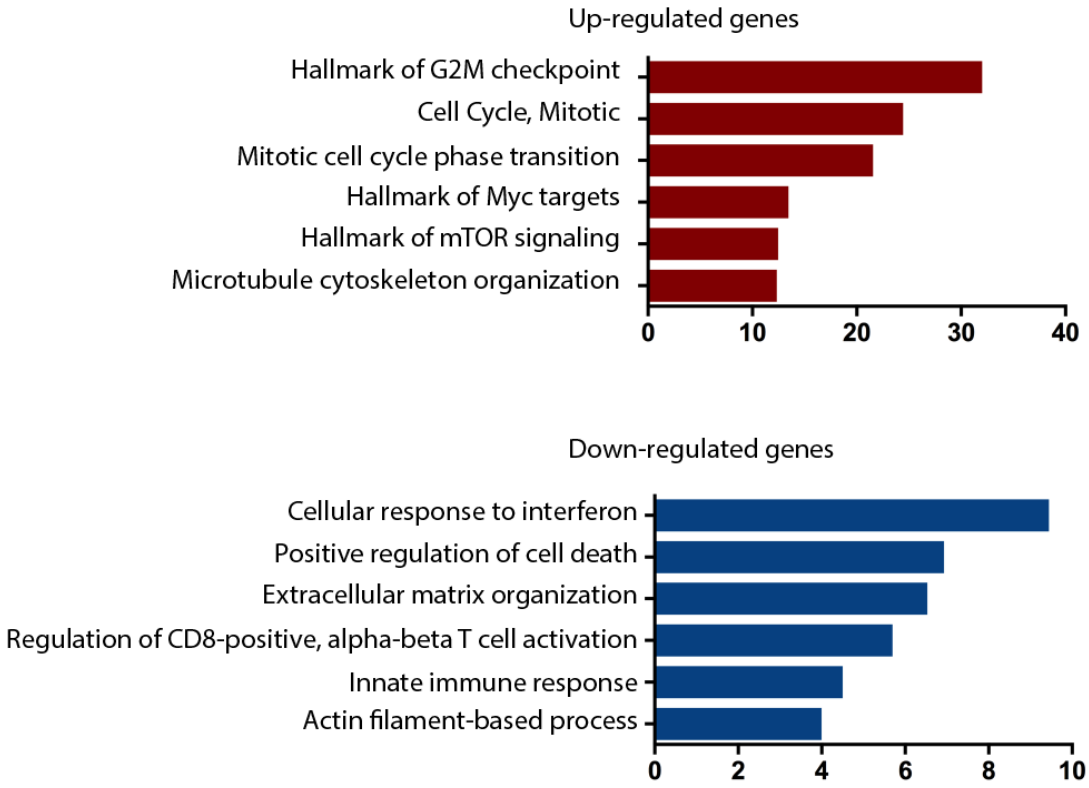

Figure 4.8. GO analysis of differential expressed genes from isolated fibroblasts of hearts 3 days after tamoxifen injection. (Upper panel, red), up-regulated genes in *Lats1/2* CKO cells compared with control includes genes associated with cell cycle and Myc targets; (Lower panel, blue), down-regulated genes in *Lats1/2* CKO cells compared with control contains genes associated with immune response and extracellular matrix organization.

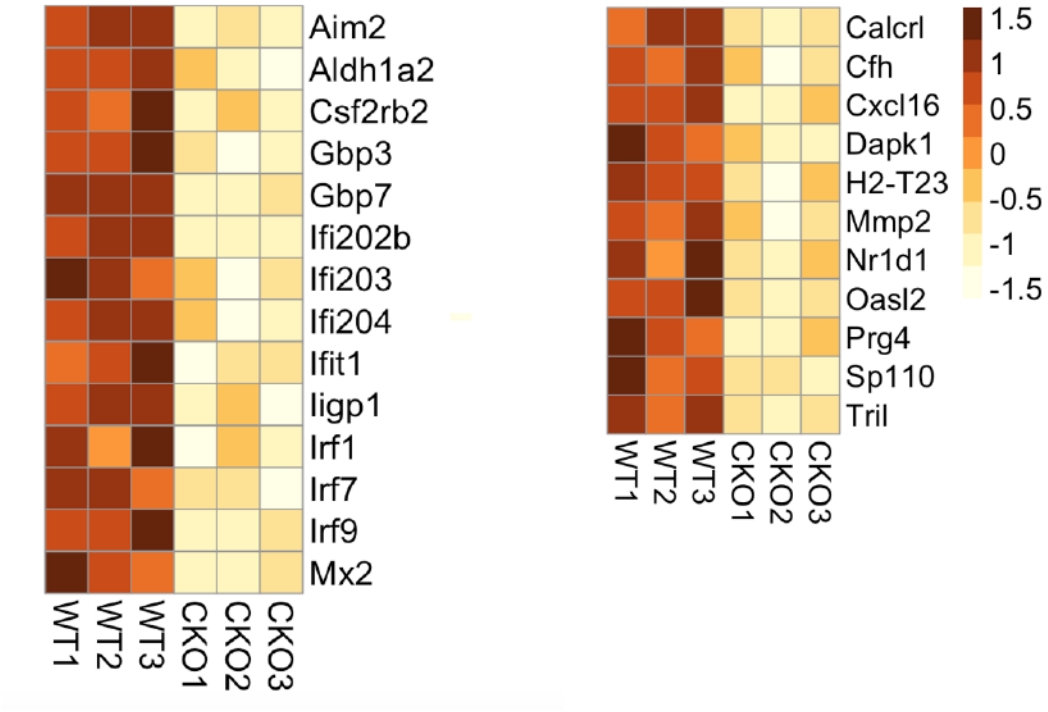

Figure 4.9 Interferon responding genes and innate immune regulatory genes were down-regulated.

We next validated the c-Myc expression level *in vitro* and *in vivo*. We used siRNA to knockdown *Lats1/2* in mouse fibroblast cell line 3T3 cells and c-Myc were increased in cells treated with siRNA against *Lats1/2*(Fig.4.10). We also examined c-Myc on tissue sections from heart without surgery. We found mutant cells which were GFP positive had significantly enhanced c-Myc level (Fig.4.11).

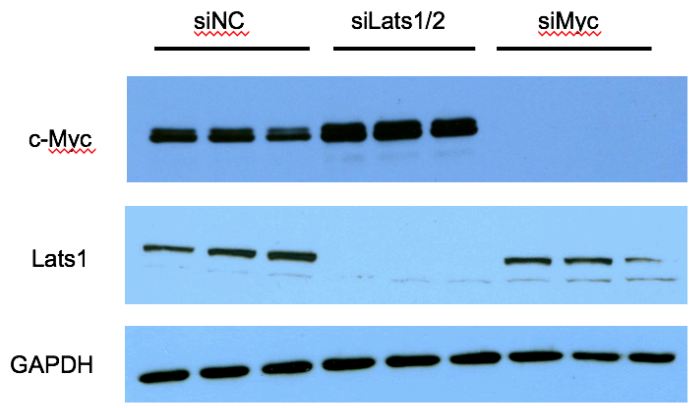

Figure 4.10. Increased c-Myc expression in *Lats1/2* knockdown cells. NIH 3T3 cells were treated with siRNA against Lats and cells were hearvested 48hours. Protein level was detected by Western blotting.

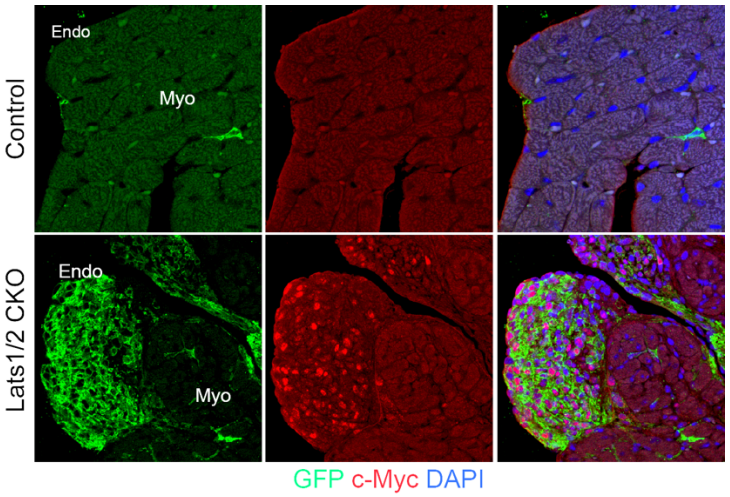

Figure 4.11. Enhanced c-Myc expression in *Lats1/2* deficient fibroblasts. Tissue were collect at 3 week post tamoxifen. GFP labelled Tcf21 derived cells.

Since c-Myc has been shown to act together with Hippo signaling component TEAD to drive cell competition(79), and blood vessel associated genes were down-regulated in TRAP RNA-seq (Fig.4.4), we performed PECAM staining to detect endothelial cell distribution. In control hearts or intact myocardium in mutant hearts, endothelial cells were densely distributed. However, in the region where abnormally occupied by hyperproliferative mutant fibroblasts showed sparse endothelial cells(Fig.4.12). Furthermore, TUNEL assay for detecting cell apoptosis demonstrated significantly increased cell death in *Lats1/2* CKO hearts, and this mainly took place in GFP negative, non-cardiac fibroblasts (Fig.4.13). Collectively, these data suggested cell competitive interaction between super competitor *Lats1/2* deficient fibroblasts and other weak competitors such as endothelial cells, which was eliminated by cell apoptosis.

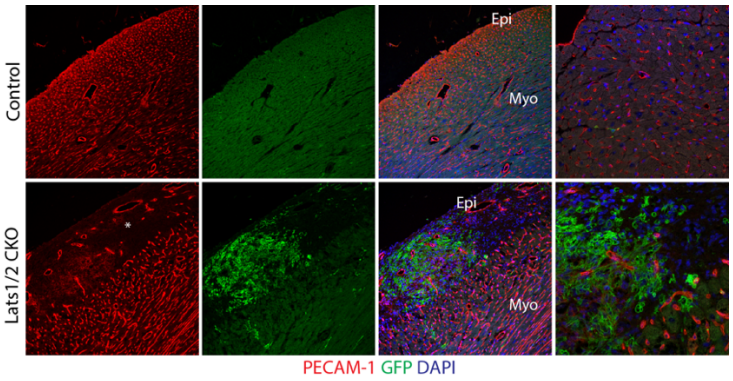

Figure 4.12 Reduction of endothelial cell density in *Lats1/2* CKO hearts. Regions with abnormal tissue accumulation in *Lats1/2* CKO showed reduced endothelial cell density(star). Tissue were collect at 3 week post tamoxifen. GFP labelled Tcf21 derived cells.

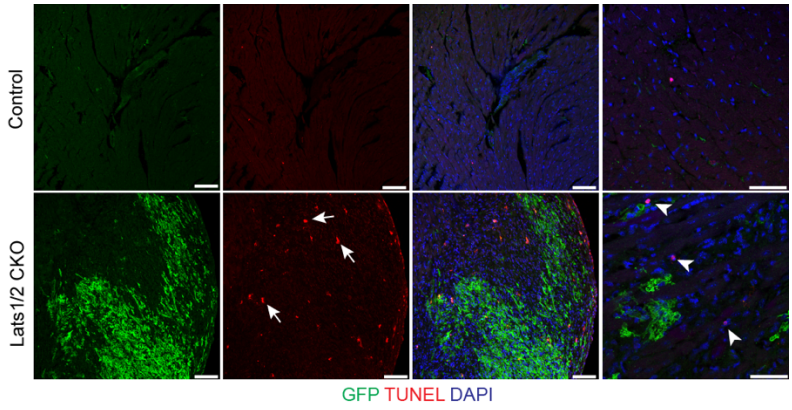

Figure 4.13. Pronounced cell death in *Lats1/2* CKO hearts detected by TUNEL assay. TUNEL staining (red, arrows, left three columns) indicated cell apoptosis and GFP labelled Tcf21 derived cells. Cell death was mainly in non-cardiac fibroblasts (arrowheads, right column). Tissue were collect at 3 week post tamoxifen.

Discussion

Interferon mediated cross-talk between fibroblast and immune cell

As two major cell types involving injury response and cardiac fibrosis, fibroblasts and immune cells their studies mostly have been done under injury model. However, little is know about how they are at resting condition to interact with each other and maintain homeostatic balance. Investigating the interaction mechanism at resting condition would help us understand the disease progression when this balance is disrupted, such as myocardial infarction.

Previously studies have shown that mesenchymal stromal cells and fibroblast are not immunologically inert. However, to exert immunoregulatory effect, they have to be exposed to certain inflammatory milieu as a prerequisite.

Here in our study *Lats1/2* deficient genetic model specifically in cardiac fibroblast resulted in abnormal cardiac fibroblast expansion. It appeared to be a good interfering model to interrupt the interaction between fibroblasts and other cell types. Surprisingly, *Lats1/2* CKO fibroblasts showed significantly down-regulation of the genes responding to inflammatory cytokines interferon gamma and interferon beta, such as Ifi202b, Ifi203, Ifi204, Aim2, Irf1, Irf7 and Irf9(80-82). These data suggest that fibroblasts are constantly under the stimulation of immune cytokines, which are partly from resident immune cells. On the other hand, we also observed the immunoregulatory role of fibroblasts were attenuated as well. Chemokine Cxcl16, major histocompatibility complex (MHC), class I, and hemochromatosis protein Hfe, which are associated with T cell activation and MHC I antigen presentation were down-regulated(83,84).

Overall, our data support a model that the crosstalk between cardiac fibroblast and resident immune cells in the heart under homeostasis is mainly mediated through interferon family.

Cell competition and cardiac homeostasis

Cell competition is an evolutionarily conserved mechanism to maintain tissue homeostasis that “fit” cells with higher anabolic capacity eliminate “unfit”

cells with lower anabolic capacity(85). Cell with relatively higher activity of Myc are supercompetitor which induce death of their neighboring cells(86).Hippo signaling components TEAD and Yap have been shown to initiate cell competition(79). However, all these studies are either studied in *Drosophila*, or *in vitro* system.

Here we exhibited a good system for studying Hippo signaling and cell competition *in vivo*. In *Lats1/2* deficient fibroblasts, we observed pronounced Myc up-regulation, while non-mutant cell in *Lats1/2* CKO hearts, such as endothelial cells, number decreased. Importantly, these non-mutant regions showed high apoptosis rate, which agrees with typical cell competition phenotype. So far very few cell competition studies in heart, and our study is the first time to offer an insight of cell competition among different cardiac cell types. although the mechanisms of inducing non-mutant cell death remain to be elucidated.

CHAPTER V

SUMMARY

In our studies, we uncovered an essential of Hippo signaling Kinase Lats1/2 in epicardial development and adult heart homeostasis. During epicardial development, Lats1/2 kinases is required to maintain fibroblast and smooth muscle cell differentiation. Moreover, Lats1/2 kinases and mechanical stress coordinately suppress endothelial fate derived from epicardium. In adult heart, Lats1/2 in cardiac fibroblast is essential for heart homeostasis. It prevents cardiac fibroblast from over-proliferation and maintains normal fibroblast function such as collagen production. It is required for common cross-talk between fibroblast and immune cells and inhibits of Myc activity from hyperactivated cell-competition.

REFERENCES

1. Heallen, T., Morikawa, Y., Leach, J., Tao, G., Willerson, J. T., Johnson, R. L., and Martin, J. F. (2013) Hippo signaling impedes adult heart regeneration. *Development* 140, 4683-4690
2. Morikawa, Y., Zhang, M., Heallen, T., Leach, J., Tao, G., Xiao, Y., Bai, Y., Li, W., Willerson, J. T., and Martin, J. F. (2015) Actin cytoskeletal remodeling with protrusion formation is essential for heart regeneration in Hippo-deficient mice. *Sci Signal* 8, ra41
3. Heallen, T., Zhang, M., Wang, J., Bonilla-Claudio, M., Klysik, E., Johnson, R. L., and Martin, J. F. (2011) Hippo pathway inhibits Wnt signaling to restrain cardiomyocyte proliferation and heart size. *Science* 332, 458-461
4. Wessels, A., and Perez-Pomares, J. M. (2004) The epicardium and epicardially derived cells (EPDCs) as cardiac stem cells. *Anat Rec A Discov Mol Cell Evol Biol* 276, 43-57
5. Lepilina, A., Coon, A. N., Kikuchi, K., Holdway, J. E., Roberts, R. W., Burns, C. G., and Poss, K. D. (2006) A dynamic epicardial injury response supports progenitor cell activity during zebrafish heart regeneration. *Cell* 127, 607-619
6. Huang, G. N., Thatcher, J. E., McAnally, J., Kong, Y., Qi, X., Tan, W., DiMaio, J. M., Amatruda, J. F., Gerard, R. D., Hill, J. A., Bassel-Duby, R., and Olson, E. N. (2012) C/EBP transcription factors mediate epicardial activation during heart development and injury. *Science* 338, 1599-1603

7. Halder, G., and Johnson, R. L. (2011) Hippo signaling: growth control and beyond. *Development* 138, 9-22

8. Macosko, E. Z., Basu, A., Satija, R., Nemesh, J., Shekhar, K., Goldman, M., Tirosh, I., Bialas, A. R., Kamitaki, N., Martersteck, E. M., Trombetta, J. J., Weitz, D. A., Sanes, J. R., Shalek, A. K., Regev, A., and McCarroll, S. A. (2015) Highly parallel genome-wide expression profiling of individual cells using nanoliter droplets. *Cell* 161, 1202-1214

9. Zhou, B., Ma, Q., Rajagopal, S., Wu, S. M., Domian, I., Rivera-Feliciano, J., Jiang, D., von Gise, A., Ikeda, S., Chien, K. R., and Pu, W. T. (2008) Epicardial progenitors contribute to the cardiomyocyte lineage in the developing heart. *Nature* 454, 109-113

10. Xin, M., Kim, Y., Sutherland, L. B., Qi, X., McAnally, J., Schwartz, R. J., Richardson, J. A., Bassel-Duby, R., and Olson, E. N. (2011) Regulation of insulin-like growth factor signaling by Yap governs cardiomyocyte proliferation and embryonic heart size. *Sci Signal* 4, ra70

11. Muzumdar, M., Tasic, B., Miyamichi, K., Li, L., and Luo, L. (2007) A global double-fluorescent Cre reporter mouse. *Genesis* 45, 593-605

12. Dyer, L. A., and Patterson, C. (2013) Isolation of embryonic ventricular endothelial cells. *Journal of Visualized Experiments* 77,e50463

13. Shekhar, K., Lapan, S. W., Whitney, I. E., Tran, N. M., Macosko, E. Z., Kowalczyk, M., Adiconis, X., Levin, J. Z., Nemesh, J., Goldman, M., McCarroll, S. A., Cepko, C. L., Regev, A., and Sanes, J. R. (2016)

Comprehensive classification of retinal bipolar neurons by single-cell transcriptomics. *Cell* 166,1308-1323

14. Dobin, A., Davis, C. A., Schlesinger, F., Drenkow, J., Zaleski, C., Jha, S., Batut, P., Chaisson, M., and Gingeras, T. R. (2013) STAR: ultrafast universal RNA-seq aligner. *Bioinformatics* 29, 15-21
15. Satija, R., Farrell, J. A., Gennert, D., Schier, A. F., and Regev, A. (2015) Spatial reconstruction of single-cell gene expression data. *Nat Biotechnol* 33, 495-502
16. Leek, J. T., Johnson, W. E., Parker, H. S., Jaffe, A. E., and Storey, J. D. (2012) The sva package for removing batch effects and other unwanted variation in high-throughput experiments. *Bioinformatics* 28, 882-883
17. Maaten, L., and Hinton, G. (2008) Visualizing data using t-SNE. *J Mach Learn Res* 9, 2579-2605
18. McDavid, A., Finak, G., Chattopadyay, P. K., Dominguez, M., Lamoreaux, L., Ma, S. S., Roederer, M., and Gottardo, R. (2013) Data exploration, quality control and testing in single-cell qPCR-based gene expression experiments.*Bioinformatics* 29,461-467
19. Qiu, X., Hill, A., Packer, J., Lin, D., Ma, Y.-A. A., and Trapnell, C. (2017) Single-cell mRNA quantification and differential analysis with Census. *Nat Methods* 14,309-315
20. Janky, R., Verfaillie, A., Imrichova, H., Van de Sande, B., Standaert, L., Christiaens, V., Hulselmans, G., Herten, K., Naval Sanchez, M., Potier,

D., Svetlichnyy, D., Kalender Atak, Z., Fiers, M., Marine, J. C., and Aerts, S. (2014) iRegulon: from a gene list to a gene regulatory network using large motif and track collections. *PLoS Comput Biol* 10, e1003731

21. Tripathi, S., Pohl, M. O., Zhou, Y., Rodriguez-Frandsen, A., Wang, G., Stein, D. A., Moulton, H. M., DeJesus, P., Che, J., Mulder, L. C., Yanguez, E., Andenmatten, D., Pache, L., Manicassamy, B., Albrecht, R. A., Gonzalez, M. G., Nguyen, Q., Brass, A., Elledge, S., White, M., Shapira, S., Hacohen, N., Karlas, A., Meyer, T. F., Shales, M., Gatorano, A., Johnson, J. R., Jang, G., Johnson, T., Verschueren, E., Sanders, D., Krogan, N., Shaw, M., Konig, R., Stertz, S., Garcia-Sastre, A., and Chanda, S. K. (2015) Meta- and orthogonal integration of influenza "OMICs" data defines a role for UBR4 in virus budding. *Cell Host Microbe* 18, 723-735
22. Singhal, N., and Martin, P. T. (2015) A role for Galgt1 in skeletal muscle regeneration. *Skeletal Muscle* 5, 3
23. Mukouyama, Y. S., James, J., Nam, J., and Uchida, Y. (2012) Whole-mount confocal microscopy for vascular branching morphogenesis. *Methods Mol Biol* 843, 69-78
24. Ma, L., Lu, M.-F. F., Schwartz, R. J., and Martin, J. F. (2005) Bmp2 is essential for cardiac cushion epithelial-mesenchymal transition and myocardial patterning. *Development* 132,5601-5611

25. Jiang, R., Lan, Y., Norton, C. R., Sundberg, J. P., and Gridley, T. (1998) The Slug gene is not essential for mesoderm or neural crest development in mice. *Dev Biol* 198, 277-285

26. Li, P., Cavallero, S., Gu, Y., Chen, T. H., Hughes, J., Hassan, A. B., Bruning, J. C., Pashmforoush, M., and Sucov, H. M. (2011) IGF signaling directs ventricular cardiomyocyte proliferation during embryonic heart development. *Development* 138, 1795-1805

27. Singh, A., Ramesh, S., Cibi, D. M., Yun, L. S., Li, J., Li, L., Manderfield, L. J., Olson, E. N., Epstein, J. A., and Singh, M. K. (2016) Hippo signaling mediators Yap and Taz are required in the epicardium for coronary vasculature development. *Cell Rep* 15, 1384-1393

28. Amir, E.-a. D. l.-A. D., Davis, K. L., Tadmor, M. D., Simonds, E. F., Levine, J. H., Bendall, S. C., Shenfeld, D. K., Krishnaswamy, S., Nolan, G. P., and Pe'er, D. (2013) viSNE enables visualization of high dimensional single-cell data and reveals phenotypic heterogeneity of leukemia. *Nat Biotechnol* 31,545-552

29. Anchang, B., Hart, T. D., Bendall, S. C., Qiu, P., Bjornson, Z., Linderman, M., Nolan, G. P., and Plevritis, S. K. (2016) Visualization and cellular hierarchy inference of single-cell data using SPADE.*Nat Protoc* 11,1264-1279

30. Levine, J. H., Simonds, E. F., Bendall, S. C., Davis, K. L., Amir, E.-a. D. l.-A. D., Tadmor, M. D., Litvin, O., Fienberg, H. G., Jager, A., Zunder, E. R.,

Finck, R., Gedman, A. L., Radtke, I., Downing, J. R., Pe'er, D., and Nolan, G. P. (2015) Data-driven phenotypic dissection of AML reveals progenitor-like cells that correlate with prognosis. *Cell* 162, 184-197

31. Acharya, A., Baek, S. T., Huang, G., Eskiocak, B., Goetsch, S., Sung, C. Y., Banfi, S., Sauer, M. F., Olsen, G. S., Duffield, J. S., Olson, E. N., and Tallquist, M. D. (2012) The bHLH transcription factor Tcf21 is required for lineage-specific EMT of cardiac fibroblast progenitors. *Development (Cambridge, England)* 139, 2139-2149
32. Trapnell, C., Cacchiarelli, D., Grimsby, J., Pokharel, P., Li, S., Morse, M., Lennon, N. J., Livak, K. J., Mikkelsen, T. S., and Rinn, J. L. (2014) The dynamics and regulators of cell fate decisions are revealed by pseudotemporal ordering of single cells. *Nat Biotechnol* 32,381-386
33. Theriault, B. L., Shepherd, T. G., Mujoomdar, M. L., and Nachtigal, M. W. (2007) BMP4 induces EMT and Rho GTPase activation in human ovarian cancer cells. *Carcinogenesis* 28, 1153-1162
34. Rosano, L., Spinella, F., Di Castro, V., Nicotra, M. R., Dedhar, S., de Herreros, A. G., Natali, P. G., and Bagnato, A. (2005) Endothelin-1 promotes epithelial-to-mesenchymal transition in human ovarian cancer cells. *Cancer Res* 65, 11649-11657
35. Perez-Pinera, P., Alcantara, S., Dimitrov, T., Vega, J. A., and Deuel, T. F. (2006) Pleiotrophin disrupts calcium-dependent homophilic cell-cell

adhesion and initiates an epithelial-mesenchymal transition. *Proc Natl Acad Sci U S A* 103, 17795-17800

36. Rudat, C., and Kispert, A. (2012) Wt1 and epicardial fate mapping. *Circ Res* 111, 165-169

37. Terai, Y., Abe, M., Miyamoto, K., Koike, M., Yamasaki, M., Ueda, M., Ueki, M., and Sato, Y. (2001) Vascular smooth muscle cell growth-promoting factor/F-spondin inhibits angiogenesis via the blockade of integrin alphavbeta3 on vascular endothelial cells. *J Cell Physiol* 188, 394-402

38. Lavine, K. J., Yu, K., White, A. C., Zhang, X., Smith, C., Partanen, J., and Ornitz, D. M. (2005) Endocardial and epicardial derived FGF signals regulate myocardial proliferation and differentiation in vivo. *Dev Cell* 8, 85-95

39. Ou, X., O'Leary, H. A., and Broxmeyer, H. E. (2013) Implications of DPP4 modification of proteins that regulate stem/progenitor and more mature cell types. *Blood* 122, 161-169

40. Sridurongrit, S., Larsson, J., Schwartz, R., Ruiz-Lozano, P., and Kaartinen, V. (2008) Signaling via the Tgf-beta type I receptor Alk5 in heart development. *Dev Biol* 322, 208-218

41. Wu, Q. H., Ma, Y., Ruan, C. C., Yang, Y., Liu, X. H., Ge, Q., Kong, L. R., Zhang, J. W., Yan, C., and Gao, P. J. (2017) Loss of osteoglycin promotes angiogenesis in limb ischaemia mouse models via modulation

of vascular endothelial growth factor and vascular endothelial growth factor receptor 2 signalling pathway. *Cardiovas Res* 113, 70-80

42. Billings, S. E., Pierzchalski, K., Butler Tjaden, N. E., Pang, X. Y., Trainor, P. A., Kane, M. A., and Moise, A. R. (2013) The retinaldehyde reductase DHRS3 is essential for preventing the formation of excess retinoic acid during embryonic development. *FASEB J* 27, 4877-4889
43. Li, G., Xu, A., Sim, S., Priest, J. R., Tian, X., Khan, T., Quertermous, T., Zhou, B., Tsao, P. S., Quake, S. R., and Wu, S. M. (2016) Transcriptomic profiling maps anatomically patterned subpopulations among single embryonic cardiac cells. *Dev Cell* 39, 491-507
44. Zhang, H., von Gise, A., Liu, Q., Hu, T., Tian, X., He, L., Pu, W., Huang, X., He, L., Cai, C. L., Camargo, F. D., Pu, W. T., and Zhou, B. (2014) Yap1 is required for endothelial to mesenchymal transition of the atrioventricular cushion. *J Biol Chem* 289, 18681-18692
45. Boggiano, J. C., and Fehon, R. G. (2012) Growth control by committee: intercellular junctions, cell polarity, and the cytoskeleton regulate Hippo signaling. *Dev Cell* 22, 695-702
46. Zhou, B., Honor, L. B., He, H., Ma, Q., Oh, J.-H. H., Butterfield, C., Lin, R.-Z. Z., Melero-Martin, J. M., Dolmatova, E., Duffy, H. S., Gise, A. v., Zhou, P., Hu, Y. W., Wang, G., Zhang, B., Wang, L., Hall, J. L., Moses, M. A., McGowan, F. X., and Pu, W. T. (2011) Adult mouse epicardium

modulates myocardial injury by secreting paracrine factors. *J Clin Invest* 121, 1894-1904

47. Riley, P. R. (2011) An epicardial floor plan for building and rebuilding the mammalian heart. *Curr Top Dev Biol* 100, 233-251

48. Khurana, S., Margamuljana, L., Joseph, C., Schouteden, S., Buckley, S. M., and Verfaillie, C. M. (2013) Glypican-3-mediated inhibition of CD26 by TFPI: a novel mechanism in hematopoietic stem cell homing and maintenance. *Blood* 121, 2587-2595

49. Dupont, S., Morsut, L., Aragona, M., Enzo, E., Giulitti, S., Cordenonsi, M., Zanconato, F., Le Digabel, J., Forcato, M., Bicciato, S., Elvassore, N., and Piccolo, S. (2011) Role of YAP/TAZ in mechanotransduction. *Nature* 474, 179-183

50. Lopez, A. D., Mathers, C. D., Ezzati, M., Jamison, D. T., and Murray, C. J. (2006) Global and regional burden of disease and risk factors, 2001: systematic analysis of population health data. *Lancet* 367, 1747-1757

51. Duffey OJ, Smart N. (2016) Approaches to augment vascularisation and regeneration of the adult heart via the reactivated epicardium. *Glob Cardiol Sci Pract* 4: e201628

52. Smart, N., Bollini, S., Dubé, K. N., Vieira, J. M., Zhou, B., Davidson, S., Yellon, D., Riegler, J., Price, A. N., Lythgoe, M. F., Pu, W. T., and Riley, P. R. (2011) De novo cardiomyocytes from within the activated adult heart after injury. *Nature* 474, 640-644

53. van Wijk, B., Gunst, Q. D., Moorman, A. F., and van den Hoff, M. J. (2011) Cardiac regeneration from activated epicardium. *PloS One* 7,e44692

54. Katz, T. C., Singh, M. K., Degenhardt, K., Rivera-Feliciano, J., Johnson, R. L., Epstein, J. A., and Tabin, C. J. (2012) Distinct compartments of the proepicardial organ give rise to coronary vascular endothelial cells. *Dev Cell* 22, 639-650

55. Mammoto, A., and Ingber, D. E. (2009) Cytoskeletal control of growth and cell fate switching. *Curr Opin Cell Biol* 21, 864-870

56. Engler, A. J., Sen, S., Sweeney, H. L., and Discher, D. E. (2006) Matrix elasticity directs stem cell lineage specification. *Cell* 126, 677-689

57. Halder, G., Dupont, S., and Piccolo, S. (2012) Transduction of mechanical and cytoskeletal cues by YAP and TAZ. *Nat Rev Mol Cell Biol* 13, 591-600

58. Wada, K., Itoga, K., Okano, T., Yonemura, S., and Sasaki, H. (2011) Hippo pathway regulation by cell morphology and stress fibers. *Development* 138, 3907-3914

59. Huang, Y., Harrison, M. R., Osorio, A., Kim, J., Baugh, A., Duan, C., Sucov, H. M., and Lien, C. L. (2013) Igf signaling is required for cardiomyocyte proliferation during zebrafish heart development and regeneration. *PLoS One* 8, e67266

60. Gunning, A. P., Chambers, S., Pin, C., Man, A. L., Morris, V. J., and Nicoletti, C. (2008) Mapping specific adhesive interactions on living human intestinal epithelial cells with atomic force microscopy. *FASEB J* 22, 2331-2339

61. Tse, J. R., and Engler, A. J. (2010) Preparation of hydrogel substrates with tunable mechanical properties. *Curr Protoc Cell Biol* Chapter 10, Unit 10.16

62. Zhou, B., and Pu, W. T. (2012) Genetic Cre-loxP assessment of epicardial cell fate using Wt1-driven Cre alleles. *Circ Res* 111, e276-280

63. Hayashi, S., and McMahon, A. P. (2002) Efficient recombination in diverse tissues by a tamoxifen-inducible form of Cre: a tool for temporally regulated gene activation/inactivation in the mouse. *Dev Biol* 244, 305-318

64. Takeichi, M., Nimura, K., Mori, M., Nakagami, H., and Kaneda, Y. (2012) The transcription factors Tbx18 and Wt1 control the epicardial epithelial-mesenchymal transition through bi-directional regulation of Slug in murine primary epicardial cells. *PloS One* 8, e57829

65. Cenni, B., Gutmann, S., and Gottar-Guillier, M. (2012) BMX and its role in inflammation, cardiovascular disease, and cancer. *Int Rev Immunol* 31, 166-173

66. Kleaveland, B., Zheng, X., Liu, J. J., Blum, Y., Tung, J. J., Zou, Z., Sweeney, S. M., Chen, M., Guo, L., Lu, M. M., Zhou, D., Kitajewski, J.,

Affolter, M., Ginsberg, M. H., and Kahn, M. L. (2009) Regulation of cardiovascular development and integrity by the heart of glass-cerebral cavernous malformation protein pathway. *Nat Med* 15, 169-176

67. Meiri, D., Marshall, C. B., Greeve, M. A., Kim, B., Balan, M., Suarez, F., Bakal, C., Wu, C., Larose, J., Fine, N., Ikura, M., and Rottapel, R. (2012) Mechanistic insight into the microtubule and actin cytoskeleton coupling through dynein-dependent RhoGEF inhibition. *Mol Cell* 45, 642-655

68. Gonzalez-Mariscal, L., Dominguez-Calderon, A., Raya-Sandino, A., Ortega-Olvera, J. M., Vargas-Sierra, O., and Martinez-Revollar, G. (2014) Tight junctions and the regulation of gene expression. *Semin Cell Dev Biol* 36, 213-223

69. Mathur, A. B., Collinsworth, A. M., Reichert, W. M., Kraus, W. E., and Truskey, G. A. (2001) Endothelial, cardiac muscle and skeletal muscle exhibit different viscous and elastic properties as determined by atomic force microscopy. *J Biomech* 34, 1545-1553

70. Mahaffy, R. E., Shih, C. K., MacKintosh, F. C., and Kas, J. (2000) Scanning probe-based frequency-dependent microrheology of polymer gels and biological cells. *Phys Rev Lett* 85, 880-883

71. Engler, A. J., Sen, S., Sweeney, H. L., and Discher, D. E. (2006) Matrix elasticity directs stem cell lineage specification. *Cell* 126, 677-689

72. Mosqueira, D., Pagliari, S., Uto, K., Ebara, M., Romanazzo, S., Escobedo-Lucea, C., Nakanishi, J., Taniguchi, A., Franzese, O., Di

Nardo, P., Goumans, M. J., Traversa, E., Pinto-do, O. P., Aoyagi, T., and Forte, G. (2014) Hippo pathway effectors control cardiac progenitor cell fate by acting as dynamic sensors of substrate mechanics and nanostructure. *ACS Nano* 8, 2033-2047

73. Yin, F., Yu, J., Zheng, Y., Chen, Q., Zhang, N., and Pan, D. (2013) Spatial organization of Hippo signaling at the plasma membrane mediated by the tumor suppressor Merlin/NF2. *Cell* 154, 1342-1355

74. Codelia, V. A., Sun, G., and Irvine, K. D. (2014) Regulation of YAP by mechanical strain through Jnk and Hippo signaling. *Curr Biol* 24, 2012-2017

75. Trembley, M. A., Velasquez, L. S., de Mesy Bentley, K. L., and Small, E. M. (2015) Myocardin-related transcription factors control the motility of epicardium-derived cells and the maturation of coronary vessels. *Development (Cambridge, England)* 142, 21-30

76. Esnault, C., Stewart, A., Gualdrini, F., East, P., Horswell, S., Matthews, N., and Treisman, R. (2014) Rho-actin signaling to the MRTF coactivators dominates the immediate transcriptional response to serum in fibroblasts. *Genes Dev* 28, 943-958

77. Fernandez, B. G., Gaspar, P., Bras-Pereira, C., Jezowska, B., Rebelo, S. R., and Janody, F. (2011) Actin-capping protein and the Hippo pathway regulate F-actin and tissue growth in Drosophila. *Development* 138, 2337-2346

78. Riley, P. R., and Smart, N. (2011) Vascularizing the heart. *Cardiovasc Res* 91, 260-268

79. Mamada, H., Sato, T., Ota, M., and Sasaki, H. (2015) Cell competition in mouse NIH3T3 embryonic fibroblasts is controlled by the activity of Tead family proteins and Myc. *J Cell Sci* 128, 790-803

80. Asefa, B., Klarmann, K. D., Copeland, N. G., Gilbert, D. J., Jenkins, N. A., and Keller, J. R. (2004) The interferon-inducible p200 family of proteins: a perspective on their roles in cell cycle regulation and differentiation. *Blood Cells Mol Dis* 32, 155-167

81. Zhao, G. N., Jiang, D. S., and Li, H. (2015) Interferon regulatory factors: at the crossroads of immunity, metabolism, and disease. *Biochim Biophys Acta* 1852, 365-378

82. Horiuchi, M., Hayashida, W., Akishita, M., Yamada, S., Lehtonen, J. Y., Tamura, K., Daviet, L., Chen, Y. E., Hamai, M., Cui, T. X., Iwai, M., and Minokoshi, Y. (2000) Interferon-gamma induces AT(2) receptor expression in fibroblasts by Jak/STAT pathway and interferon regulatory factor-1. *Circ Res* 86, 233-240

83. Day, C., Patel, R., Guillen, C., and Wardlaw, A. J. (2009) The chemokine CXCL16 is highly and constitutively expressed by human bronchial epithelial cells. *Exp Lung Res* 35, 272-283

84. Reuben, A., Chung, J. W., Lapointe, R., and Santos, M. M. (2017) The hemochromatosis protein HFE 20 years later: An emerging role in antigen presentation and in the immune system. *Immun Inflamm Dis* 5, 218-232

85. Claveria, C., and Torres, M. (2016) Cell competition: mechanisms and physiological roles. *Annu Rev Cell Dev Biol* 32, 411-439

86. Levayer, R., Hauert, B., and Moreno, E. (2015) Cell mixing induced by myc is required for competitive tissue invasion and destruction. *Nature* 524, 476-480